UNIVERSITY OF BELGRADE

FACULTY OF TECHNOLOGY AND METALLURGY

Alsadek Ali Alguail

BATTERY TYPE HYBRID SUPERCAPACITOR BASED ON CONDUCTING POLYMERS

Doctoral Dissertation

Belgrade, 2018

UNIVERZITET U BEOGRADU

TEHNOLOŠKO-METALURŠKI FAKULTET

Alsadek Ali Alguail

HIBRIDNI SUPERKONDENZATORI AKUMULATORSKOG TIPA NA BAZI PROVODNIH POLIMERA

doktorska disertacija

Beograd, 2018

Mentor:

Dr Branimir Grgur, redovni profesor,

Univerzitet u Beogradu, Tehnološko-metalurški fakultet

Članovi komisije:

Dr Milica Gvozdenović, vanredni profesor,

Univerzitet u Beogradu, Tehnološko-metalurški fakultet

Dr Branimir Jugović, naučni savetnik,

Institut tehničkih nauka – SANU, Beograd

Datum odbrane: ___ ___ _____ god.

ACKNOWLEDGEMENT

BATTERY TYPE HYBRID SUPERCAPACITOR BASED ON CONDUCTING POLYMERS

ABSTRACT

The electrochemically synthesized polypyrrole and lead-lead sulfate are examined as a potential electrodes for battery-type hybrid supercapacitors in acidic solution. Discharge in the specific current range of ~0.6–2.27 A g^{-1} based on the active masses, can deliver capacity of 90–72 Ah kg^{-1}, energy of 58–40 Wh kg^{-1} and power of 40–1350 W kg^{-1}, with the specific capacitance of the cell in the range of 300–250 F g^{-1}. The device exhibits battery-type behavior at low discharge rate, e.g. <0.5 A g^{-1}, and supercapacitors-type behavior at a higher discharge rate. It is estimated that cell will lose 20% of initial capacitance after ~500-600 cycles.

The electrochemically synthesized polyaniline and lead sulfate are investigated as a possible active material of the aqueous based hybrid asymmetric supercapacitors. The electrochemical characteristics of polyaniline (doping-dedoping reactions), as well as electrical characteristics (specific capacitance, capacity, energy, and power) of the $PbSO_4$|PANI cell, are determined. The cell capacitance, ranging from 216 F g^{-1} to 230 F g^{-1} is determined. In the specific current range of 0.3–1.5 A g^{-1} based on the active masses, the specific energy decrease from 30 to 20 Wh kg^{-1}, while specific power increased from 200 to ~800 W kg^{-1}. The specific capacity of the cell, slightly decreased from 47 Ah g^{-1} to 40 Ah g^{-1} by increasing the specific current. It is estimated that cell will lose 20% of initial capacitance after ~550 cycles.

Based on the estimated specific energy and power, it is suggested that investigated cells could be classified as hydride asymmetric battery type supercapacitors or "supercapattery" type of electrochemical power sources.

HIBRIDNI SUPERKONDENZATORI AKUMULATORSKOG TIPA NA BAZI PROVODNIH POLIMERA

REZIME

Elektrohemijski sintetizovani polipirol i olovo-olovo sulfat ispitani su kao potencijalne elektrode za hibridne superkondenzatore akumulatora tipa u kiselom rastvoru. Pražnjenjem u strujnom opsegu od ~0,6-2,27 A g^{-1} na bazi aktivnih masa, određene su vrednosti specifični kapaciteti od 90-72 Ah kg^{-1}, energija od 58-40 Wh kg^{-1} i snaga od 40-1350 W kg^{-1}, sa specifičnom kapacitivnošću ćelije u opsegu od 300-250 F g^{-1}. Sistem pokazuje ponašanje tipa akumulatora pri malim strujama pražnjenja, npr. <0,5 A g^{-1} i superkondenzatorsko ponašanje pri većom strujama pražnjenja. Procenjeno je da će ćelija izgubiti 20% početnog kapaciteta posle ~ 500-600 ciklusa punjenja i pražnjenja.

Elektrohemijski sintetizovani polianilin i olovo sulfat ispitani su kao mogući aktivni materijal hibridnih asimetričnih superkondenzatora. Određene su elektrohemijske karakteristike polianilina (reakcije dopovanja i dedopovanja), kao i električne karakteristike (specifična kapacitivnost, kapacitet, energija i snaga) ćelije. Određuene su kapacitivnosti ćelije, u opsegu od 216 F g^{-1} do 230 F g^{-1}. Pri strujama pražnjenja u opsegu od 0.3-1.5 A g^{-1} na osnovu aktivnih masa, specifična energija se smanjuje sa 30 na 20 Wh kg^{-1}, dok se specifična snaga povećana sa 200 na ~ 800 W kg^{-1}. Specifični kapacitet ćelije, malo je smanjen sa 47 Ah g^{-1} na 40 Ah g^{-1}. Procenjeno je da će ćelija izgubiti 20% početne kapacitivnosti nakon ~550 ciklusa.

Na osnovu procenjenih vrednosti specifične energije i snage, predloženo je da ispitane ćelije mogu biti klasifikovane kao asimetrični hibridni superkondenzatori akumulatorskog tipa ili a "superkapabaterijska" vrsta elektrohemijskih izvora energije.

Ključne reči: polianilin, polipirol, superkapabaterija, specifična energija, specifična snaga

Naučna oblast: Tehnološko inženjerstvo

Uža naučna oblast: Hemijsko inženjerstvo

CONTENTS

1. INTRODUCTION REVIEW

In response to the climate changes, energy has become a primary focus of the major world powers and scientific community [1]. There has been great interest in developing and refining more efficient energy storage devices. One such device, the supercapacitor, has matured significantly over the last decade and emerged with the potential to facilitate major advances in energy storage. Supercapacitors, also known as ultracapacitors or electrochemical capacitors, utilize high surface area electrode materials and thin electrolytic layer to achieve capacitances several orders of magnitude larger than conventional electrical capacitors [2,3,4,5]. Electrochemical supercapacitors are able to achieve greater energy densities while still maintaining the characteristic high power density of conventional capacitors.

The performance improvement for a supercapacitor is shown in Figure 1.1, a graph conventionally called a "Ragone plot". This type of graph presents the power densities of different energy storage devices, measured along the vertical axis, versus their energy densities, shown along the horizontal axis. In Figure 1.1, it can be seen that electrochemical supercapacitors occupy a region between conventional capacitors and batteries [3]. Regardless of greater capacitances than conventional capacitors, supercapacitors have yet to match the energy densities of mid to high-end batteries and fuel cells.
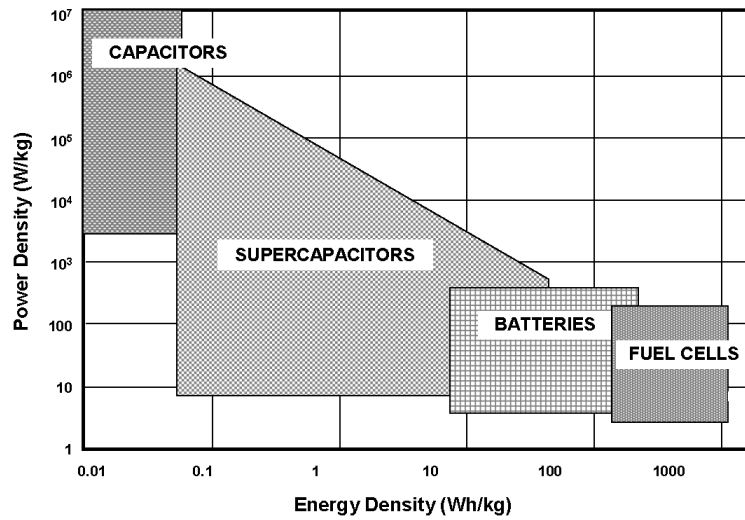
Figure 1.1. Ragone plot of energy storage devices [3].

Figure 1.2 shows the constant current discharge curves of battery, electrostatic capacitor and electrochemical supercapacitors (EC). It is obvious that the battery curve has discharge plateau, and the voltage keeps in invariant. The discharge curves of electrostatic capacitor and EC are similar, which are linear, the voltage decreases linearly with the increase of discharge charge. There is a linear relationship between voltage and time in the process of constant current discharge for the EC, the dU/dI keeps constant value.
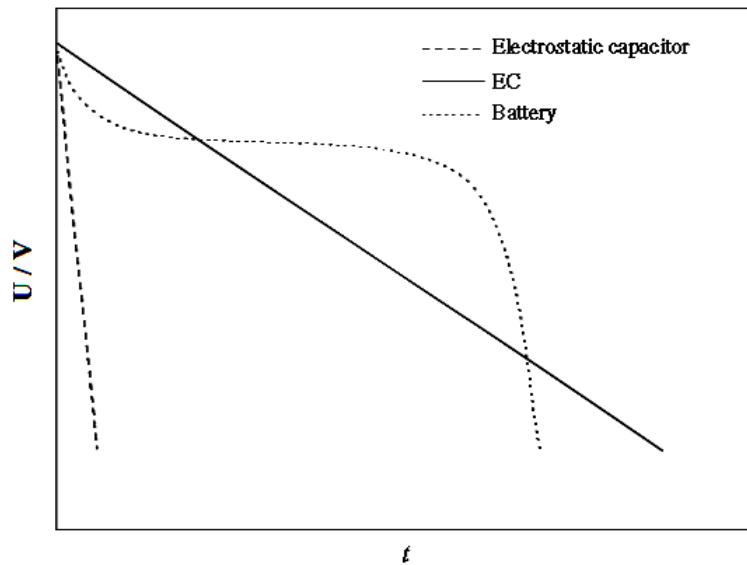
Figure. 1.2. Discharge characteristics of battery, electrostatic capacitor and electrochemical supercapacitors (EC) [6].

In Table 1.1 are given in typical values of the basic parameters of the battery, classical and supercapacitors for comparison [7].

Table 1.1. Typical values of the basic parameters of the battery, classic and electrochemical supercapacitor (EC) [7].

	Batteries	Capacitors	EC
Charge time	1 – 5 h	$10^{-3} – 10^{-6}$ s	0.3-30 s
Discharge time	0.5 – 3 h	$10^{-3} – 10^{-6}$ s	0.3-30 s
Specific energy, Wh kg^{-1}	10 - 100	<0.1	1 - 10
Specific power, W kg^{-1}	50 - 200	>10.000	~1000
Efficiency	0.7 - 0.85	~1	0.85 – 0.95
Cycle life	500 - 2000	>500.000	>100.000

Based upon current R&D trends, supercapacitors can be divided into three general classes: electrochemical double-layer capacitors, pseudocapacitors, and hybrid capacitors, Fig. 1.3 [3]. Each class is characterized by its unique mechanism for storing charge. These are, respectively, non-Faradaic, Faradaic, and a combination of the two. Faradaic processes, such as oxidation-reduction reactions, involve the transfer of charge between electrode and electrolyte. A non-Faradaic mechanism, by contrast, does not use a chemical mechanism. Rather, charges are distributed on surfaces by physical processes that do not involve the making or breaking of chemical bonds.
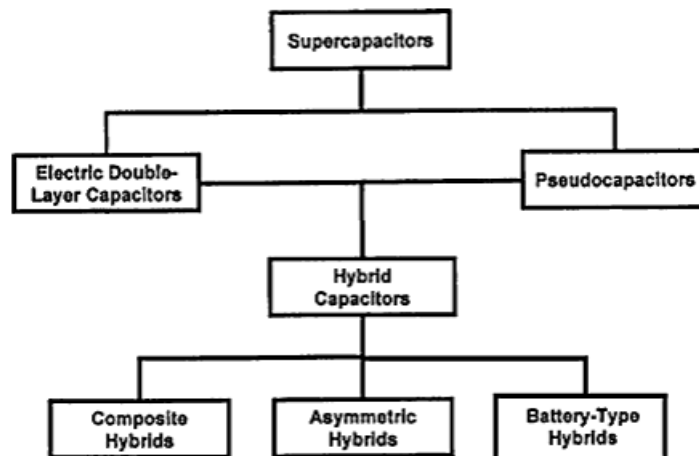
Figure 1.3. Division of supercapacitors by type [3].

In Fig. 1.4, the typical cyclic voltammograms and galvanostatic charge-discharge response of pure capacitive, pseudocapacitive and pure battery type electrodes, are shown. The series shows the transition from a typical capacitive behavior (EDLC) (a, b) to a typical (two phase) battery electrode (e, f) with a pseudocapacitive oxide electrode as an intermediate case (c, d). It should be noted that even for the same Co_3O_4 material different degrees of capacitive and faradaic components can be appreciated depending on the specific microstructure of the active phase [8]
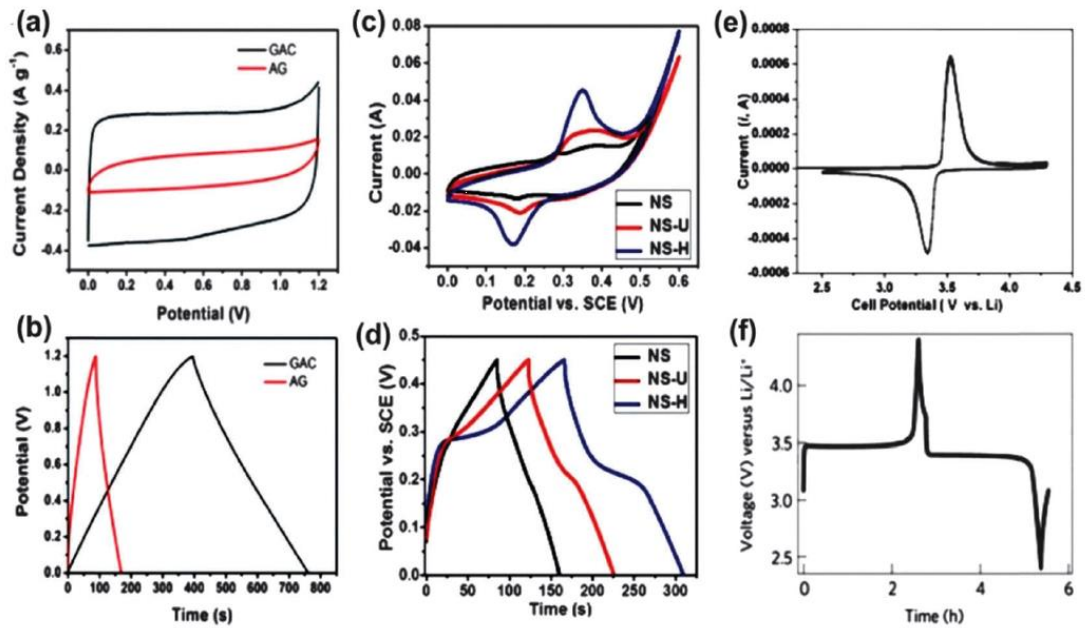
Figure 1.4. Cyclic voltammograms (top) and charge–discharge cycles (bottom) for different types of electrode materials: (a, b), carbon-based double-layer supercapacitors; (c, d) Co_3O_4 pseudocapacitor; (e, f) $LiFePO_4$ battery electrode [8].

Among different types of supercapacitors, *e.g.* double-layer (EDLC) and pseudocapacitors, very promising type are hybrid supercapacitors [8]. Utilizing both faradaic and non-faradaic processes to store charge, hybrid supercapacitors have achieved energy and power densities greater than EDLC's without the sacrifices in cycling stability and affordability that have limited the success of pseudocapacitors [9, 10]. According to the recent review paper by Dubal et al. [8] characteristics of the hybrid supercapacitors are at the top of other types, and possess specific energy in the range of 30-100 Wh kg^{-1} and specific power ranging from 0.1 up to ~10 kW kg^{-1}.

Research has focused on three different types of hybrid capacitors, distinguished by their electrode configuration: composite, asymmetric and battery-type, respectively. In order to improve characteristics of supercapacitors, different combinations of hybrid nanostructures were investigated, including binary and ternary combinations of various carbon and graphene materials, intrinsically conducting polymers (ICP's) and metal oxides/hydroxides, such as RuO_2, MnO_2, $NiO/Ni(OH)_2$, $Co_3O_4/Co(OH)_2$, Fe_2O_3, Fe_3O_4 etc. [8,9,10,11]. A hybrid device based on a battery type electrode and an electrochemical capacitor electrode defined by Cericola and Kötz [3] as an "internal serial hybrid" (ISH) in principle could combine good characteristics of supercapacitors and battery [8]. Recently, such configuration was named "supercapattery" (from: **supercapa**citors -ba**tteries**) [12, 13]. Practically, all the electrode materials of the commercial battery systems can be used for the battery-type electrode in the suitable electrolyte, from lead–acid batteries to metal/air systems, but in practice, metallic compounds like SnO_2, MnO_2 and $LiFePO_4$ are usually investigated [12]. Although there is less experimental data on battery-type hybrids than on other types of hybrid supercapacitors, the data that is available suggests that these hybrids may be able to bridge the gap between supercapacitors and batteries [8]. The battery-type, usually combine one battery-type, faradaic electrode (as an energy source) with the other capacitive electrode (as a power source) in the cell [8, 14].

One example of such hybrid system based on electrodeposited PbO_2 on graphite in combination with activated carbon negative electrode in 5.3 mol dm^{-3} H_2SO_4 aqueous solutions were recently investigated by Wang et al. [15]. The authors reported a specific capacitance of 63 F g^{-1} in the voltage window from 1.88 to 0.65 V at 5 C rate. The reported specific energy was in the range of 18 to 27 Wh kg^{-1} with a specific power in the range of 690 to 150 W kg^{-1}.

Supercapacitor that utilize conductive polymers, or from more recently **_intrinsically conductive polymers (ICP's)_**, as a representative of pseudocapacitive electrode materials [16], are envisaged to bridge the gap between existing carbon-based double-layer supercapacitors and batteries to form units of intermediate specific energy [17,18]. ICP's could improve the device as they undergo a redox reaction to store charge in the bulk of the material, thereby, increase the stored energy, and reduce self-

discharge. [17]. Intrinsically conducting polymers represents a distinct group of pseudocapacitive materials that can accumulate energy via both redox and pseudo-capacitive properties [17,19,20,21,22]. The ability of ICP's to store charges originate from a doping-dedoping process, and capability to provide the capacitive response through a fast redox reaction of the conjugated areas of the polymer matrix. The most extensively studied ICP's, due to the low cost of the monomer, easy synthesis and environmental friendliness are polyaniline (PANI) and polypyrrole (PPy) with the wide range of the reported specific capacitance in both aqueous and non-aqueous electrolytes [13,21,22].

Among different ICP's, polypyrrole (PPy) is currently one of the preferred, due to its high electrical conductivity, facile synthesis in both aqueous and organic media, relatively good stability and reversibility at different pH [8, 23]. The theoretical specific capacitance of the PPy doped with single charged anions is 630 F g^{-1}, while experimentally measured are in the range of 150 up to 500 F g^{-1}, depending on morphology and synthesis conditions [8,11,19,24,25,26,27].

The theoretical specific capacitance of PANI is as high as 750 F g^{-1} [22], while the experimentally obtained in the sulfuric acid based electrolytes were reported to be in the range of 200-550 F g^{-1} with potential windows of ~0.8 V [28,29].

Hence, the aim of this work is to test the possible characteristics of simple hybrid devices based on typical pseudocapacitive, polypyrrole and polyaniline, materials and lead-lead sulfate as typical battery materials, in the battery-type hybrid supercapacitor.

2. THEORETICAL PART

2.1. Electrostatic capacitors

The classical capacitors are consisted of a dielectric materials, with thickness d, between two conducting plates with area, A, as shown in Fig. 2.1.
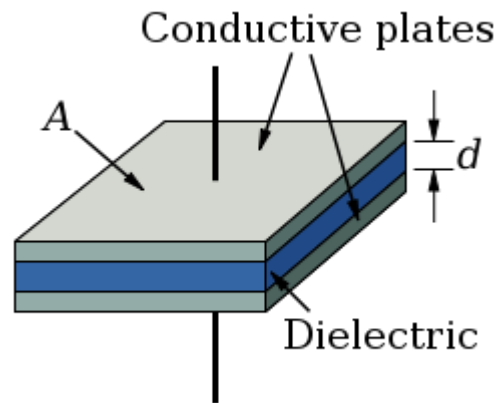
Figure. 2.1. Schematic presentation of the classical capacitors.

The capacitance of a capacitors is equivalent to stored charge, Q, divided by applied voltage, U [30]:

$$C = \frac{Q}{U} \tag{2.1}$$

On the other hand capacitance is given by:

$$C = \varepsilon_0 \varepsilon_r \frac{A}{d} \tag{2.2}$$

where, ε_0 is dielectric constant (permittivity) of vacuum, 8.854×10^{-12} F·m^{-1}, and ε_r is relative permittivity of isolating materials. The values of ε_r for the common isolating materials are given in Table 2.1.

Table 2.1. The values of ε_r for the common isolating materials [31]

Material	Dielectric Constant
Vacuum	1
Glass	5-10
Mica	3-6
Neoprene	6.70
Plexiglas	3.40
Polyethylene	2.25
Polyvinyl chloride	3.18
Teflon	2.1
Water	80.4
Air (1 atm)	1.00059

The unit of capacitance is the farad (F), while the SI system unit are s^{4}A^{2}m^{-2}kg^{-1}. Connection with other electric units is given by the following equation:

$$F = \frac{As}{V} = \frac{J}{V^2} = \frac{Ws}{V^2} = \frac{C}{V} = \frac{C^2}{J}$$ (2.3)

Real capacitors is always connected with equivalent serial resistance (ESR) caused by Ohmic resistance of the used materials. The charge of capacitors with electrical circuit, shown in Fig. 2.2, is linear function of time. Discharge starts with small voltage drop, defined by value of ESR, and proceed linearly to zero voltage, Fig. 2.2.

The energy, W, stored in an electric capacitors can be evaluated [32]:

$$dW = \Delta U dQ = \frac{Q}{C} dq$$ (2.4)

$$dW = \int_0^\varrho \frac{Q}{C} dQ = \frac{1}{C} \int_0^\varrho Q dQ = \frac{Q^2}{2C}$$ (2.4)

or:

$$W = \frac{Q^2}{2C} = \frac{1}{2}Q\Delta U = \frac{1}{2}C(\Delta U)^2 \qquad (2.5)$$
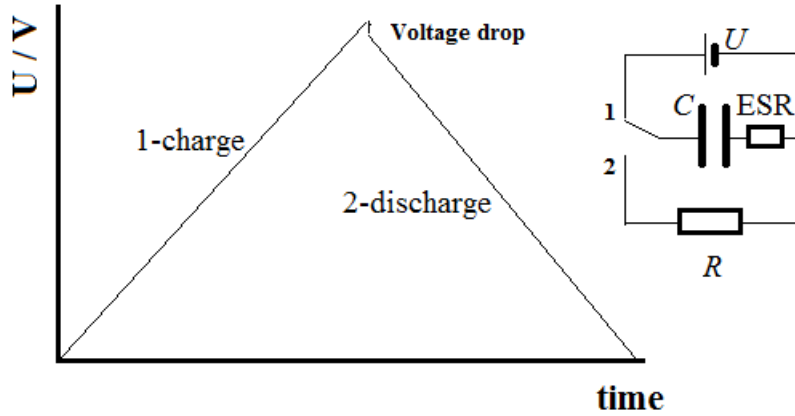
Figure. 2.2. Charge and discharge of electric capacitors with direct current.

The power, P, of electric capacitors is dependent on time of discharge and can be estimated by following equation:

$$P = \frac{W}{\Delta t} = \frac{1}{2\Delta t}C(\Delta U)^2 \qquad (2.6)$$

The maximum power is determined by the value of the equivalent serial resistor (ESR), when external resistance is zero ($R = 0$), according to the equation [30]:

$$P_{max} = \frac{(\Delta U)^2}{4ESR} \qquad (2.7)$$

Electrical capacitors usually has capacitance between 1 pF to few hundred µF, and can store huge power depending on size, for example 10 kW. But the typical discharge

times are in the range of micro to milli-seconds, so the stored energy are relatively low, see Table 1.1, and does not have appropriate values to be used as energy sources.

2.2. Electrochemical capacitors

In principle, electrochemical capacitors or supercapacitors are governed by the same basic principles as conventional electrostatic capacitors. However, they incorporate electrodes with much higher surface areas A, and much thinner dielectrics that decreased distance, d, between the electrodes. By the development of electrochemistry, the new type of electrochemical supercapacitors were developed. The first electrochemical supercapacitors (or sometime ultracapacitor) were developed in the early 1950s, by General Electric, which engineers began experimenting with porous carbon electrodes and electrolytes, in the design of capacitors. The principle of these devices was based on existence of the electrochemical double layer which exist on every conductor – electrolyte interfaces due adsorption of different ions from the electrolyte, as shown in Fig. 2.3 [33]. Accumulated charge and potential drop across boundary layer provoke the capacitance of the electrode. The typical value of the electrochemical double layer capacitance for ideally smooth electrode is 20 µF cm^{-2}. So, by using high surface area materials, the capacitance can dramatically increase.
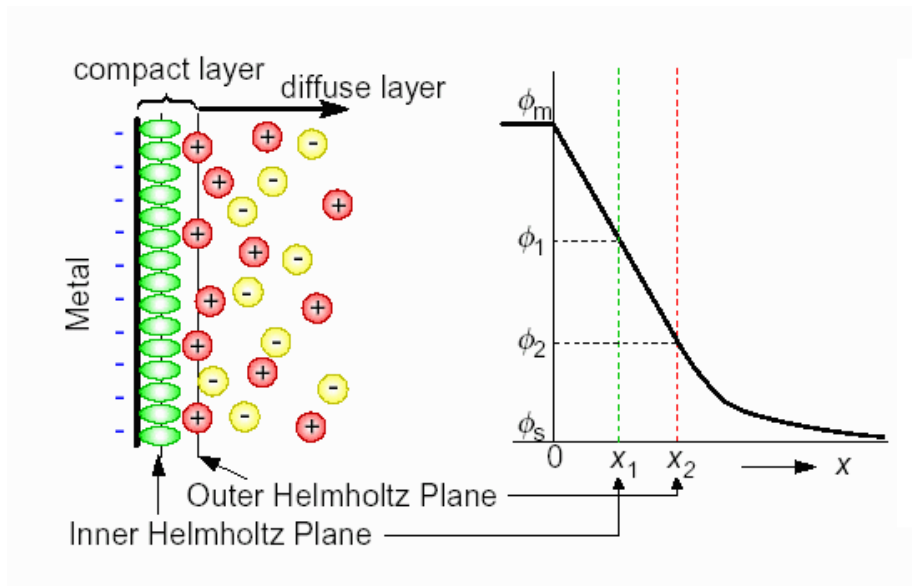
Figure. 2.3. Schematic representation of the electrochemical double layer [33].

2.3. Types of electrochemical supercapacitor

In principle, electrochemical supercapacitors can be divided in a three main groups, as shown in Fig. 2.4 [30]:

1) Electrochemical double layer capacitors (EDLC)

2) Pseudocapacitors

3) Hybrid (or asymmetric) capacitors

Each group of supercapacitors is characterized by its unique mechanism for storing charge [30]. These are, respectively, non-Faradaic (double layer capacitors), Faradic (pseudocapacitors), and a combination of the two (hybrid capacitors). Non-Faradic mechanism, does not involve a chemical reaction mechanism. Rather, charges are distributed on surfaces by physical processes that do not involve the making or breaking of the chemical bonds. Faradic processes, such as oxidation-reduction reactions, contain the transfer of charge among electrode and electrolyte.
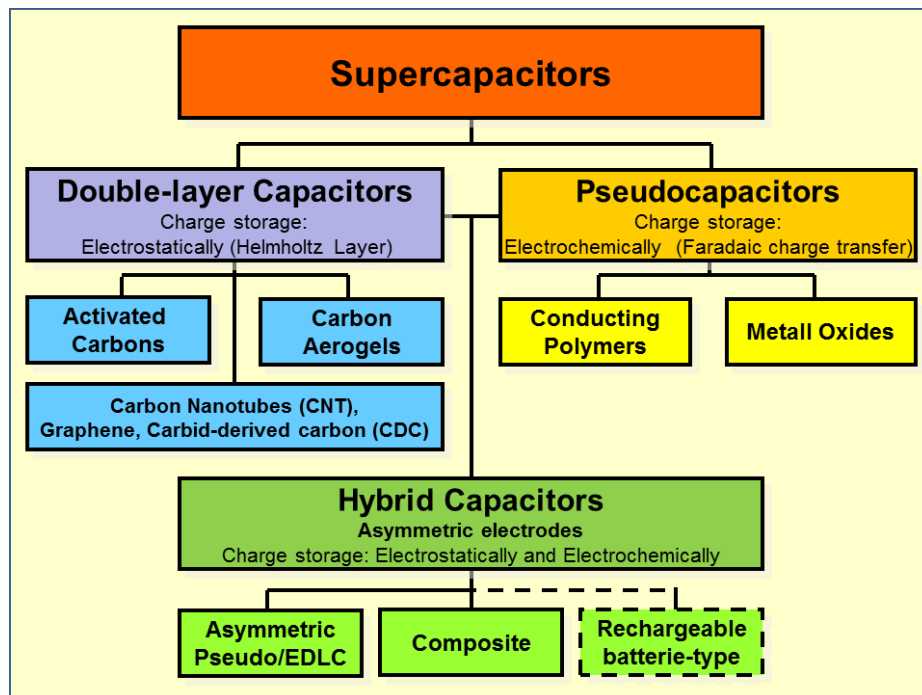
Figure 2.4. Taxonomy of the supercapacitor materials [34]

Development of the supercapacitors was connected with development of the materials used for electrode preparations, Fig 2.5 [35].
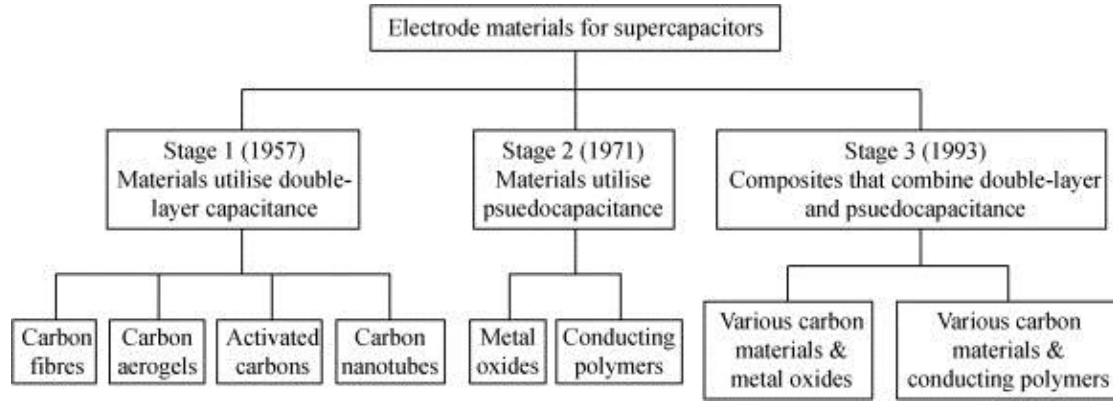
Figure 2.5. Development of of the supercapacitor materials [35].

In 1950's double layer capacitor was first developed [35]. This devices usually used high surface carbon materials like: porous carbons, activated carbon, graphite, graphene, carbon onions, nanotubes, etc [36]. Following stage was development of pseudocapacitive materials in the beginning of 1970's. Those materials can be divided in materials with fast surface redox pseudocapacitance due to adsorption and/or fast intercalation of ions, for examples: hydrated RuO_2, birnessite MnO_2, Ti_3C_2, NiO, Co_2O_3 etc. After discovery of conducting polymer or ***intrinsically conducting polymers (ICP's)*** in 1977. which was distinguished in the form of Nobel Prize in chemistry received by MacDiarmid, Heeger and Shirakawa [37,38,39], those materials was very fast introduced as materials for pseudocapacitors. The firs group suffer from low energy and possess high power density, and the second suffer from low cyclability, so the next stage which started at 1993. combine those two materials in the hybrid asymmetric devices. For example combination of negative carbon and positive metal oxide supercapacitors. During the time, for both electrode, composite materials has been investigated, for example combining conducting polymers deposited on the activated carbons. Recently, combination of ECDL or pseudocapacitive materials with battery type materials, with increased energy and moderate power density, like: Nb_2O_5, $LiCoO_2$, $LiFePO_4$ in the form of battery type supercapacitors so called "supercapattery", have begun to examine [12,13,36].

2.4. Principles and materials of electrochemical supercapacitors

2.4.1. Electrochemical double layer supercapacitors

Electrochemical double layer supercapacitors use for both electrode the same material based mainly on some high surface carbon materials. Schematic presentation of an electrical double-layer supercapacitor is shown in Fig. 2.6 [40]. Because, both electrode are the same, such supercapacitors is usually named symmetric supercapacitors. Two electrode are in an electrolyte, and separated by a separator. Due high corrosion resistivity of the carbon materials many different electrolytes like: acid, strong bases or neutral solutions could be used.
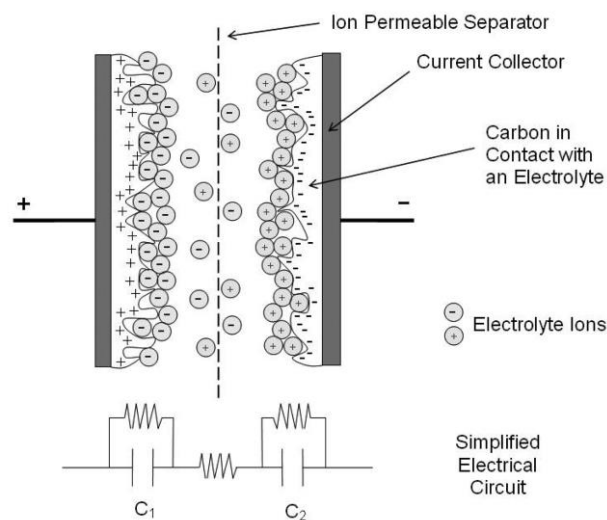
Figure 2.6. Representation of a charged electrochemical double layer capacitor [40].

In Fig. 2.7a the typical rectangular shape cyclic voltammogram recorded for a symmetric carbon/carbon electrochemical capacitor in 1 M H_2SO_4 electrolyte is shown [41]. The galvanostatic charge/discharge profile of the cell is nearly triangular with a Coulombic efficiency of over 97%, as can be seen in Fig 2.7b. The shape of the galvanostatic charge/discharge profile for each individual electrode is also nearly triangular, as can be seen in Fig. 2.7c.
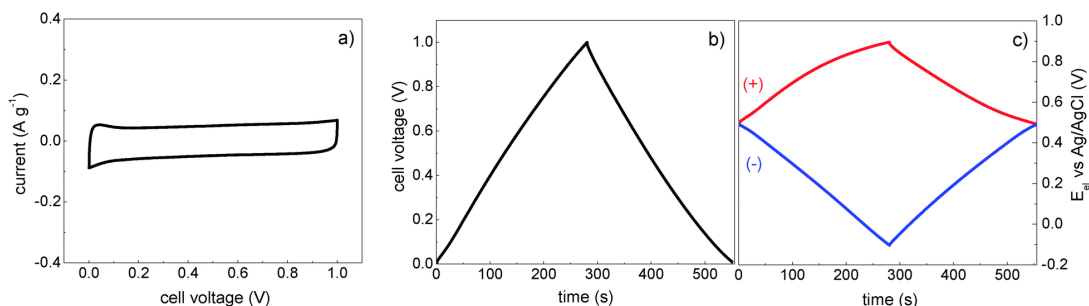
Figure 2.7. Cyclic voltammogram (a), galvanostatic charge/discharge profiles for the cell (b, left axis) and separately for positive and negative electrodes (c, right axis) of a symmetric carbon/carbon electrochemical capacitor with 1 M H_2SO_4 electrolyte, at current density of 90 mA g^{-1}. [41]

Different forms of carbon materials that can be used to store charge in EDLC electrodes are: activated carbons, carbon aerogels, carbon nanotubes, carbon fibers, graphite and graphene as well as their functionalized, oxidized and reduced forms [40]. The capacitive properties of different carbon materials are given in Table 2.2. [42, 43].

Table 2.2. The capacitive performance for carbon electrodes [42, 43]

Materials	Specific surface area, m^2 g^{-1}	Density g cm^{-3}	Capacitance F g^{-1}	Capacitance F cm^{-3}
Activated carbon	1000-3500	0.4 - 0.7	< 200	< 80
Functionalized porous carbon	300-2200	05 - 0.9	150 - 300	< 180
Carbon nanotubes (CNT's)	150 - 200	0.6	50 - 100	< 60
Carbon cloth	2500	0.4	100-200	40-80
Activated carbon fibers (ACF)	1000-3000	0.3-0.8	120 - 370	< 150
Carbon aerogels	400-1000	0.1-0.7	100-125	< 80
Graphene	900	0.1 - 2.0 mg cm^{-2}	100-120	-

Activated carbons are made from many different materials like coconut shell, peat, hard and soft wood, lignite coal, bituminous coal, olive pits and various carbonaceous specialty materials [43]. Activated carbon with highly porous adsorptive medium that has a complex structure composed primarily of carbon atoms. The networks of pores in the activated carbons are channels created within a rigid skeleton of disordered layers of carbon atoms, linked together by chemical bonds, stacked unevenly, creating a highly porous structure of nooks, crannies, cracks and crevices between the carbon layers, as can be seen in Fig. 2.8. The active carbons possess macro, mezzo and micro porosity.

Figure 2.8. SEM images of an activated carbon materials [43].

Carbon nanotubes. A significant nanoparticle discovery that came to light in 1991 by Japanese researcher Sumio Iijima [44] was carbon nanotubes (CNT's). Where buck-balls are round and nanotubes are cylinders [45]. Carbon nanotubes are composed of carbon atoms linked in hexagonal shapes, with each carbon atom covalently bonded to three other carbon atoms. Carbon nanotubes have diameters as small as 1 nm and lengths up to several centimeters. Although, like buck-balls, carbon nanotubes are strong, and they are not brittle. Carbon nanotubes that have only one cylinder are called single-walled carbon nanotubes (SWCTs) with diameters ranging from 0.5 to 1.5 nm and lengths ranging from 100 nm up to several micrometers, Fig. 2.9. Carbon nanotubes can occur as multiple concentric cylinders of carbon atoms, called multi-walled carbon nanotubes (MWCTs), Fig. 2.9 [45]. SWCNT is formed by only one rolled-up graphene sheet, while MWCNT is composed of more than one rolled-up concentric graphene sheet having larger diameters (more than 100 nm) and lengths ranging from 0.1 to 50 µm. [44].
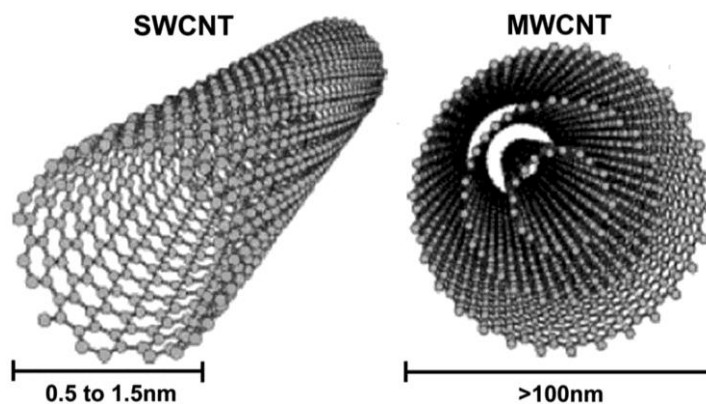
Figure 2.9. Schematic representation of single-walled carbon nanotubes (SWCNT) and multi-walled carbon nanotubes (MWCNT). [45]

Graphene. is an allotrope of carbon in the form of a two-dimensional, atomic-scale, honey-comb lattice in which one atom forms each vertex, Fig 2.10a [46].The material was rediscovered, isolated from graphite and characterized in 2004 by Andre Geim and Konstantin Novoselov at the University of Manchester [47].
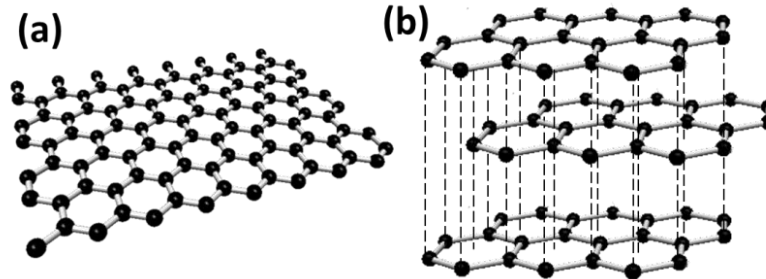
Figure 2.10. a) Graphene is a single layer honeycomb lattice of carbon atoms. b) Graphite viewed as a stack of graphene layers [46].

2.4.2. Symmetric pseudo-supercapacitors

Symmetric supercapacitors based on pseudocapacitive materials, are the similar constructions as the ECDL supercapacitors, Fig. 2.6, but use different metal oxides or conducting polymers for both electrodes. There is a numerous materials which shows pseudo-supercapacitive properties, with high variation in specific capacitance as can be seen in Fig. 2.11 [42].
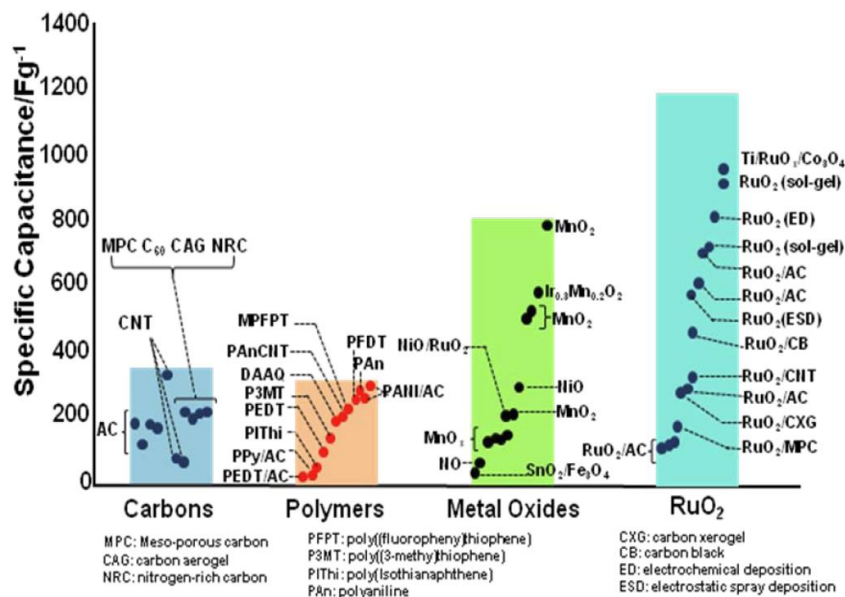
Figure 2.11. Comparisons of the capacitive performance for carbon and pseudocapacitor electrode materials [42].

The charge-storage mechanism of metal based pseudocapacitive materials (e.g. RuO_2, MnO_2, NiO, Co_2O_3, Fe_2O_3 etc. [48]) are based on surface adsorption of electrolyte cations C^+ (K^+, Na^+, Li^+…) as well as proton incorporation according to the reactions for example MnO_2 [49]:

$$MnO_2 + xC^+ + yH^+ + (x+y)e^- \rightleftarrows MnOOC_xH_y \qquad (2.8)$$

or for RuO_2 [50]

$$RuO_a(OH)_b + \delta H^+ + \delta e^- \rightleftarrows RuO_{a-\delta}(OH)_{b+\delta} \qquad (2.9)$$
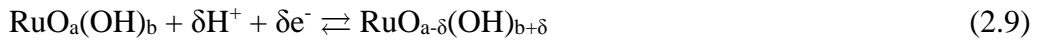
Figure 2.12 shows a typical cyclic voltammogram of MnO_2 electrode in neutral aqueous electrolyte. The fast, reversible successive surface redox reactions define the behavior of the voltammogram, whose shape is close to that of the EDLC [49].
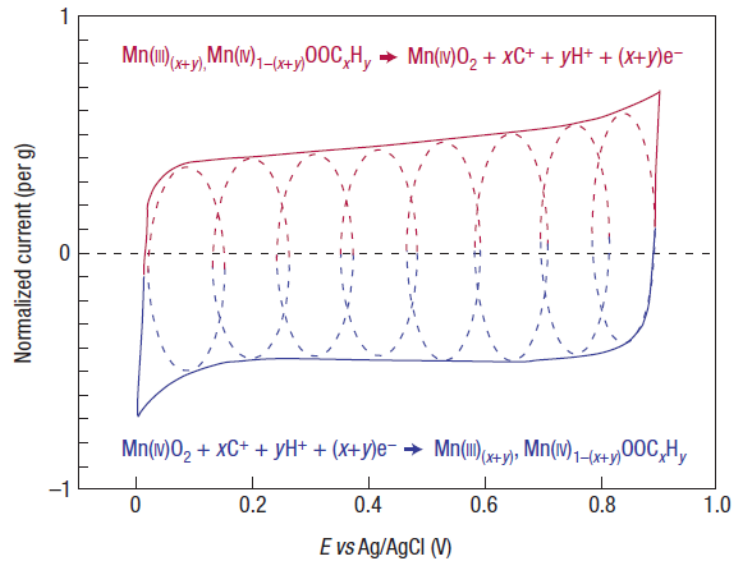
Figure 2.12. Cyclic voltammetry of MnO_2 electrode in 0.1 M K_2SO_4, shows the successive multiple surface redox reactions leading to the pseudo-capacitive charge storage mechanism. The upper part is related to the oxidation from Mn(III) to Mn(IV) and the lower part refers to the reduction from Mn(IV) to Mn(III) [49].

17

Hydrous ruthenium dioxide is one of the best and most investigated pseudocapacitive materials. In acidic or neutral solution voltage window is almost 2 V. Xai et al. [51] investigated symmetrical supercapacitors based on two identical RuO_2 electrode in 1 M Na_2SO_4. In Fig. 2.13 the cyclic voltammogram of positive and negative electrode for different ending potentials is shown.
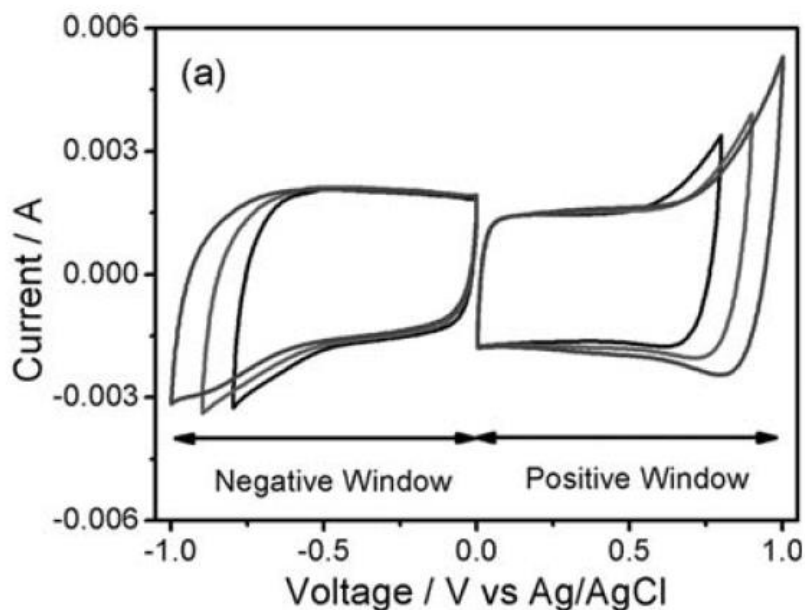
Figure 2.13. CVs of RuO_2 electrode in various positive and negative windows in 1 M Na_2SO_4 [51].

The CVs of the symmetric RuO_2/RuO_2 supercapacitor between 0 and 1.6 V at different scan rates from 20 to 200 mV s^{-1} is shown in Fig. 2.14a. The shape of the voltammograms are similar to ECDL capacitors. The galvanostatic charge/discharge curves at different current densities, Fig. 2.14b, shows practically ideal triangular shape. The specific capacitance was in the range of 50-40 F g^{-1}, specific energy 19-15 Wh kg^{-1} with corresponding power in the range of 1000 to 10.000 W kg^{-1}, Fig. 2.14c. The cycle performance is investigated in the voltage window between 0 and 1.6 V at a current density of 2.5 A g^{-1}, showing some deterioration characteristics after 2000 cycles, Fig. 2.14d. Unfortunately, very promising results of the symmetric metallic compounds based pseudocapacitors, have huge drawback, very high price of ruthenium based

compounds, relatively small energy density, and deterioration of the characteristics of other compounds due irreversible crystal structures changes during cyclization [51].
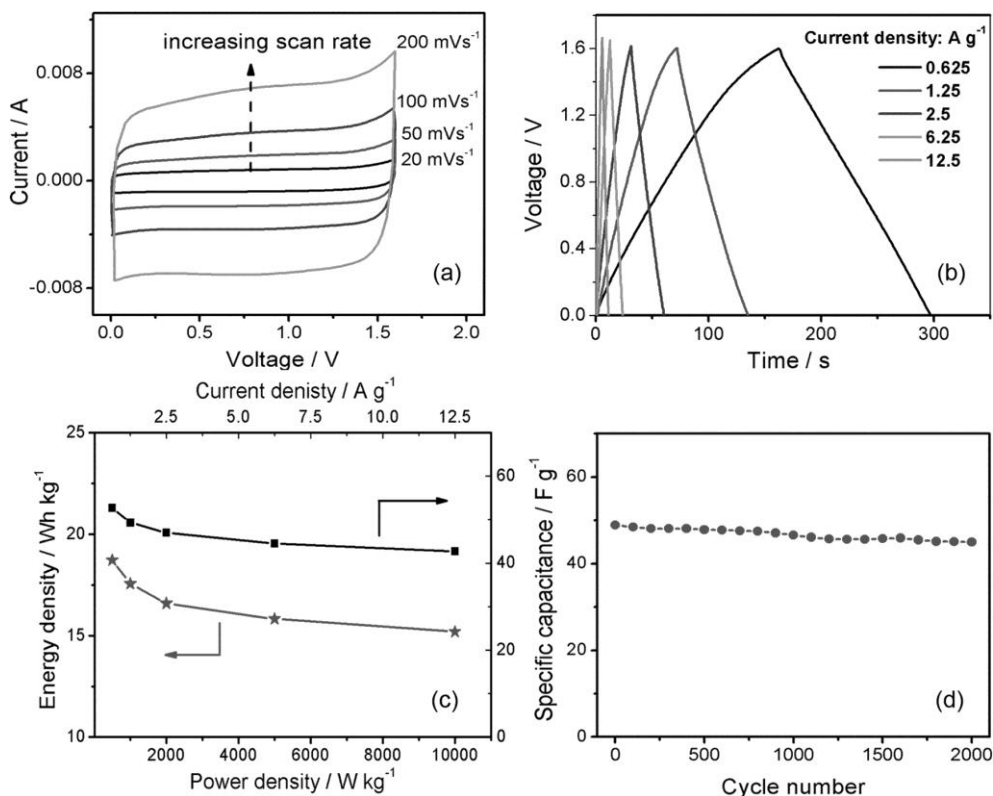
Figure 2.14. (a) The CVs of the symmetric RuO_2/RuO_2 super-pseudocapacitors (b) The galvanostatic charge/discharge curves of the symmetric supercapacitor at different current densities. (c) The specific capacitance of the symmetric supercapacitor as a function of current density and the Ragone plot of the full cell. (d) The cycle performance of the symmetric supercapacitor in the voltage window between 0 and 1.6 V at a current density of 2.5 A g^{-1} [51].

Second representatives of pseudocapacitive materials are conducting polymers or organic metals [52]. Their conductivity is connected with existence of conjugation over large length of polymer chain, in which polymer units are repeated. Conducting polymers have backbones of contiguous sp2 hybridized carbon centers. One valence electron on each center resides in a pz orbital, which is orthogonal to the other three sigma-bonds. All the pz orbitals combine with each other to a molecule wide delocalized set of orbitals. The electrons in these delocalized orbitals have high mobility

when the material is "doped" by oxidation, which removes some of these delocalized electrons. Thus, the conjugated p-orbitals form a one-dimensional electronic band, and the electrons within this band become mobile when it is partially emptied [53]. Oxidation (doping) or reduction (dedoping) is an electrochemical reaction involving anions (p-doping) or cations (n-doping), as shown in Fig. 2.15 [54].
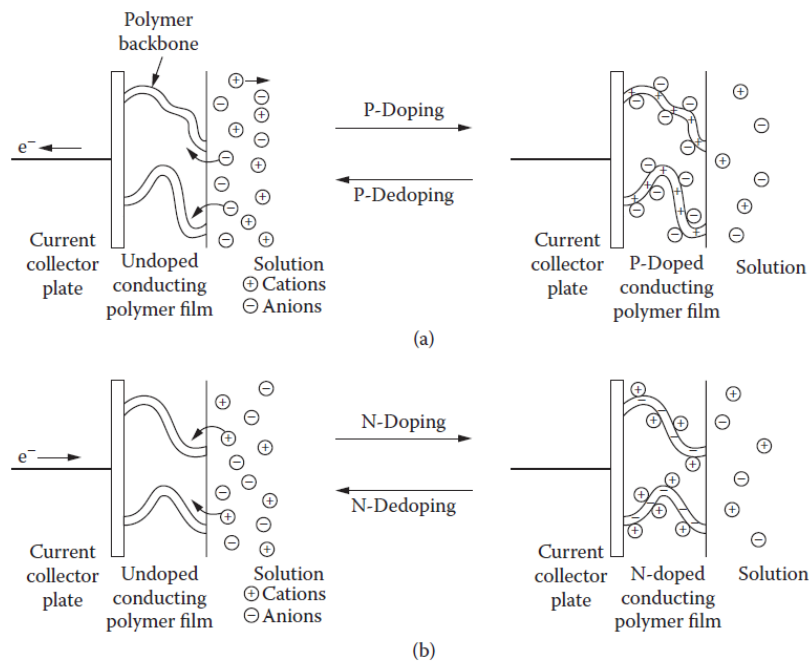
Figure 2.15. The *p*-doping (a) and *n*-doping (b) of polymers as they undergo charging and discharging [54].

The doping-dedoping reaction, Fig. 2.16, involve certain numbers of anions per polymer units, which usually contain tree or four monomer units. The number of anions per polymer units is called doping degree, *y*. Hence if polymer units contains three monomer units, and in doped state with one anions, the doping degree is $y = 0.33$.
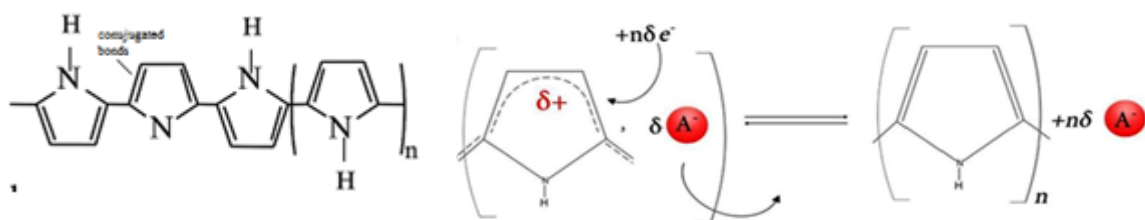
Figure 2.16. Polypyrrole structural formula (left) and dedoping reaction (right).

There is a numerous different conducting polymers [17], but the most investigates are polyaniline (PANI), polypyrrole (PPy), polythiophene (PTh) and poly(3,4-ethylenedioxythiophene) (PEDOT), which structures are shown in Fig. 2.17 [55].
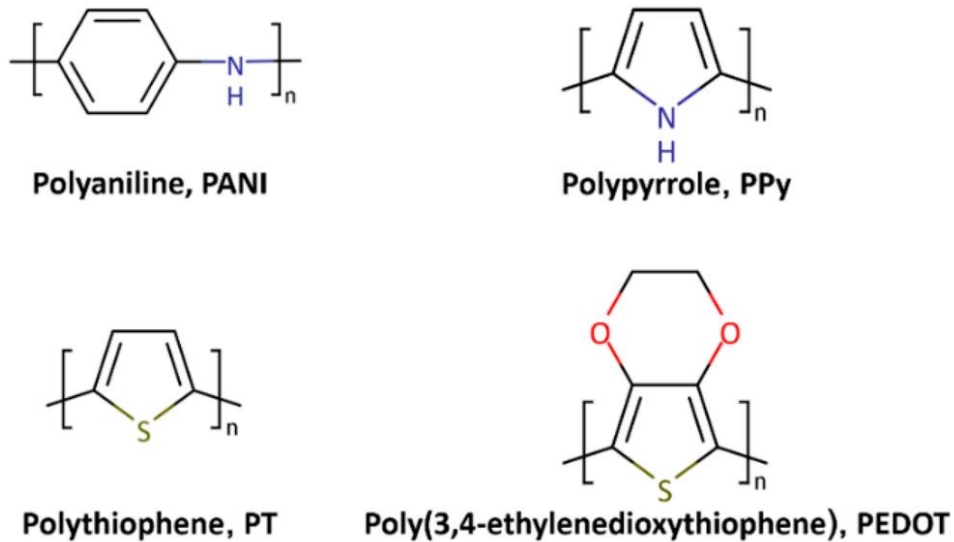
Figure 2.17. Chemical structures of the most representative conducting polymers [55].

Some of the typical characteristics of common conducting polymers are given in Table 2.3 [22].

Table 2.3. Characteristics of most common conducting polymers [22].

ICP's	M (monomer) g mol^{-1}	Doping level y	$C_{theoretical}$ F g^{-1}	C_{exp} F g^{-1}
PANI	93	0.5	750	240
PPy	67	0.33	620	530
PTh	84	0.33	485	-
PEDOT	142	0.33	210	92

Wu et a. [27] examined the behavior of polypyrrole film and nanowires (with an average diameter of 30 to 50 nm) in 1 M KCl for use as supercapacitors electrodes. Figure 2.18 shows the cyclic voltammograms of the electrodes, from which is seen that the nanowires have an increased capacity as compared to the film electrode.
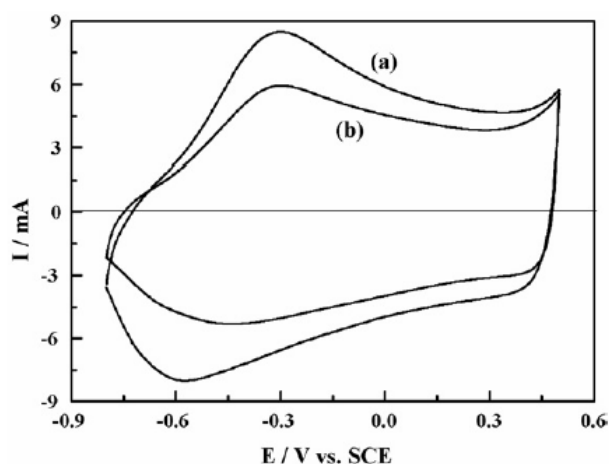
Figure 2.18. Cyclic voltamograms (10 mVs^{-1}): (a) of PPy nanowires and
(b) PPy film ($m = 3$ mg) [27].

Figure 2.19 shows the charging and discharging curve of the electrode at different currents, from which can be see that PPy in the form of nanowires have a somewhat longer charge and discharge time of than the film electrode.
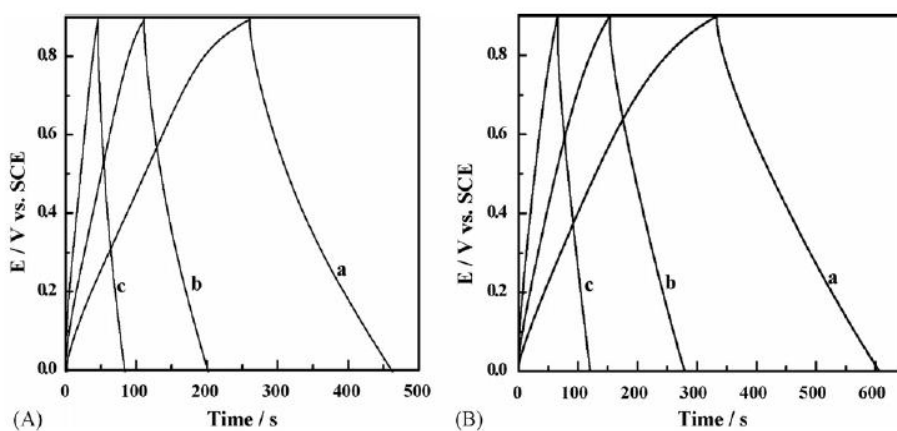
Figure 2.19. Typical charge and discharge curves of of the electrodes (a) PPy nanowires and (b) the PPy film ($m = 3$ mg), at different currents:
(a) 1.5 mA, (b) 3 mA, i (c) 6 mA [27].

Comparing the characteristics of the film electrode and the electrode of the nanowires, Table 2.4, it can be seen that PPy nanowires generate capacitance of 282 F g^{-1} and specific energy of 31.8 Wh kg^{-1} at a specific current of 1 A g^{-1} that is about 30% more than in the film electrode, which is discussed more development areas of the nanowires.

Table 2.4. Comparison of capacitance and specific energy of PPy film electrode and PPy nanowires at different specific currents [27].

I / A g⁻¹	C / F g⁻¹		w / Wh kg⁻¹	
	PPy$_F$	PPy$_{nw}$	PPy$_F$	PPy$_{nw}$
0.5	223	305	25.1	34.3
1.0	204	282	23.0	31.8
2.0	169	254	19.0	28.6

Wang et al. [56] investigated PPy nanotubes and granules in 1 M KCl, with the accent on NT's. Figure 2.20 shows the cyclic voltammograms of PPy nanotubes at different scan rates. The rectangular and symmetrical profiles of cyclic voltammograms indicated nearly ideal pseudocapacitive nature of PPy in KCl electrolyte. Authors noted the PPy nanotubes have higher current density than those of PPy granules at the same scan rate, indicating a much larger specific capacitance of PPy nanotubes. The galvanostatic charge–dischare curves of PPy nanotubes, Fig. 2.20b, and PPy granules, Fig. 2.20c, at different applied current densities confirm the good pseudocapacitive behavior. The specific capacitance obtained from discharging curves shows that nanotubes possess almost double capacitance, Fig. 2.20d.
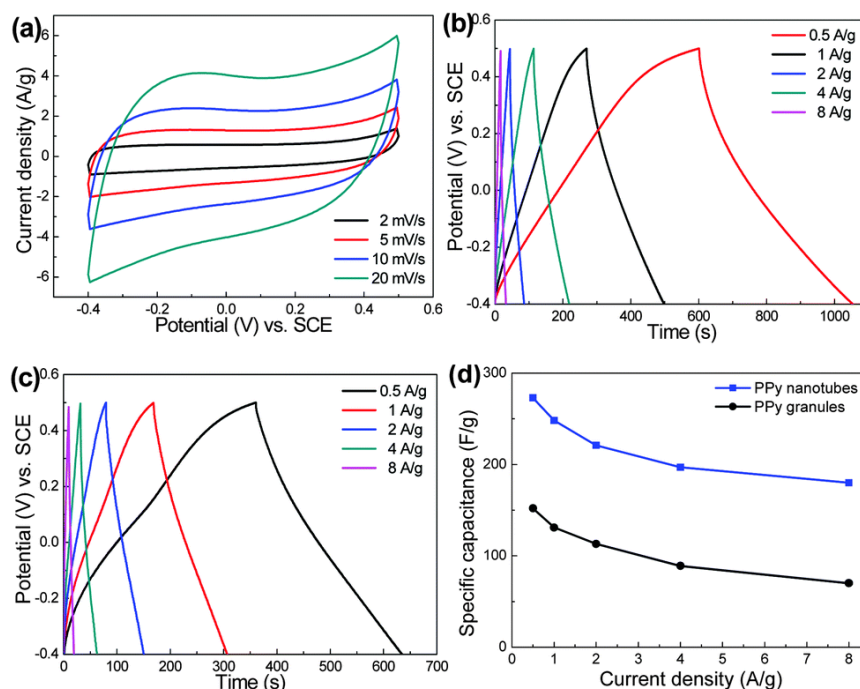
Figure 2.20. (a) CV curves of PPy nanotubes; galvanostatic charge–discharge plots of (b) PPy nanotubes and (c) PPy granules; (d) specific capacitance as a function of current density [56].

Mu et al. [57] investigated chemically synthetized polyaniline using D-tartaric acid (D-TA) as a dopant anion. They investigated PANI powder attached to glassy carbon electrode by Nafion, in 1 M H_2SO_4, using the cyclic voltammetry, Fig. 2.21a, and charge-discharge at constant current, Fig 2.21b. In the current density range from 1 to 10 A g^{-1}, specific capacitance decreases from 620 to 500 F g^{-1}, Fig. 2.21c. Specific energy was in the range of 55 to 45 Wh kg^{-1} with the corresponding specific power in the range of ~100 up to 4000 W kg^{-1}. It should be mentioned that Authors investigated behavior in both oxidation PANI states emeraldine and perningraniline, so fast deterioration of the characteristics was observed, ~30% after 500 cycles, Fig. 2.21d.
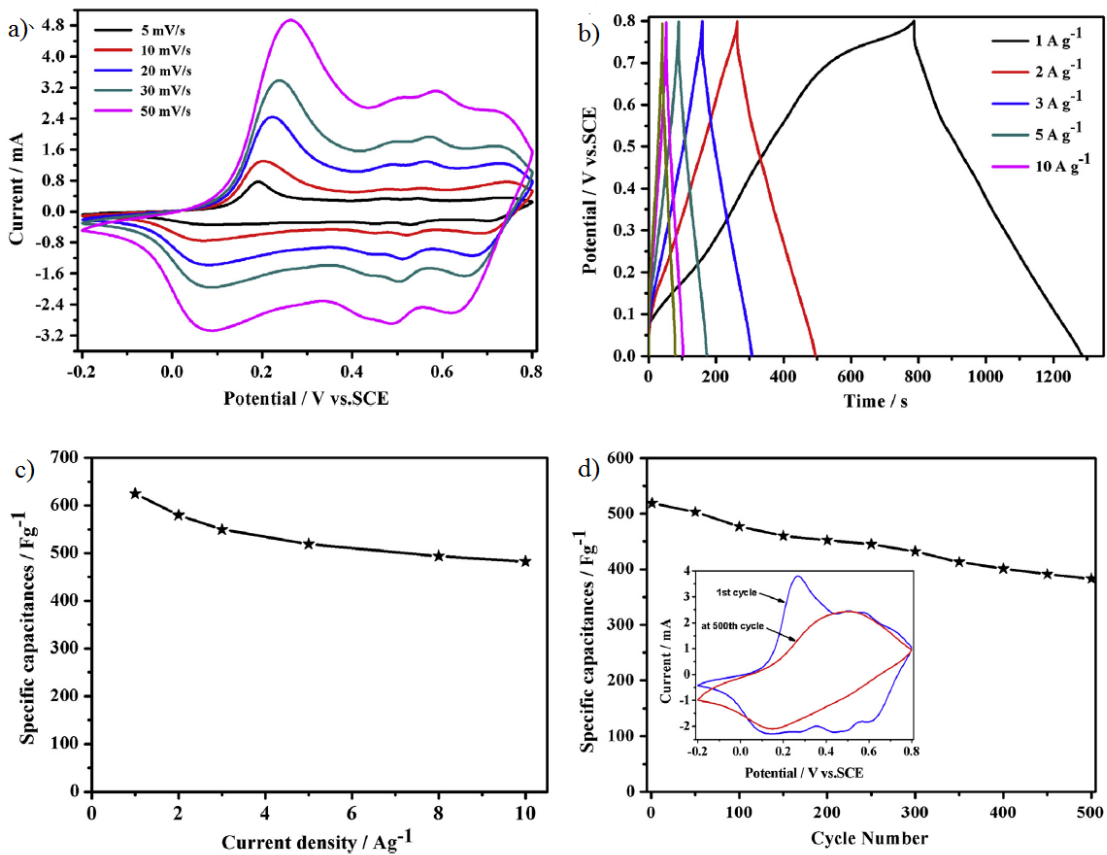
Figure. 2.21. a) CV curves of PANI-(D-TA) nanotubes electrodes with the [D-TA]/[An] ratio of 1:1 at various scan rates in 1 M H_2SO_4. b) Galvanostatic charge/discharge curves of PANI-(D-TA) electrodes at various current densities; (c) discharge capacitances at various current densities in 1 M H_2SO_4. Variations of the specific capacitances of PANI-(D-TA) electrodes as a function of cycle number measured at a scan rate of 50 mV s^{-1} and (inset) CV curves of PANI-(D-TA) at the first and 500th cycle. (Adopted from ref. [57]).

Symmetric conducting polymer pseudocapacitors are rarely investigated, mainly due to the small voltage windows. On such example is reported by Chen et al. [58] who investigated symmetric pseudocapacitors based on polyaniline nanofibers (NF) and nanotubes (NT) in 1 M H_2SO_4. The characterization of such device using different electrochemical techniques are shown in Fig. 2.22a)-f). Figures 2.22a and b show the cyclic voltammetry and galvanostatic charge – discharge curves of PANI-NT's pseudocapacitors. The operating voltage range is limited to 0.7 V. The cyclic voltammogram tests demonstrate that some redox reactions occur during the charge and discharge process. A pair of redox peaks that appears during the charge and discharge process for different scan rates are resulted from Faradaic transformation of the emeraldine–pernigraniline form of polyaniline. Specific capacitance of PANI-NT's are in the range of 500 F g^{-1} while for PANI-NFs around 400 F g^{-1}, Fig. 2.22c. From Fig. 2.22e it can be seen that NT's shows some improvement in characteristics, with estimated energy density of 25 Wh kg^{-1}, and specific power of ~3.6 kW kg^{-1} at current of 5 A g^{-1}.
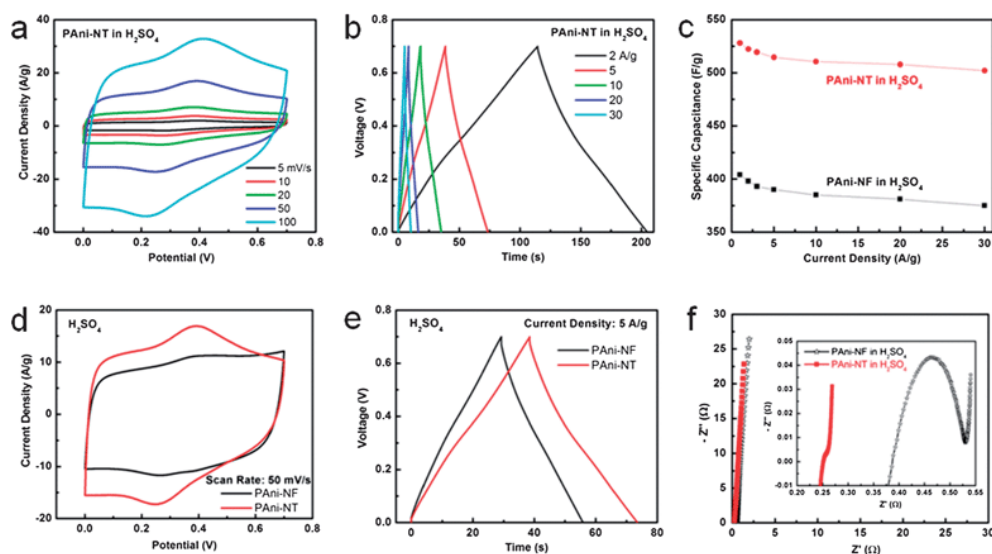
Figure 2.22. Electrochemical performance of PANI pseudocapacitors in acidic aqueous electrolytes (1 M H_2SO_4). (a) Cyclic voltammograms of PANI-NT pseudocapacitors at different scan rates. (b) Galvanostatic charge–discharge curves of PANI-NT pseudocapacitors at different current densities. (c) Specific capacitance vs. current density for PANI-NF and PANI-NT pseudocapacitors. Comparison of (d) cyclic voltammetry, (e) galvanostatic charge–discharge, and (f) electrochemical impedance spectroscopy curves of PANI-NT and PANI-NF [58].

Recently, Wang et al. [59] reported a facile approach in fabrication of the mesoporous PANI film on ultra-thin graphene nanosheet (G-mPANI) hybrid by in situ polymerization using graphene-mesoporous silica composite as template, which cyclic voltammograms and charge-discharge curves are shown in Fig. 2.23a-b. Owing its mesoporous structure, over all conductive network, G-mPANI electrode displays a specific capacitance of 749 F g^{-1} at 0.5 A g^{-1} with excellent rate capability, remains 73% even at 5.0 A g^{-1}, much higher than that of pristine PANI electrode, 315 F g^{-1} at 0.5 A g^{-1}, 39% retention at 5.0 A g^{-1} in 1 mol L^{-1} H$_2$SO$_4$ aqueous solution. More interestingly, the G-mPANI hybrid can maintain 88% of its initial capacitance compared to 45% for pristine PANI after 1000 cycles, suggesting a superior electrochemical cyclic stability. They also reported capacitance and Ragone plot for symmetric device, Fig. 2.23c and d.
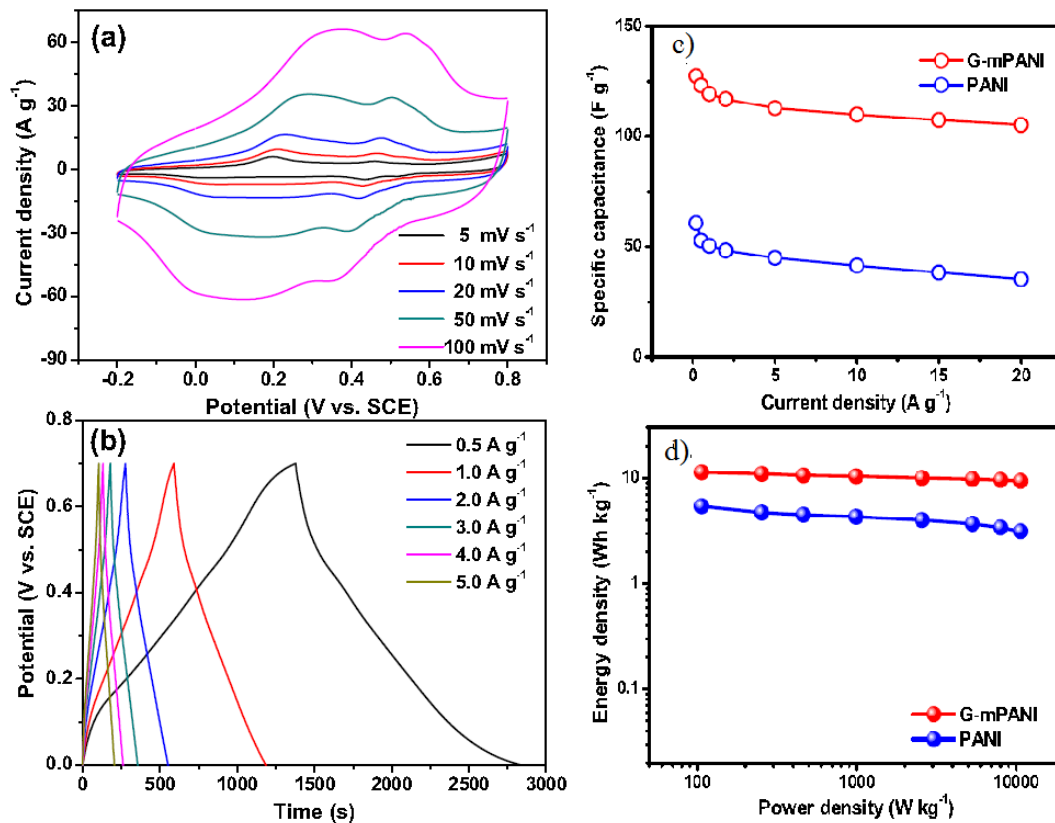
Figure 2.23. (a) CV curves of the as-prepared G-mPANI electrode at different scan rates from 5 to 100 mV s^{-1}. (b) Galvanostatic charge-discharge curves of G-mPANI electrode. (c) Specific capacitance at different current densities and (d) Ragone plots of PANI- and G-mPANI-based symmetric supercapacitors measured in 1.0 mol L^{-1} H$_2$SO$_4$ aqueous electrolyte [59].

The performance of some symmetric and asymmetric supercapacitors based on different materials with pseudocapacitive properties such as several conducting polymers (ICPs) and amorphous manganese dioxide (α-MnO_2) is reported by Khomenko et al. [60], and shown in Table 2.4. Even the obtained maximum power density is in reasonable range, it is obvious that symmetric devices suffers from low energy contents. Improvement in energy is visible for the asymmetric configurations.

Table 2.4. Electrochemical characteristics of symmetric and asymmetric capacitors based on different active materials, adopted from Ref. [60].

Positive materials	Negative materials	U	w	P_{max}	ESR
		V	Wh kg^{-1}	kW kg^{-1}	Ω cm^{-2}
PANI	PANI	0.5	3.13	10.9	0.36
PPy	PPy	0.6	2.3	19.7	0.32
PEDOT	PEDOT	0.6	1.13	23.8	0.27
MnO_2	MnO_2	0.6	1.88	3.8	1.56
MnO_2	PANI	1.2	5.86	42.1	0.57
MnO_2	PPy	1.4	7.37	62.8	0.52
MnO_2	PEDOT	1.8	13.5	120.1	0.48

2.4.3. Hybrid supercapacitors

Hybrid supercapacitors attempt to exploit the relative advantages and mitigate the relative disadvantages of EDLCs and pseudocapacitors to realize better performance characteristics. Utilizing both Faradaic and non-Faradaic processes to store charge, hybrid capacitors have achieved energy and power densities greater than EDLCs without the sacrifices in cycling stability and affordability that have limited the success of pseudocapacitors. Research has focused on three different types of hybrid capacitors, distinguished by their electrode configuration [30]:

- **Asymmetric,**
- **Composite,**
- **Battery-type.**

2.4.3.1. Asymmetric supercapacitors

Asymmetric hybrids combine Faradaic and non-Faradaic processes by coupling an EDLC electrode with a pseudocapacitive electrode [3, 30]. In principle, as a negative electrode usually carbon based material is used, and as a positive some pseudocapacitive materials, as shown in Fig. 2.24 [61].
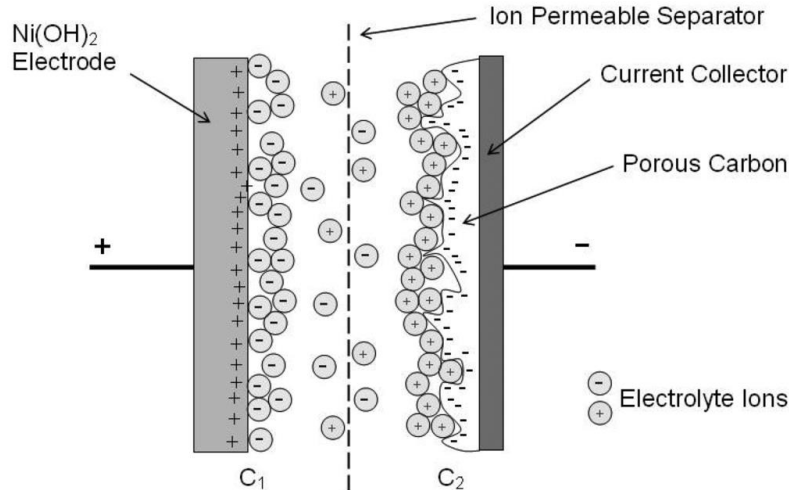
Figure 2.24. Schematic of an Ni(OH)$_2$/NiOOH–porous carbon asymmetric supercapacitor [61].

The combination of an negative carbon electrode with a conducting polymer or metal oxide positive electrode received a great deal of attention [62,63,64,65]. Asymmetric hybrid capacitors that couple these two electrodes reduce the extent of this trade-off to achieve higher energy and power densities than comparable EDLCs. Also, they have better cycling stability than comparable symmetric pseudocapacitors [30].

For example, Park and Park [65] investigated activated carbon (AC)-polyaniline, hybrid asymmetric electrochemical capacitor in 6 M KOH. The capacitor is prepared by using polyaniline as a positive electrode and activated carbon as a negative electrode, which cyclic voltammograms are shown in Fig. 2.25a and b. From a constant current charge–discharge test, a specific capacitance of 380 F g^{-1} is obtained, Fig. 2.25c. The cycling behavior of the hybrid electrochemical capacitor is examined in a two-electrode cell by means of cyclic voltammetry, achieving the cycle-life of 4000 cycles. Values for the specific energy of 18 Wh kg^{-1}, independent on power, and specific power in the

range of 20 to 1250 W kg^{-1}, Fig. 2.25d, are obtained for a cell voltage between 1 and 1.6 V.
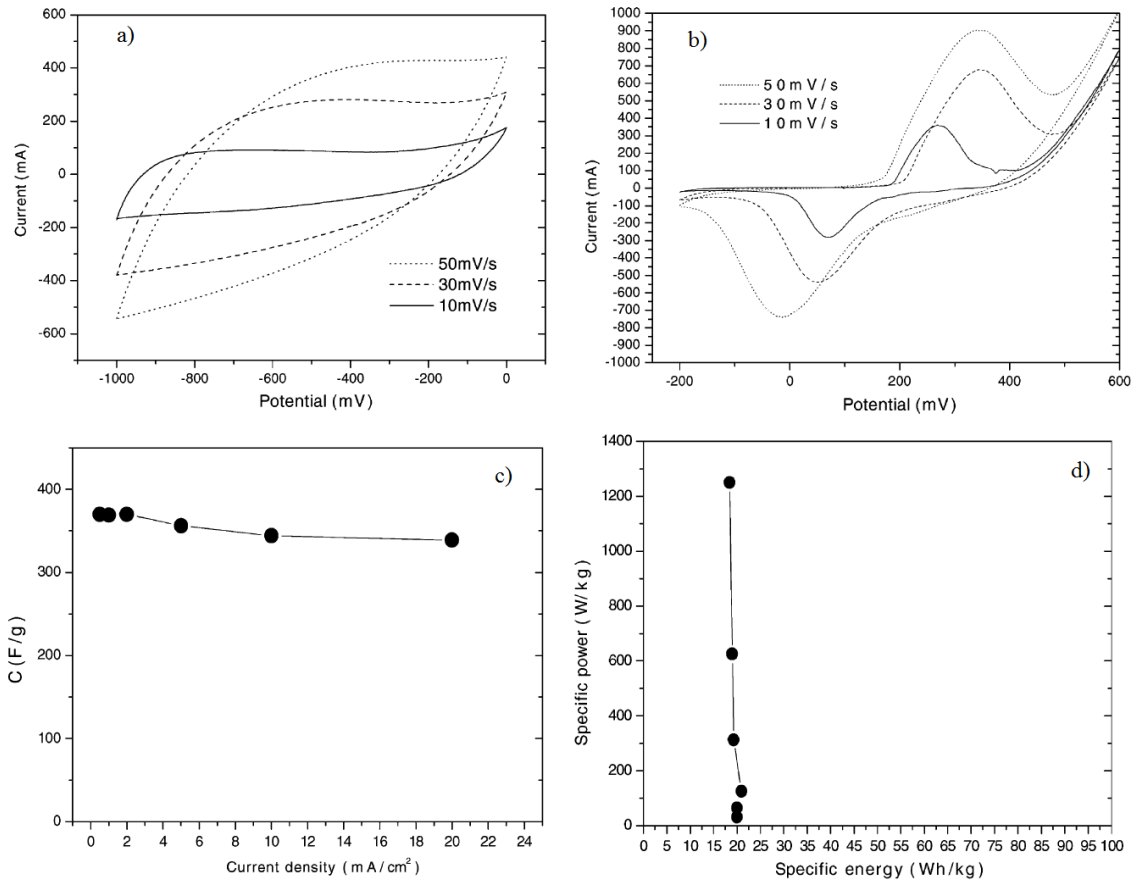
Figure 2.25. Cyclic voltammogram for (a) AC electrode and (b) PANI electrode at various potential sweep rates c) Specific capacitances of PANI–AC hybrid EC capacitor as function of charge–discharge current density, d) Ragone plot of PANI–AC hybrid EC capacitor, adopted from ref [65].

Zhou et al. [66] investigated the hierarchical CoMoO$_4$/Co$_3$O$_4$ nano-composite, obtained using one-pot hydro-thermal method. In combination with activated carbon in the asymmetric supercapacitor in 3 M KOH aqueous solution as the electrolyte, an energy density of 31 Wh kg^{-1} is achieved at a power density of 7270 W kg^{-1}. The characteristics cyclic voltammograms of each electrode and the cell are shown in Fig. 2.26a and b, while charge-discharge curve in Fig. 2.26c. From the life cycle test, it can be seen that no deterioration of the characteristics occurred over a 2000 cycles, Fig. 2.26d.
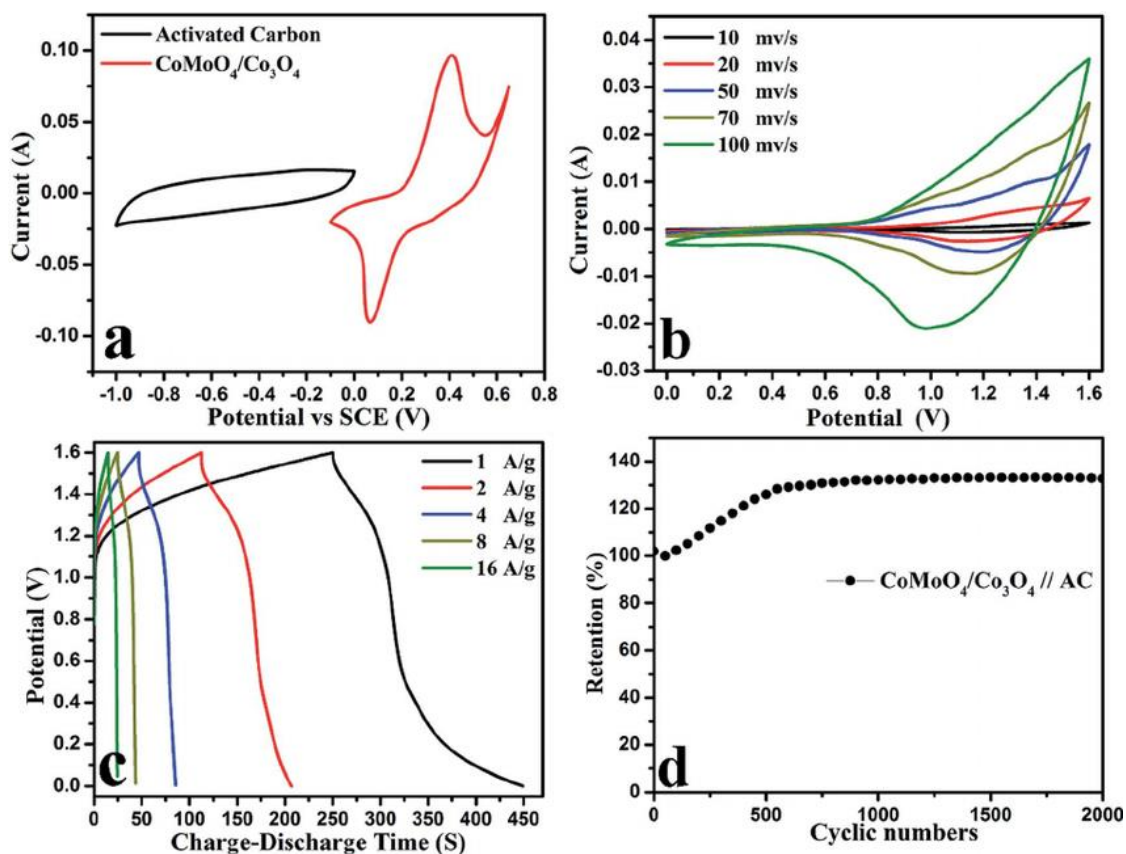
Figure 2.26. Electrochemical measurements of the asymmetric supercapacitor. Cyclic voltammetry (CV) curves of the $CoMoO_4/Co_3O_4$ and active carbon as working electrodes in three-electrode system (a), cyclic voltammetry (CV) curves of the asymmetric supercapacitor at various scan rates (b), galvanostatic charge – discharge (GCD) curves of the asymmetric supercapacitor at different current densities (c), and cyclic performance of the asymmetric supercapacitor (d) [66].

In Tables 2.5 and 2.6, the summary of the asymmetric hybrid supercapacitors using an electrode based on activated carbon (AC) and manganese oxide in an aqueous electrolyte (adopted from ref. [62]), are given, *it should be noted that values are given for device (packing factor 1/3), so for the active masses based values should be multiplied by 3* [62]. It can be seen that no significant improvement is achieved over ten year's period. Maximum specific energy is smaller than ~10 Wh kg^{-1} of device with power in the range of 1 to 10 kW kg^{-1}.

Table 2.5. Summary of the asymmetric hybrid using an electrode based on activated carbon (AC) and manganese oxide in an aqueous electrolyte [adopted from ref. 62]

	Positive electrode	Electrolyte	U, V	w^a Wh kg^{-1}	P^a kW kg^{-1}	C.L^b	Year
AC	Amorphous MnO_2	KCl/H_2O	2.0	9.6	2.7c	–	2002
AC	Amorphous MnO_2	K_2SO_4/H_2O	2.2	6.3	3.6		2004
AC	Amorphous MnO_2	KNO_3/H_2O	2.0	7.0	4.1	–	2006
AC	MnO_2	KOH/H_2O	1.5	5.2d	–	+	2006
AC	Amorphous MnO_2	K_2SO_4/H_2O	2.2	5.8	6.3	+	2006
AC	MnO_2	K_2SO_4/H_2O	2.2	5.2d	–	+	2006
AC	Amorphous MnO_2	K_2SO_4/ H_2O	2.0	3.3	5.6	+	2007
AC	MnO_2 nanorods	Na_2SO_4 or K_2SO_4/H_2O	1.8	5.7	0.7c	+	2009
AC	Mesoporous MnO_2	KOH/H_2O	1.8	10.4	0.130c	+	2009
AC	Nano-struct. MnO_2	$K_2SO_4/H2O$	1.8	5.7	0.670c	+	2009
AC	$NaMnO_2$	Na_2SO_4/H_2O	1.9	6.5	–	+	2009
AC	MnO_2	Neutral electrolyte	2.0	5.4d	–	+	2010
AC	MnO_2	$(NH_4)_2SO_4/H_2O$	1.0	7.4d	–	–	2010
AC	MnO_2	$LiOH /H_2O$	1.8	6.8d	0.3d	+	2010
AC	K-doped MnO_2	K_2SO_4/H_2O	1.8	5.9	0.7c	+	2010

a Values refer to the device mass. A packaging factor of 1/3 is assumed to estimate the device value whenever the values are provided for the active material mass.
b Cycling stability is reported for a minimum of 1000 cycles.
c Maximum power demonstrated.
d Estimated from the available information.

Table 2.6. Summary of the asymmetric supercapacitors using an electrode based on activated carbon (AC) and nickel oxide in an aqueous electrolyte [adopted from ref. 62]

	Positive electrode	Electrolyte	U, V	w^a Wh kg^{-1}	P^a kW kg^{-1}	C. L^b	Year
AC	Ni oxide	KOH/H_2O	1.4	4.0	2.7c-8.0d	–	1997
AC	Ni oxide	KOH/H_2O	1.5–1.6	10	3	+	1997–1999
AC	Ni oxide	KOH/H_2O	1.23	3	6	–	1999
AC	Co/Zn doped NiOOH	KOH/H_2O	1.5	4.1	–	–	2000
AC	Ni oxide	KOH/H_2O	1.3–1.4	2.8–6.2	1–1.5	+	2002
AC	$Ni(OH)_2$	KOH/H_2O	1.3	8.3	–	–	2002
AC	Ni oxide	KOH/H_2O	1.5	–	–	+	2003
AC	Ni oxide	KOH/H_2O	1.5	4.3	6.6	+	2003
AC	$Ni(OH)_2$	KOH/poly.	1.2	–	–	+	2006
AC	$Ni(OH)_2$/CNT	KOH/H_2O	1.6	8.6	0.9c	–	2006
AC	Ni	KOH/H_2O	1.0	3.9d	–	–	2006
AC	NiO	KOH/H_2O	1.0	1.6d	–	–	2006
AC	NiO	KOH/poly.	1.6	7.3	–	–	2006
AC	Co,Zn-doped $Ni(OH)_2$	KOH/H_2O	1.45	11.9	–	–	2008
AC	NiO	KOH/H_2O	1.5	3.7	10c	+	2008
AC	Porous NiO	KOH/H_2O	1.0–1.5	2.0d at 1.3 V	–	+	2008
AC	Al doped α-$Ni(OH)_2$	KOH/poly.	1.6	14	0.4c	+	2010

a Values refer to the device mass. A packaging factor of 1/3 is assumed to estimate the device value whenever the values are provided for the active material mass.
b Cycling stability is reported for a minimum of 1000 cycles.
c Maximum power demonstrated.
d Estimated from the available information.

2.4.3.2. Asymmetric composite supercapacitors

Composite electrodes integrate carbon-based materials with either conducting polymer or metal oxide materials and incorporate both physical and chemical charge storage mechanisms together in a single electrode [30]. The carbon-based materials facilitate a capacitive double-layer of charge and also provide a high-surface-area backbone that increases the contact between the deposited pseudocapacitive materials and electrolyte. The pseudocapacitive materials are able to further increase the capacitance of the composite electrode through Faradaic reactions [30]. The synergetic mechanism could improve corrosion stability, increased the specific capacitance and the operating potential windows. For example, the composite of carbon nanotubes (CTN) and polypyrrole can accumulate both anions (at anodic scan) and cations (at cathodic scan), as can be seen in Fig. 2.27b, in contrast with pure polypyrrole [67.
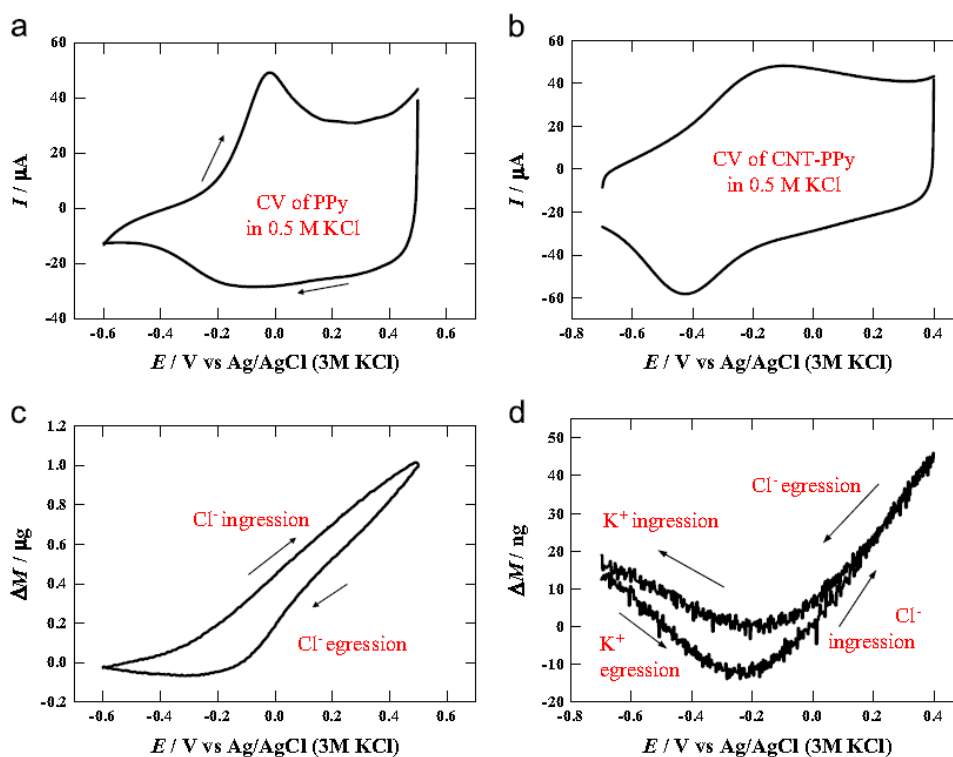
Figure 2.27. Cyclic voltammograms (a,b) and the simultaneously recorded mass changes (using quartz crystal microbalans) during the potential scan (c,d) of PPy (a,c) and CNT/PPy (b,d) films in aqueous KCl solution [67].

Improvement in capacitive behavior of multiwall carbon nanotubes modified with different mass of the PANI, is reported by Cai et al. [68]. The improvement can be clearly seen in Fig. 2.28.
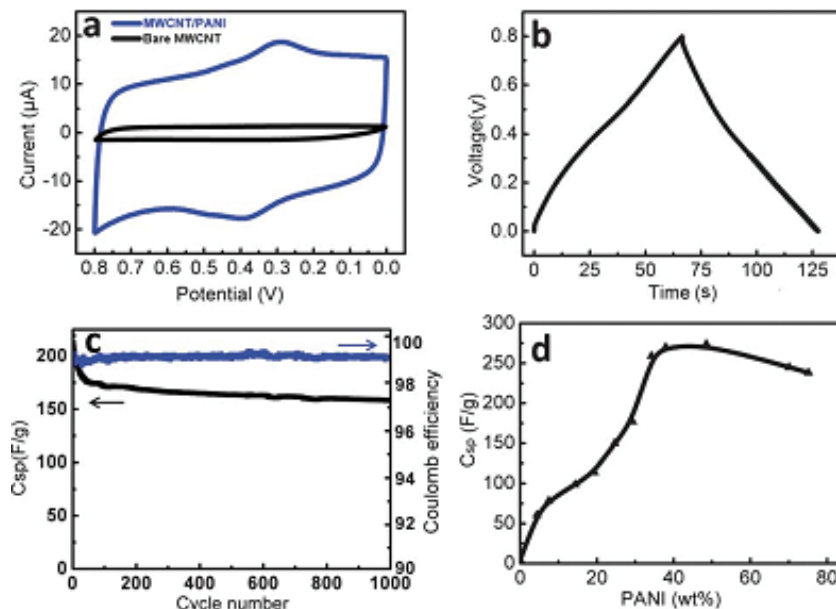
Figure 2.28. 3 Electrochemical properties of supercapacitor wires. (a) Cyclic voltammogram (10 mV s^{-1}) of a supercapacitor based on a PANI weight percentage of 24%. (b) Galvanostatic charge–discharge (2 A g^{-1}) curves of a supercapacitor based on a PANI weight percentage of 24%. (c) Dependence of specific capacitance and Coulombic efficiency on cycle number of a supercapacitor based on a PANI weight percentage of 34%. (d) Dependence of specific capacitance on the PANI weight percentage [68].

Many different materials have been investigated, mostly exotic [69,70,71,72] and very expensive (starting materials and preparation procedures) for asymmetric composite supercapacitors. For example, Deng et al. [73] investigated materials based on metal–organic frameworks-derived honeycomb-like Co_3O_4/three-dimensional graphene networks/Ni foam. Hybrid devices shows the maximum energy density of 7.5 Wh kg^{-1} with the power density of 794 W kg^{-1} and remain 4.1 Wh kg^{-1} with the power density of 15 kW kg^{-1}, with the decreases of 12% of the maximum capacitance after 2000 charge-discharge cycles. Qiu et al. [74] investigated, nickel hexacyanoferrate/hexadecyl trimethyl ammonium bromide/graphene nanocomposites synthesized by reverse microemulsion. The device shows energy density of 37 Wh kg^{-1}

but the power was only 80 W kg^{-1}. Yang et al. [75] investigated asymmetric supercapacitor based on reduced graphene oxide/multi multiwall carbon nanotube (MWCNT) and carbon fiber paper/polypyrrole electrodes, Fig. 2.29. Even with such complex structures, they obtained specific energy in the range of ~30 to 15 Wh kg^{-1} with corresponding specific power in the range of 0.7 to 7 kW kg^{-1}, Fig. 2.29f.
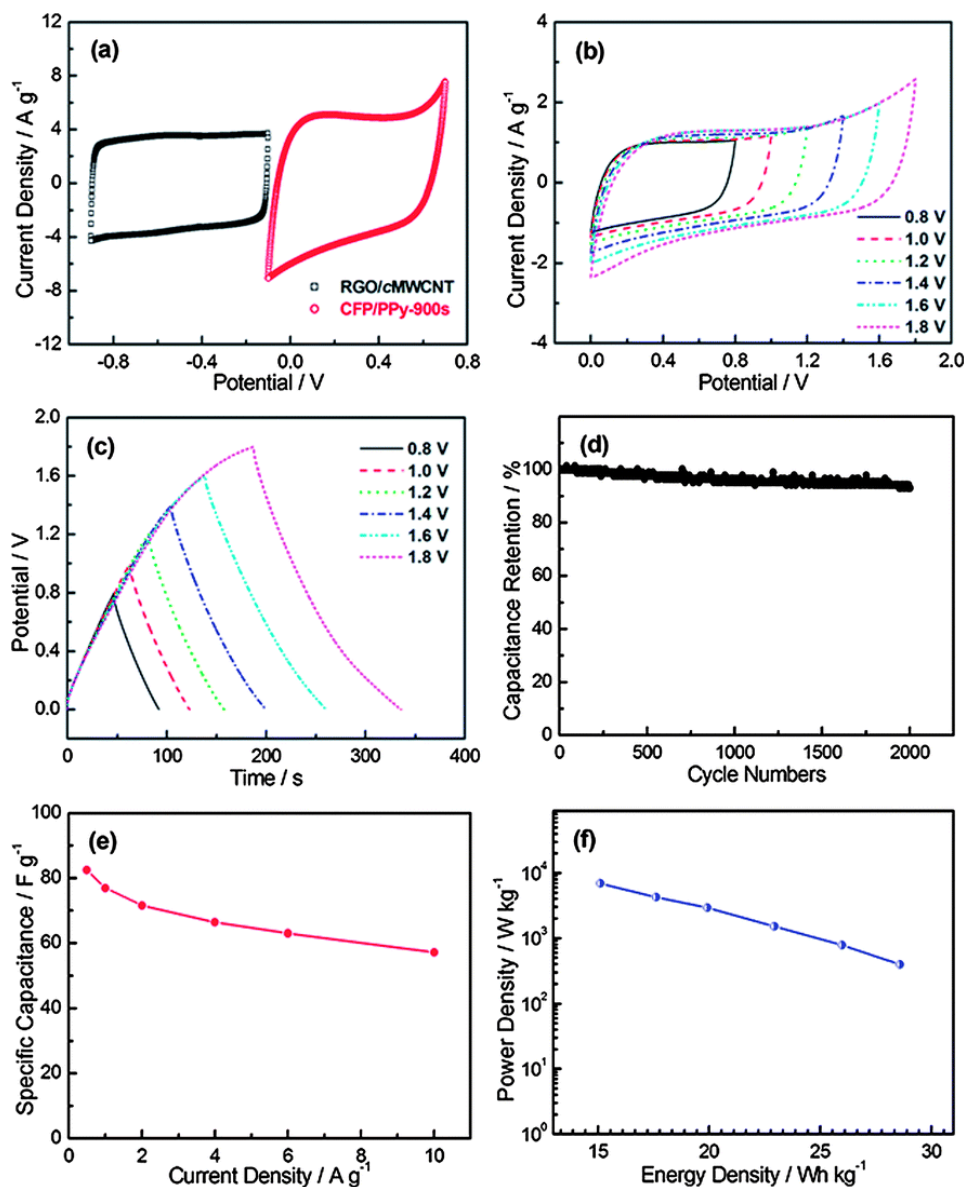
Figure 2.29. Electrochemical performance of CFP/PPy//RGO/cMWCNT asymmetric supercapacitors (a) Cyclic voltammograms of RGO/cMWCNT and CFP/PPy in three-electrode systems (20 mV s^{-1}). (b) Cyclic voltammograms at different potential windows at a scan rate of 20 mV s^{-1}. (c) Galvanostatic charge/discharge curves at different potential windows at a current density of 1 A g^{-1}. (d) Cycle performance. (e) Specific capacitance as a function of current density. (f) Ragone plot. [75].

Polypyrrole is also investigated by different Authors in hybrid-asymmetric composite supercapacitor. For examples, Song et al. [76] investigated a combination of functionalized partial-exfoliated graphite (FEG), polypyrrole film and nickel-cobalt hydroxide for asymmetric supercapacitor. In 1 M KOH, electrode based on FEG/PPy composites at a specific current in the range of 5-50 A g^{-1} shows the capacitance of 600-400 F g^{-1}, while cell FEG/PPy||FEG/NiCo(OH)$_x$ cell displays a specific capacitance of 260 F g^{-1} at a current density of 1 A g^{-1}, whit maximum energy density of 61 W h kg^{-1} at 0.65 kW kg^{-1}. Grote and Lein [77] studied SnO_2-PPy//SnO_2-MnO_2 3D core/shell NT array as asymmetric supercapacitors in 1 M Na_2SO_4 which cyclic voltammograms of half cells reaction and complete cell, are shown in Fig. 2.30. The device exhibits a voltage window of 1.7 V, specific energy of 27.2 Wh kg^{-1} at 0.85 kW kg^{-1} and remains 7.8 Wh kg^{-1} at 24.8 kW kg^{-1}.
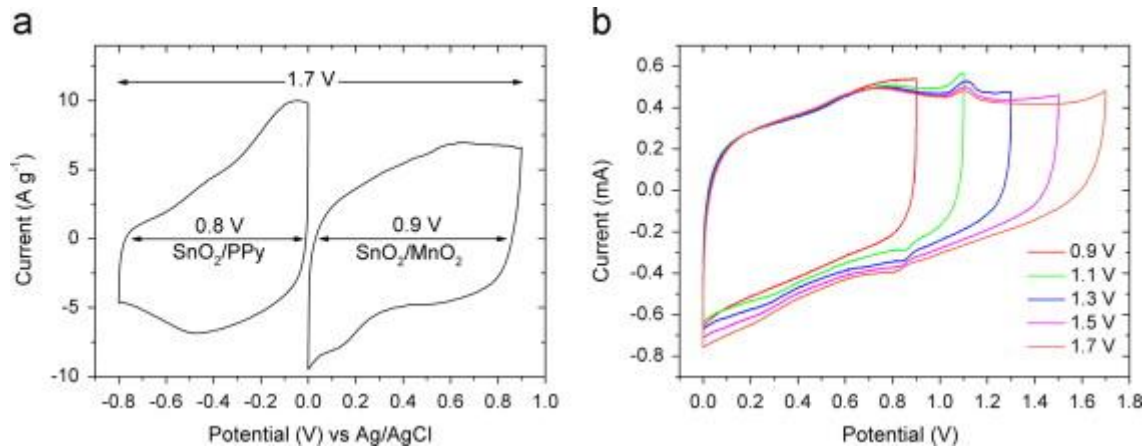
Figure. 2.30. Cyclic voltammograms of half cells reaction and complete
SnO_2-PPy//SnO_2-MnO_2 3D core/shell NT array
as asymmetric supercapacitors cell in 1 M Na_2SO_4 [77].

Liu et al. [78] investigated flexible asymmetric supercapacitors based on a new graphene foam/carbon nanotube hybrid film consisted of the GF/CNT/MnO_2 positive electrode, 0.5 M Na_2SO_4 electrolyte-soaked separator and GF/CNT/Ppy negative electrode. A maximum energy density of 22.8 Wh kg^{-1} at 860 W kg^{-1} and a high power density of 2.7 kW kg^{-1} at 6.2 Wh kg^{-1} was obtained.

Cheng et al. [79] investigated asymmetric composite supercapacitors made of activated carbon (AC) and carbon nanotubes, and an electrode made with complex composites $Co_{0.5}Ni_{0.5}(OH)_2$/graphene/CNTs. After characterization, Figs. 2.31a-c., of

the half cells materials and whole asymmetric composite supercapacitors, they obtained a specific energy in the range of 40-25 Wh kg^{-1} and corresponding specific power in the range of 0.2-4 kW kg^{-1}, Fig. 2.31d.
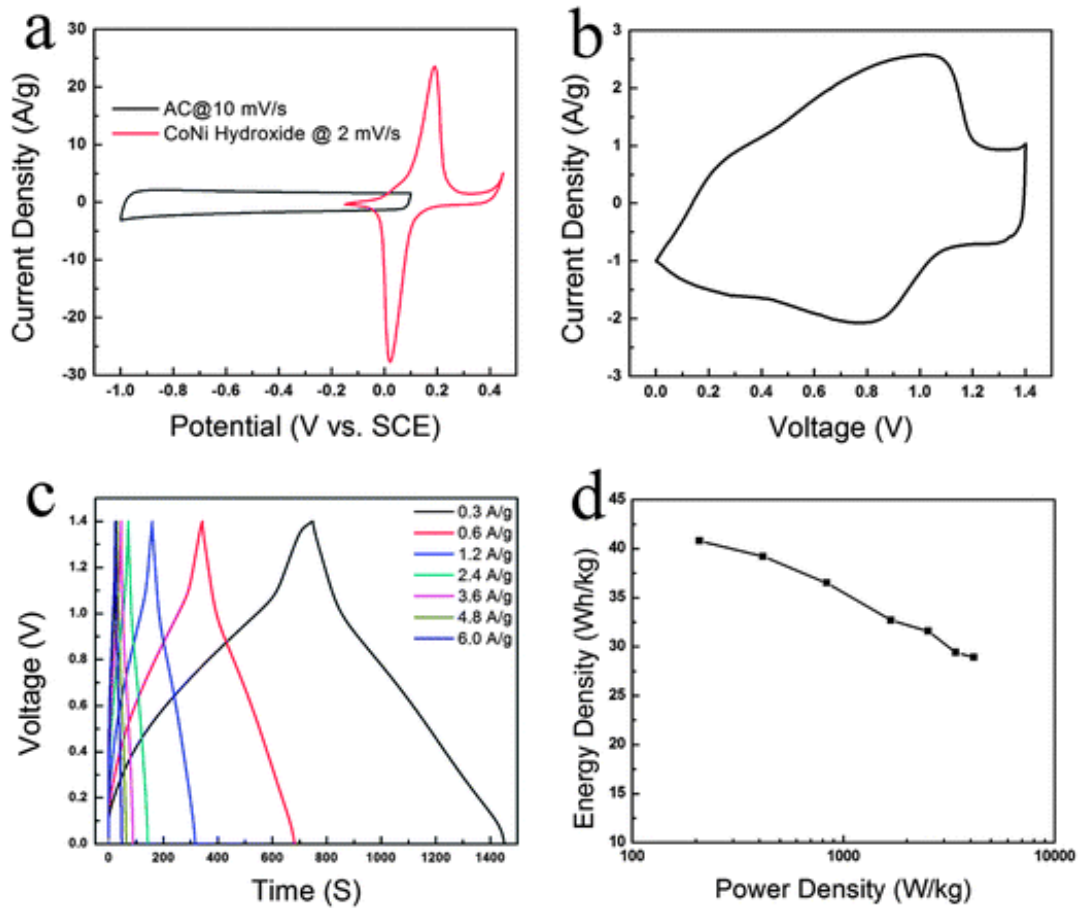
Figure 2.31. (a) Comparative CV curves of an electrode made with activated carbon (AC) and carbon nanotubes and an electrode made with $Co_{0.5}Ni_{0.5}(OH)_2$/ graphene/CNTs. (b) CV and (C) charge–discharge curves at different current densities of an asymmetric supercapacitor assembled using a $Co_{0.5}Ni_{0.5}(OH)_2$/graphene/CNT positive electrode and an AC/CNT negative electrode, and (d) the corresponding Ragone plot of the asymmetric supercapacitor [79].

2.4.3.3. Hybrids of supercapacitor and battery: "supercapattery"

Similarly, to asymmetric hybrids, the battery-type hybrids couple two different electrodes; however, the battery-type hybrids are unique in combination of a supercapacitor electrode with a battery electrode. This particular configuration replicates the demand for higher energy supercapacitors and higher power batteries, combining the energy characteristics of batteries with the power, cycle life, and recharging times of supercapacitors [30]. From the diagram, given in Fig. 2.32, the possible combinations of battery type hybrid supercapacitors could be evaluated.
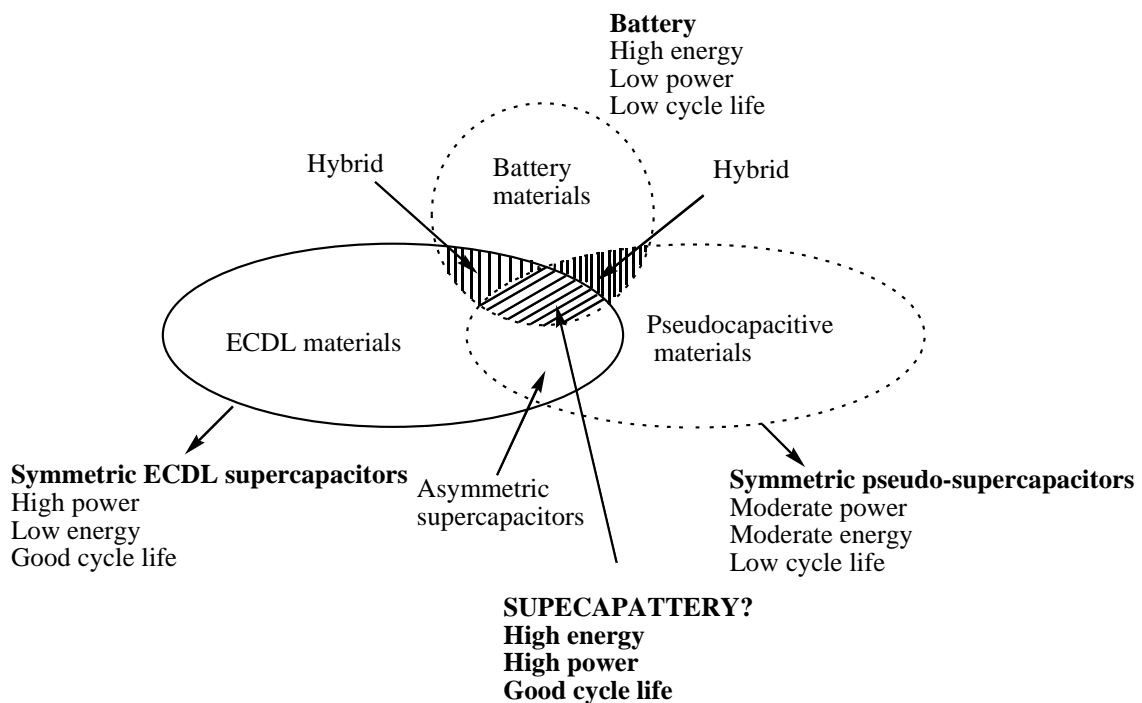
Figure 2.32. Merging the characteristics of ECDL, pseudocapacitive and battery materials in battery type hybrid supercapacitors.

Recently, such configuration was named "**supercapattery**" (from: *supercapa*citors -*batt*eries) [12, 13]. Practically, all the electrode materials of the commercial battery systems can be used for the battery-type electrode in the suitable electrolyte, from lead–acid batteries to metal/air systems. [12]. But in practice, research has focused primarily on using nickel hydroxide, lead dioxide, and LTO ($Li_4Ti_5O_{12}$) and LFP ($LiFePO_4$) as one electrode and activated carbon as the other [12,80,81,82,83,84].

Each battery technology has its own advantages and drawbacks. For example, lead-acid is the inexpensive to produce, but has low cycle-life and energy density, Ni-MH has good power capability, but lower energy and lower cycle-life than Li-ion. Supercapacitor and Li-ion devices are interesting because they stand at two ends of the spectrum: Li-ion has the highest energy density of all systems, which can vary from 120 to 200 Wh kg^{-1}. Supercapacitors have the highest power density, which can range from 2 to 5 kW kg^{-1} or more, combined with the highest cycle-life, on the order of hundreds of thousands to million cycles. But their energy density is low, from 2 to 5 Wh kg^{-1}. Recently, Telcordia Technologies [85] has been developing a new device named nonaqueous asymmetric battery hybrid (Fig. 2.33). It aims at integrating the advantages of Li-ion batteries and supercapacitors, e.g. combining high energy density, high power capability and long cycle-life. Unfortunately, such devices are very expensive and use non-aqueous electrolytes.
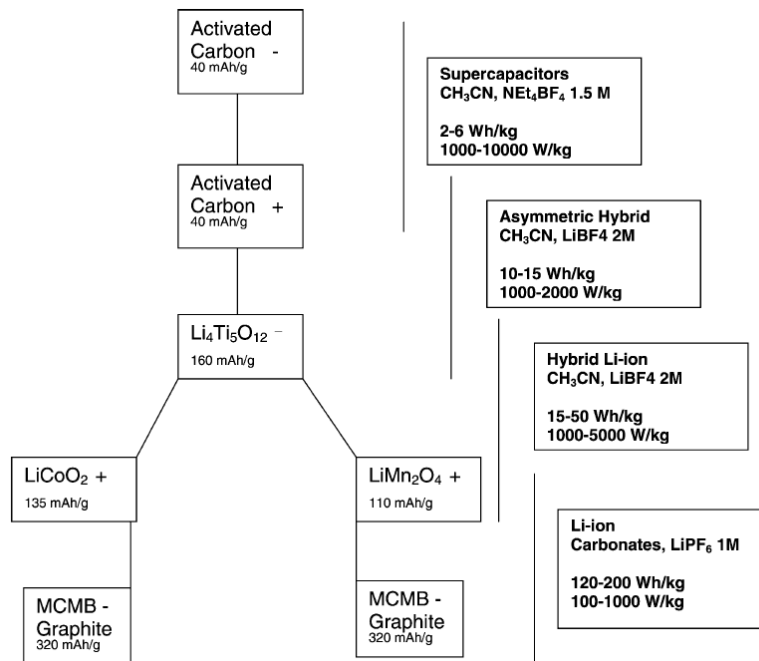
Figure 2.33. 1. Overview of the components used in the family of electrochemical storage devices developed by Telcordia Technologies [85].

Although there is less experimental data on battery type hybrids than on other types of supercapacitors, the data that is available suggests that these hybrids may be able to bridge the gap between supercapacitors and batteries. **In spite of the promising results, the general consensus is that more research will be necessary to determine**

the full potential of battery-type hybrids [30,82,83]. As a guidance in Fig. 2.34 the illustration comparison of the galvanostatic charging and discharging plots of a conventional supercapacitor, and a battery are shown, so the battery-type hybrids should have charge-discharge characteristics between those limiting cases.
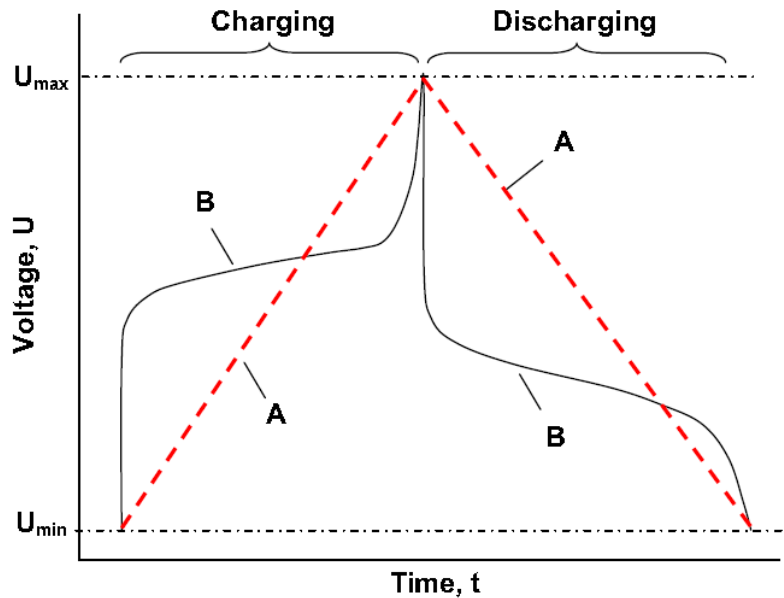
Figure 2.34. Illustrative comparison of the galvanostatic charging and discharging plots of a conventional supercapacitor (plot A, linear), and a battery (B nonlinear) [82].

2.4.3.4. Supercapattery and Supercabattery

The electrochemical characterizations of the battery, supercapacitor and the so called *supercapattery* are illustrated in Fig. 2.35 by the schematically given response of the electrode materials using cyclic voltammograms (CV) and galvanostatic charging and discharging plots (GCD) [86]. In Fig. 2.35c, the supercapattery performance is presented at the device level with one electrode displaying battery like properties and the other displaying capacitor like properties. At the electrode materials level, one or both of the electrode materials can be the nanostructured composite of an EDLC material and a battery material. CV and GCD of the supercapattery in Fig. 2.35c are sufficiently similar to those of the supercapacitor. However, it is also possible that the battery electrode dominates over the supercapacitor electrode, and the hybrid device performs more like a battery as shown in Fig. 2.35a instead of Fig. 2.35c. In that case the energy storage capacity in a battery-like hybrid should be derived in the same way

as for a battery. **To differentiate between capacitor-like and battery-like hybrids, and also to aid discussion,** Chen et al. [86] **propose to name the former as "*supercapattery*" and the latter "*supercabattery*"**.
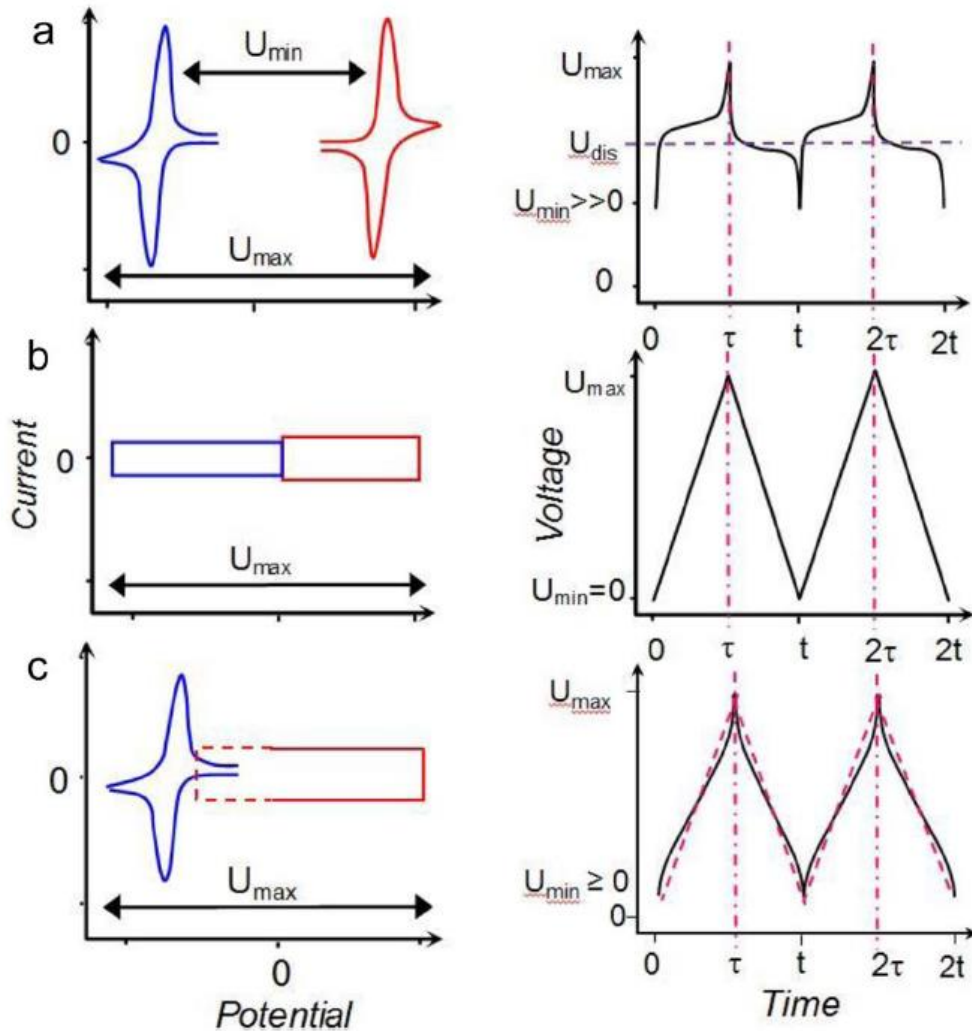
Figure 2.35. Schematic illustration of the electrochemical characteristics of (a) battery, (b) supercapacitor, and (c) supercapattery represented by (left) the cyclic voltammograms and (right) galvanostatic charging and discharging plots. [86].

There are numerous combinations of capacitive, peseudocapapacitive and battery type electrodes in the configuration of the supercapattery and supercabattery, as can be evaluated from Fig. 2.36. Calculated electrode potential (black and blue lines) and cell voltage (dashed lines) as a function of normalized time for galvanostatic charging and discharging of three typical types of supercapattery [86,87,88] with Fig 2.36a a negative

40

electrode of the lithium metal or litheated carbon and a positive electrode of activated carbon, Fig 2.36b a lithium metal or litheated carbon as a negative electrode, and a pseudocapacitive positive electrode, and Fig 2.36c a negative electrode of the typical battery type and a pseudocapacitive positive electrode, are shown in.
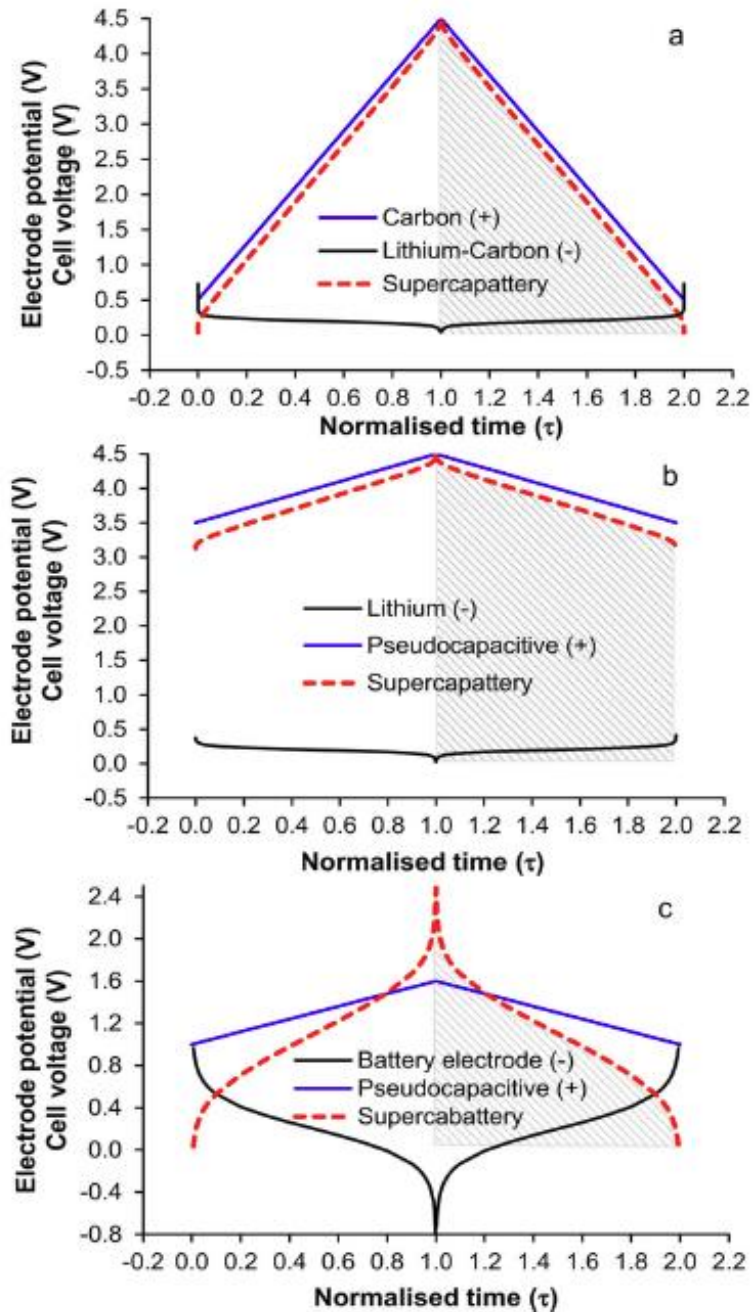
Figure 2.36. Calculated electrode potential (black and blue lines) and cell voltage (red dashed lines) as a function of normalised time for galvanostatic charging and discharging of three types of supercapattery [86,87,88].

Up to date, there is a limited numbers of studies connected with battery type hybrid supercapacitors.

Ni et al. [15] investigated system based on electrodeposited PbO_2 on graphite substrate as a pozitive electrode, with activated carbon (AC) as a negative electrode in 5.3 mol dm^{-3} H_2SO_4, Fig. 2.37. The AC/PbO_2 supercapacitor operated from 1.88 to 0.65V, Fig. 2.37b, and provides a specific capacitance in the range of 65 to 40 F g^{-1} (based on the active masses) at a discharge currenst of 150 to 600 mAg^{-1}. The hybrid system shows attractive energy and power performance. The specific energy ranges from 27 Wh kg^{-1} at a specific power of 152 W kg^{-1}, and at a power of 691 W kg^{-1}, the energy remains at 18 Wh kg^{-1}. After 3000 deep cycles under 300 mA g^{-1}, the capacity fades 20% from its initial value.
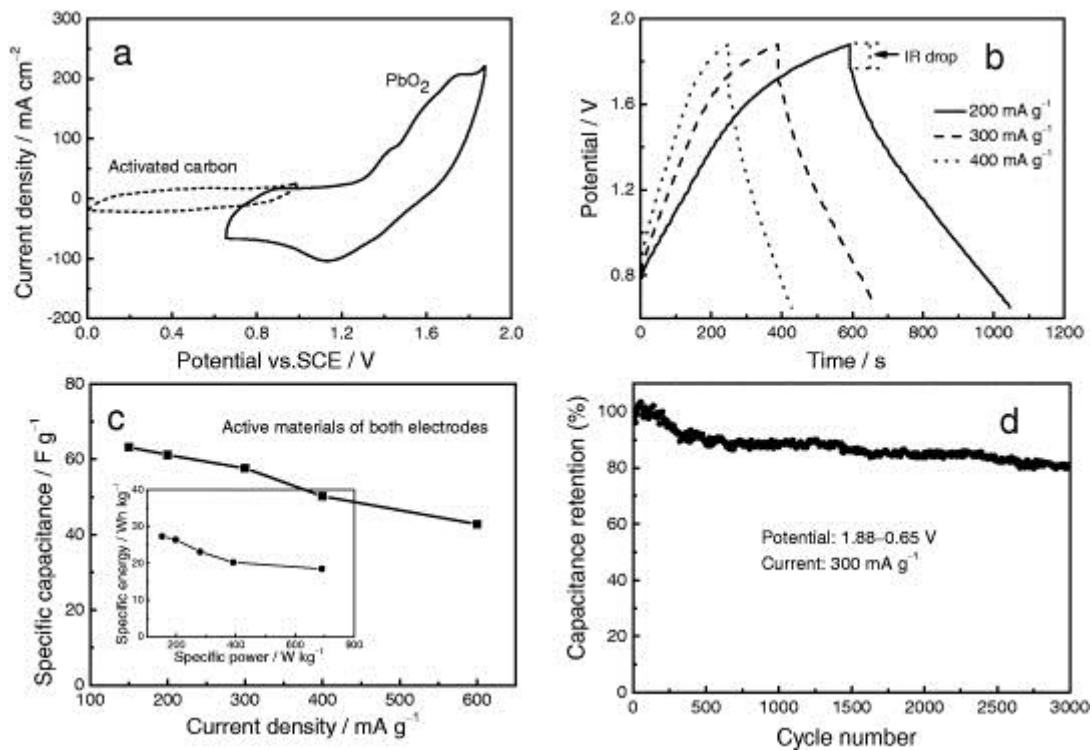
Figure 2.37. Electrochemical performance of the AC/PbO_2 hybrid supercapacitor in 5.3 mol l^{-1} H_2SO_4 solution. (a) CV profiles of PbO_2 film and AC electrodes at a scan rate of 10mVs^{-1}. (b) Charge-discharge profiles at various current rates of the hybrid capacitor. (c) The dependence of specific capacitance on the current densities; the inset shows a Ragone plot of the hybrid capacitor. (d) Cycle performance at a current of 300 mAg^{-1} (10 C rate) [15].

Hao et al. [89] investigated a hybrid supercapacitor based on spinel $Li_2Mn_4O_9$ and activated carbon (AC), Fig. 2.38. The electrochemical performance of the capacitor was studied by cyclic voltammetry, electrochemical impedance spectroscopy and galvanostatic charge/discharge in different aqueous electrolytes such as 1 M $LiNO_3$, Li_2SO_4, $NaNO_3$ and KNO_3 solution. A maximum specific capacitance of 261 F g^{-1} was obtained for the $Li_2Mn_4O_9$ single electrode between 0 and 1.4 V. The AC/$Li_2Mn_4O_9$ hybrid supercapacitor showed a sloping voltage profile from 0 to 1.4 V and delivered an energy density of 53 Wh kg^{-1} based on the total weight of the active electrode materials. The hybrid capacitor exhibited a desirable profile and maintained over 80% of its initial energy density after 1000 cycles, indicating that $Li_2Mn_4O_9$ has good cycling performance and structural stability in aqueous electrolyte. The hybrid supercapacitor also exhibited good rate capability, even at a power density of 1250 W kg^{-1}, it had a specific energy 29 Wh kg^{-1} compared with 48 Wh kg^{-1} at the power density of about 417 W kg^{-1}.
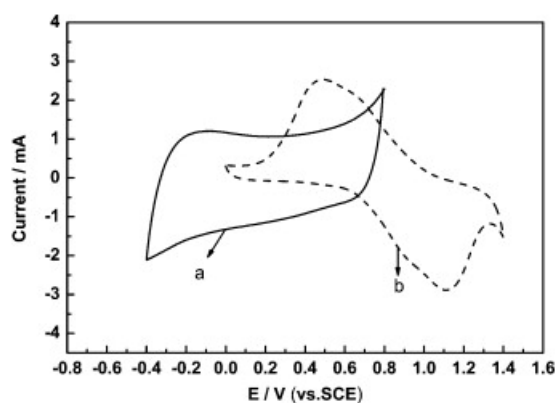
Figure 2.38. CV curves of (a) AC electrode and (b) the $Li_2Mn_4O_9$ electrode at 5 mV s^{-1} in 1 M $LiNO_3$ solution [89].

Pseudocapacitive materials based on conducting polymers has been investigated as anode in aqueous based lithium intercalation battery but with no attempt to evaluate power of the system [22,90,91,92,93,94,95]. The principle of this system is based on anions doping/dedoping of PPy, or other ICP's, as a negative electrode, and lithium ion intercalation/deintercalation of positive electrode ($LiCoO_2$, $Li_2Mn_2O_4$). During the charge, lithium ions deintercalate from the positive electrode into the solution and anions are dedoped from the negative electrode into the solution. During the discharge

process, lithium ions intercalate into the positive electrode, and anions are doped into the negative electrode [22]. For example, Wang et al. [91, 92] investigated PPy|Mn$_2$O$_4$ and PPy|LiCoO$_2$ cell in saturated Li$_2$SO$_4$ solution. For the PPy|Mn$_2$O$_4$ system, authors reported open circuit voltage of 1.6 V, and specific capacity of ~45 mAh g-1, while, for the PPy|LiCoO$_2$ system, which cyclic voltammograms is shown in Fig. 2.39, reported the open circuit voltage of 1.2 V, average discharge voltage of 0.8 V, and specific capacity of ~30 mAh g^{-1}.
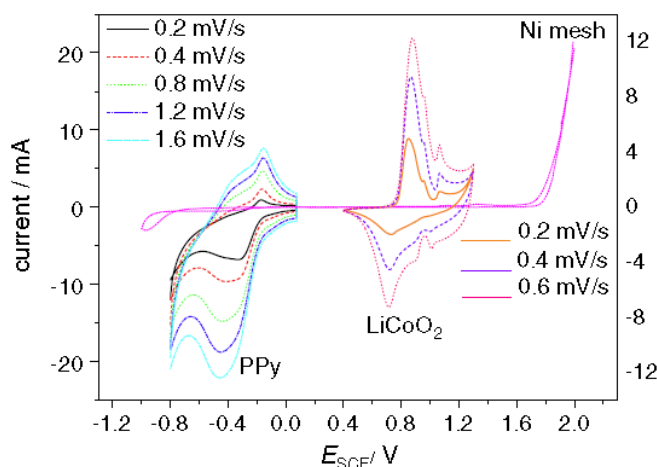
(a)
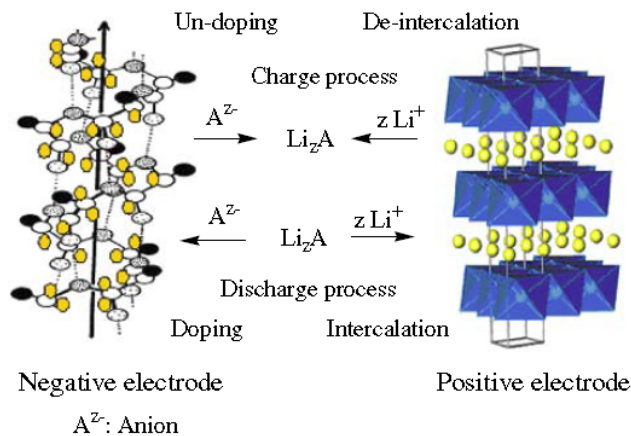
(b)

Figure 2.39. a) CVs of PPy, LiCoO$_2$, and nickel mesh in saturated Li$_2$SO$_4$ solution and b) principle of the system based on doping/undoping (negative) and deintercalation/intercalation (positive) electrodes [92]

Liu et al. [96] investigated aqueous based rechargeable lithium battery consisting of a combination of polyaniline (PANI) anode, LiMn$_2$O$_4$ cathode, and a saturated LiNO$_3$

electrolyte, Fig. 2.40. They obtained an average discharge voltage of the battery about 1.1 V. Also it is observed that during 52 initial cycles, there is an activation process for this battery, Fig 2.40c. After the 52nd cycle, it continues to run 98 cycles, battery loses ~20% of its discharge capacity. The can battery delivers a capacity of 90 mAh g^{-1} at the 150th cycle.
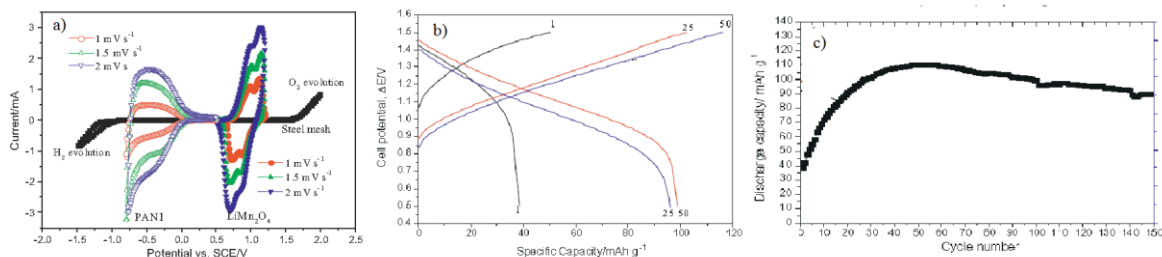
Figure 2.40. a) CVs of PANI, LiMn$_2$O$_4$, and steel mesh in saturated LiNO$_3$ solution. b) Charge and discharge profiles (b) and cycle life data (c) of the battery based on doping PANI and intercalation (LiMn$_2$O$_4$) compounds at a current density of 75 mA g^{-1} [adopted from ref. 96]

Unfortunately, lithium based systems are very expensive due high price of lithium salts. The classical battery systems based on, for example zinc or lead, and polypyrrole or polyaniline as the electrode materials in the aqueous electrolyte which could show supercapattery characteristics has been rarely reported [97,98,99,100,101]

A schematic Ragone plot, Fig. 2.41 show the position of supercapattery relative to other energy technologies [35].The energy-power curve for the novel supercapattery concept is shown bridging the gap between the high power of conventional supercapacitors and the greater energy storage of batteries.

To summarize, supercapacitors can deliver up to 10 Wh kg^{-1} of specific energy and up to 10 kW kg^{-1} of specific power. Battery can deliver more specific energy up to 100 Wh kg^{-1}, but with reduced specific power <100 W kg^{-1}.

Hence, the system which will have specific energy up to 100 Wh kg^{-1}, and increased specific power >1000 W kg^{-1} could be considered as an supercapattery systems.
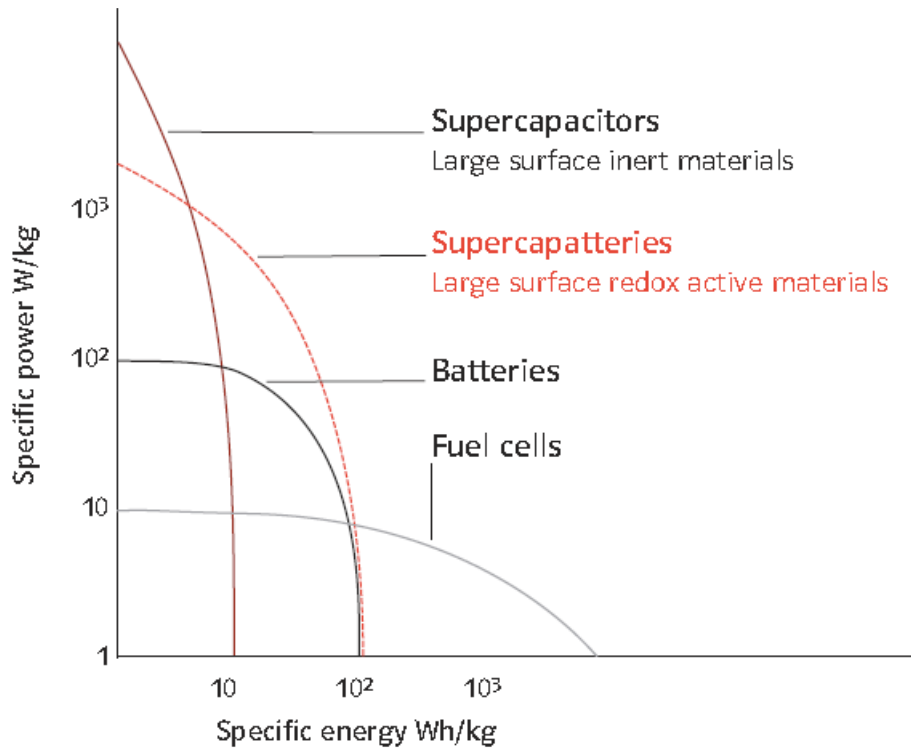
Figure 2.41. A schematic Ragone plot showing the position of supercapattery relative to other energy technologies [35].The energy-power curve for the novel supercapattery concept is shown bridging the gap between the high power of conventional supercapacitors and the greater energy storage of batteries.

2.5. Synthesis and characteristics of the polypyrrole and polyaniline

As mentioned, the battery systems based on, for example zinc or lead, and polypyrrole or polyaniline as the electrode materials in the aqueous electrolyte which could show supercapattery characteristics has been rarely reported. So, the aim of this thesis is to investigate possible characteristics of classical battery well studied lead sulfate electrode in combination with polypyrrole and polyaniline. For that reasons in following chapters the characteristics of polypyrrole and polyaniline will be presented.

2.5.1. Synthesis and characteristics of the polypyrrole

Polypyrrole can be synthetized chemically using an oxidizing agents (for example ammonium persulfate) or electrochemically [102,103]. Electrochemical synthesis could be performed potetiodynammially (using cyclic voltammetry, CV), galvanostatically (under constant current, GS), and potentiostatically (at constant potential, PS) techniques, as shown in Fig. 2.42 [104].
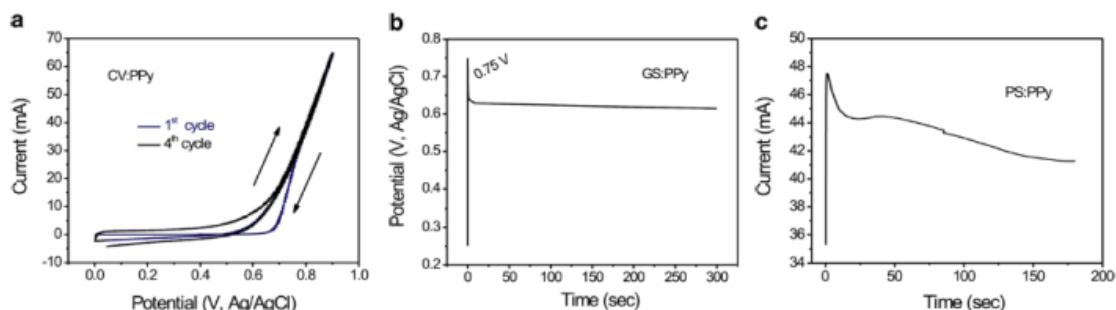
Figure 2.42. Synthesis of polypyrrole thin films by different electrodeposition modes: a) cyclic voltammetry (CV) mode by scanning between 0 and + 0.9 V for 12 cycles; b) galvanostatic (GS) mode at 10 mA/cm^2 for 5 min; and c) potentiostatic (PS) mode at 0.8 V (vs Ag/AgCl) for 3 min. 0.1 mol/L of distilled pyrrole and 0.5 mol/L H_2SO_4 [104]

The mechanism of the electrochemical polymerization of the pyrrole, described by Diaz et al. [105,106] which was later supported by the theoretical studies of Waltman et al. [107,108] is the most often discussed mechanism in the literature [109,110]. According to Diaz's approach, schematically shown in Fig 2.43, following the first

electrochemical step (E), which consists of the oxidation of the monomer into a radical cation, the coupling of the two radicals cations results in the formation of a dihydro dimer-cation. Consecutively, the chemical step (C) occurs, which leads to dimer formation followed by the loss of two protons and rearomatization. Because of the extended conjugation over two rings, having lower oxidation potential than the monomer, the dimer readily oxidizes to form the radical cation (E) and undergoes coupling with a monomeric radical. Electropolymerization is proposed to proceed through to a general $E(CE)_n$ mechanism, in which consecutive electrochemical and chemical steps takes place until the oligomers become insoluble and precipitate onto the electrode surface as polypyrolle [111].
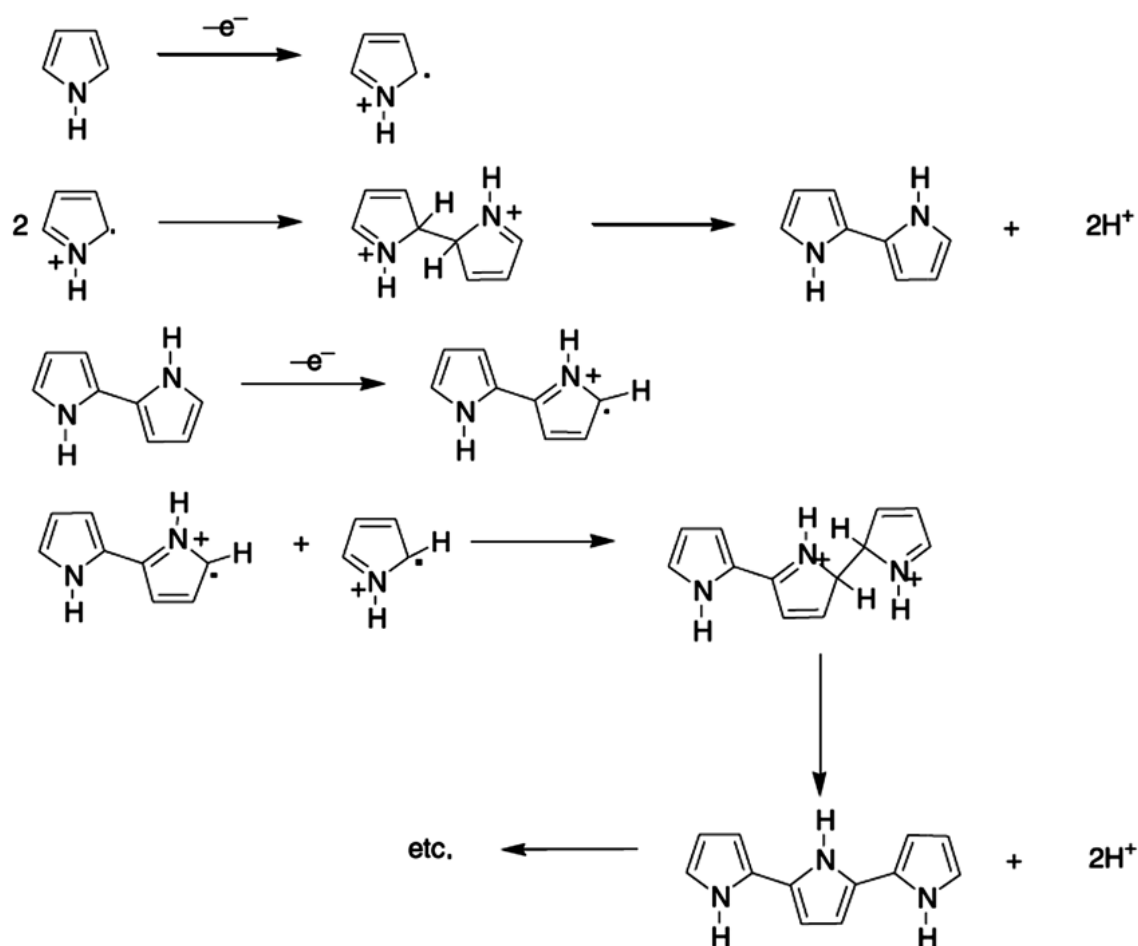
Figure 2.43. Proposed mechanism for electropolymerization of pyrrole by Diaz et al. [105, 109]

However, further studies have shown the presence of many other competitive multistep reactions, and the susceptible nature of the radical cation intermediates

regarding the nucleophilicity of the polymerization medium [112]. Typically, one electron is removed from the polymeric backbone for every three to four monomer units, which results in the intrinsic electrical conductivity and provides a delocalized p-electron band structure. In the oxidized state, the polymer is charge balanced with anions, termed also as 'dopants', which are incorporated into the chain to maintain electrical neutrality.

Schematic illustration of the electrochemical oxidation process in polypyrrole, starting from the neutral-insulating state (top) to a partially oxidized state (middle) to the fully oxidized conducting state (bottom) with corresponding cyclic voltammogram is presented in Fig. 2.44. To retain charge neutrality, an anion (A⁻) is inserted into the material for each positive charge on the chain. Fully doped, the dopant concentration in PPy is approximately 1 dopant for every 3-4 pyrrole rings [113].
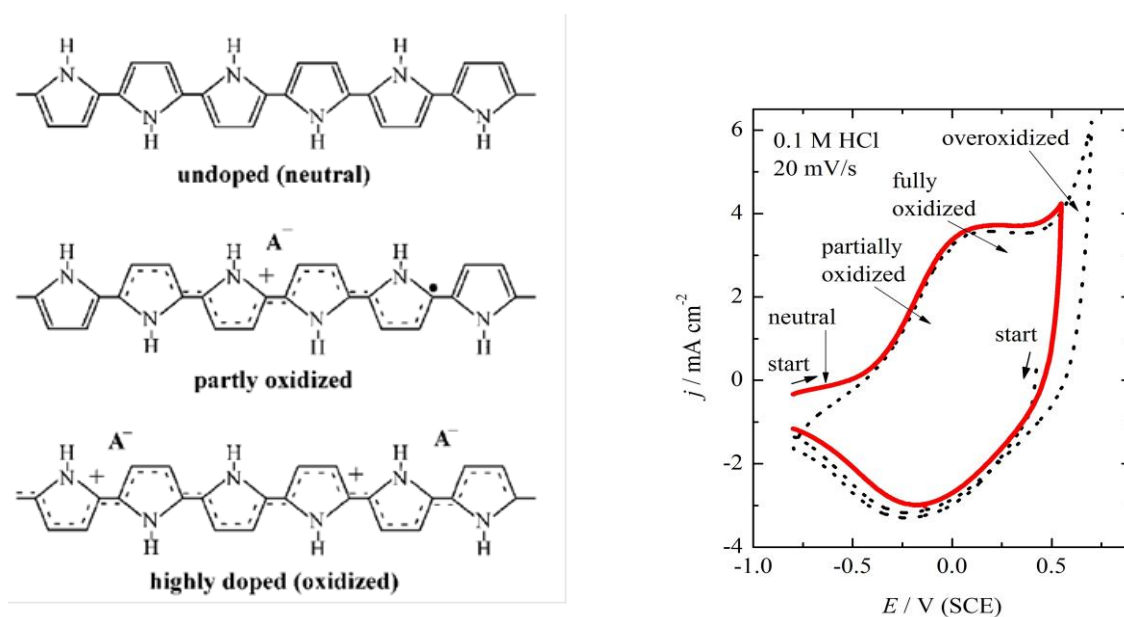
Figure 2.44. PPy at different oxidation levels. Anionic dopants (A⁻) are incorporated to maintain charge neutrality in the oxidized state (right). Cyclic voltammogram of the PPy in 0.1 M HCl (right)

The molecular structures of protonated polypyrrole (polypyrrole salt) proposed in the literature to a certain degree vary [114], but there is agreement about the structure of the polypyrrole base (undoped state) obtained after deprotonation, which is composed

of both the oxidized and reduced pyrrole constitutional units, Fig. 2.45. The localization of positive charges on polymer chain, as well as the presence of unpaired spins, polarons, detected by electron paramagnetic resonance, is still open to discussion.
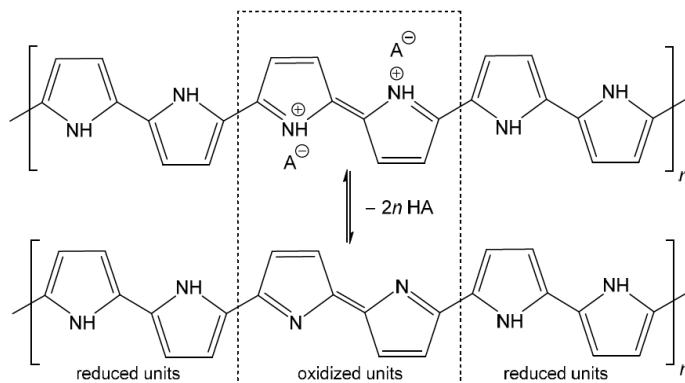
Figure 2.45. Conducting polypyrrole salt converts to non-conducting

polypyrrole base under alkaline conditions.

HA is an arbitrary acid, A^- a corresponding counter-ion [114].

The rearrangement of electrons within polypyrrole chain that lead to the formation of charge carriers was proposed by Stejskal et al. [114] (Fig. 2.46). The rearrangement of electrons in polypyrrole salt may generate bipolarons and finally polarons by delocalization over the polymer chain, as shown in Fig. 2.46. Polarons act as charge carriers.
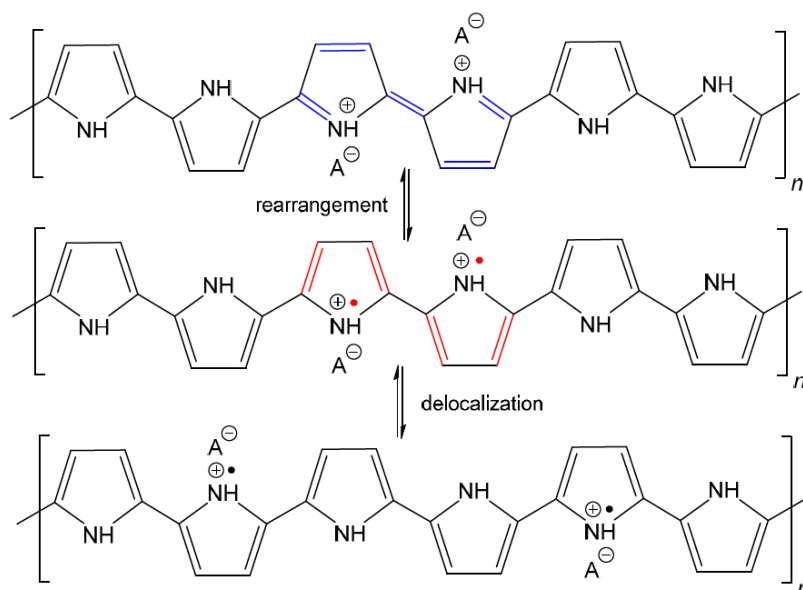
Figure 2.46. The rearrangement of electrons in polypyrrole salt [114].

Above the certain potentials, e.g. 0.5 V in Fig. 2.44, the undesirable reaction so called overoxidation, which leads to corruption of conjugation and loss of conductivity, could occur. The overoxidation is an irreversible degradation process that results in the shortening of the polymer chain length and/or formation of defects and pores along the PPy chain [115]. Figure 2.47 shows the sequence of reactions that occur during the overoxidation in the presence of small amount of the oxygen in the electrolyte. So, to avoid this phenomena the charging potentials must be limited to a certain value.
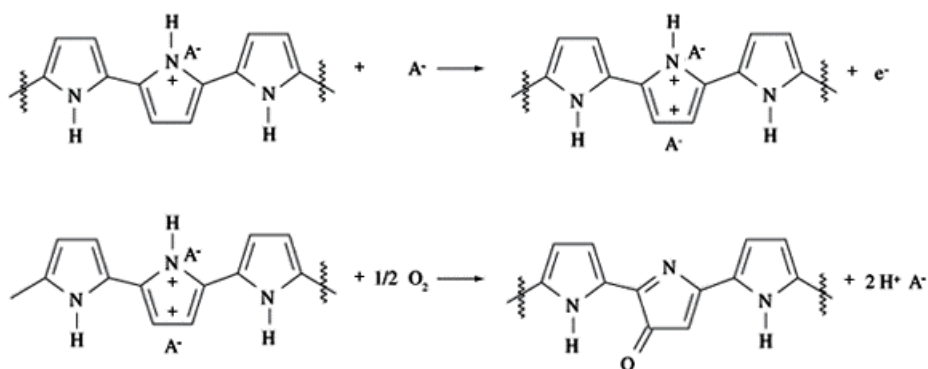
Figure. 2.47. Reaction that occur during the overoxidation of the polypyrrole [115].

2.5.2. Synthesis and characteristics of the polyaniline

Similarly like polypyrrole, polyaniline can be electrochemically synthetized applying mostly galvanostatic and cyclic voltammetry techniques, as shown in Fig. 2.48 [116]. During the cyclic voltammetry synthesis, throughout each step polyaniline film grow to the desirable thickness, which can be calculated by the determination of pased charge through each cycle. During the galvanostatic synthesis, after applying certain current density the polymerization occurred at constant potentials. Galvanostatic synthesis is favorable due easy control of film thickens simply by measuring the polymerization time. The film synthesis is usually performed on an inert electrode materials, like platinum, gold or different carbon based materials due high polymerization potentials.
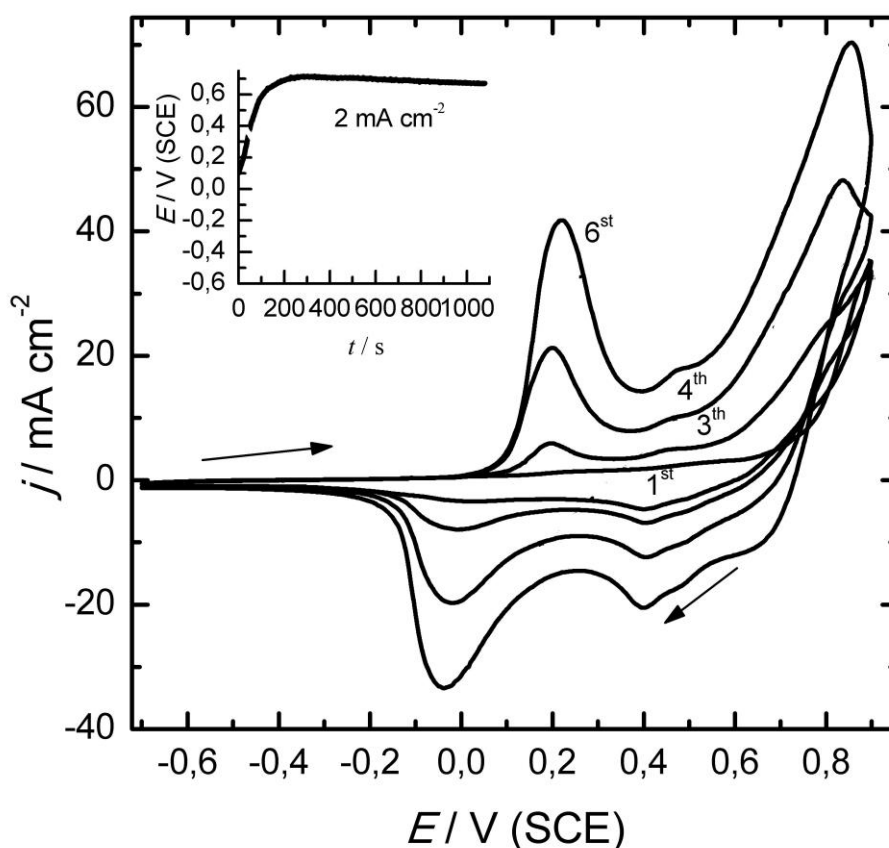
Figure 2.48. Electrochemical synthesis of polyaniline at graphite electrode by cyclic voltammetry (v = 20 mV s^{-1}) from 1.0 mol dm^{-3} HCl containing 0.25 mol dm^{-3} aniline. Insert: Chronopotenciometric curve (j = 2.5 mA cm^{-2}) of electrochemical synthesis of polyaniline from the same electrolyte [116].

The most generalized polymerization mechanism of aniline was suggested by Wei et al. [117, 118] which schematic representation is shown in Fig. 2.49. According to the authors, the rate determining step in the polymerization of the aniline is the oxidation of aniline monomer to form dimeric species (*i.e. p*-aminodiphenylamine, PADPA, *N*-*N*9-diphenylhydrazine and benzidine), because the oxidation potential of the aniline is higher than those of dimers, subsequently formed oligomers and polymer. After formation, the dimers are immediately oxidized and then react with an aniline monomer via an electrophilic aromatic substitution, followed by further oxidation and deprotonation to afford the trimers. This process is repeated, leading to the formation of polyaniline.
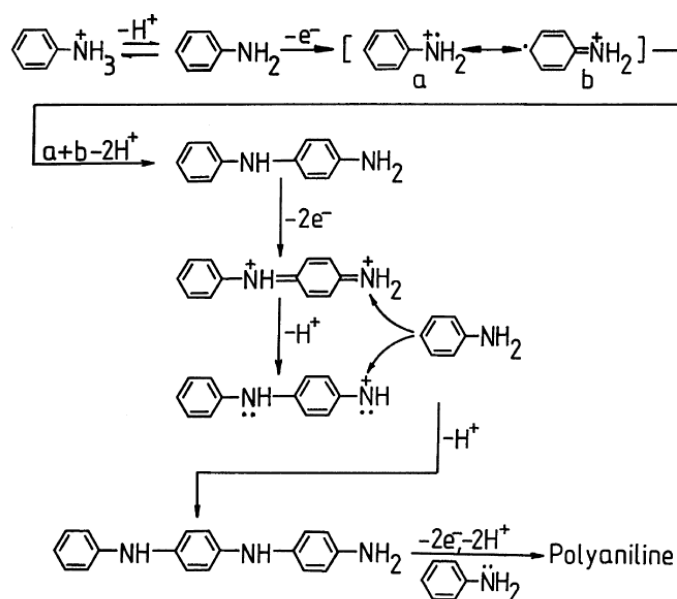
Figure 2.49. Mechanism of the aniline polymerization, proposed by Wei et al. [117, 118].

Chemically, PANI consists of "*y*" reduced benzenoid diamine and "*1-y*" oxidized quinoid diamine repeating units, where the oxidation state of PANI depends on the value of "*y.*" as shown in the scheme below. Leucoemeraldine, emeraldine, and pernigraniline are the three different redox forms of PANI having *y* : (1-*y*) ratio as 1:0; 1:1, and 0:1, respectively [119].

Benzenoid (reduced)   **Quinoid** (oxidized)

y = 1; leucoemeraldine
y = 0.5; emeraldine
y = 0; pernigraniline
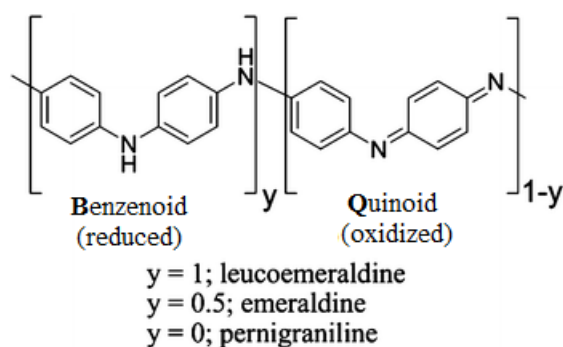
Predominately quinoid diamine repeating units groups in PANI chains can be further protonated in the presence of H^+ (acidic) ion or the dopant (X^-) anion to generate the cationic defects (polarons, bipolarons) that are responsible for the conductivity and

redox behavior of PANI. The shown stucture of the polyaniline is the only conducting and called emeraldine salt [119].

$X^- = anion$
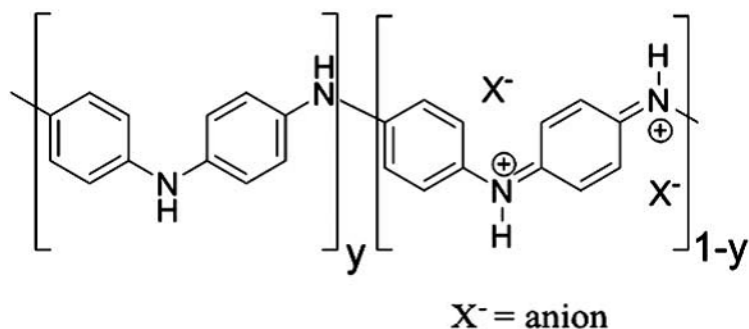
The unprotonated and protonated forms of PANI are known as base and salt, respectively. Figure 2.50 shows different base and salt forms of PANI in its three redox forms [119]. Conclusively, the conductivity of PANI can be tuned by using different doping agents, varying the extent of doping, and also by controlling the chain length and morphology including the dimensions and porosity of PANI.

Figure 2.50. Basic structure of PANI and different redox forms of PANI with its doped states [119].
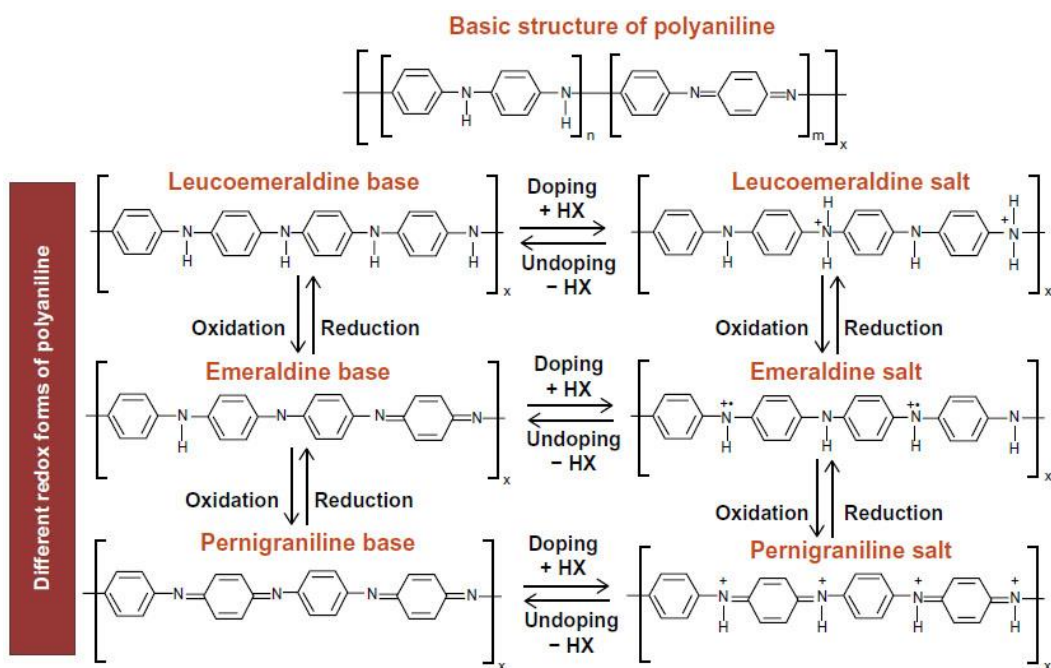
Even though the electrical properties of PANI are strongly related with the presence of polarons the bipolaron–polaron relationship, it is important to characterize

54

the doping state of PANI-based materials [120]. Figure 2.51 shows that further protonation of the polymeric chains (termed overdoping) may lead to the decrease of polaron population, due its conversion to bipolarons. Considering that the conduction mechanism is associated with polarons, the overdoping of polymeric chains is unfavorable for the electronic properties of PANI. This effect was reported for PANI doped in very high acidic media, such as 75% sulfuric acid. Besides protonation aspects, conformational changes of the polymeric chains may also occur, inducing the formation of a high number of polarons by the organization of the polymer backbone. Therefore, this effect (called secondary doping) may lead to a great improvement of the electrical properties of PANI and is one of the most desirable features for designing hybrid materials of PANI.
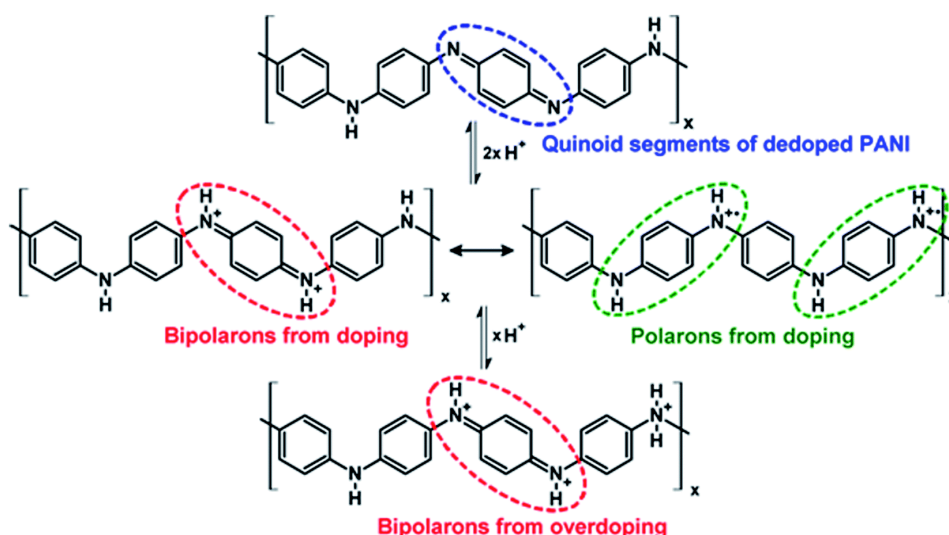
Figure 2.51. Rearrangements between polarons and bipolarons in the polyaniline [120].

Cyclic voltammogram of the polyaniline electrode in 0.5 mol dm^{-3} HCl for different anodic potential limits are shown in Fig. 2.52 [121].First anodic peak occurring at potential of about 0.25 V could be connected to doping of polyaniline with chloride anions via transition of leucoemeraldine form of PANI to emeraldine salt, while further increase of the potential above 0.50 V represents transition of emeraldine salt to pernigraniline salt. Between these two well defined anodic peaks, small peak at potential of about 0.45 V could be assigned to degradation reaction of PANI. Different forms of PANI oxidation states wich exist in different potentials are schematically represented in Fig. 2.53 [121]. Leucemeraldine is fully reduced form with doping

degree, $y = 0$, emeraldine salt is half oxidized form ($y = 0.5$), while pernigraniline salt refers to fully oxidized form ($y = 1$).
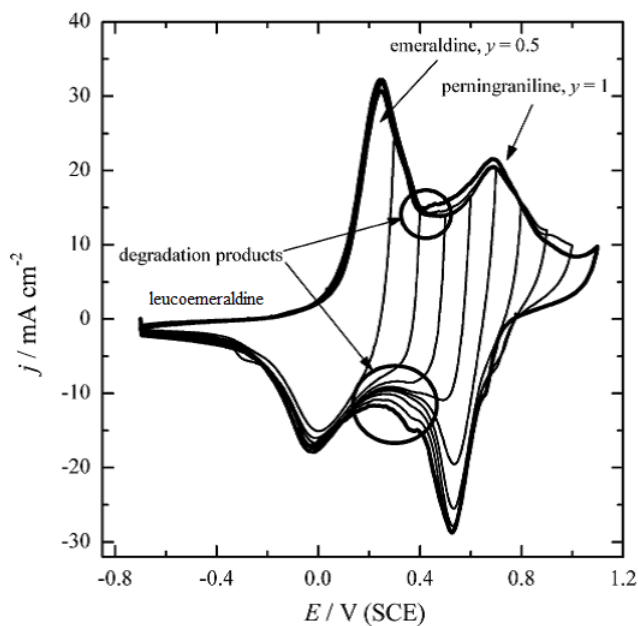
Figure. 2.52. Cyclic voltammograms of PANI electrode in 0.5 mol dm^{-3} HCl for anodic potential limits from 0.3 to 1.1 V (SCE), $v = 20$mVs^{-1} [121].
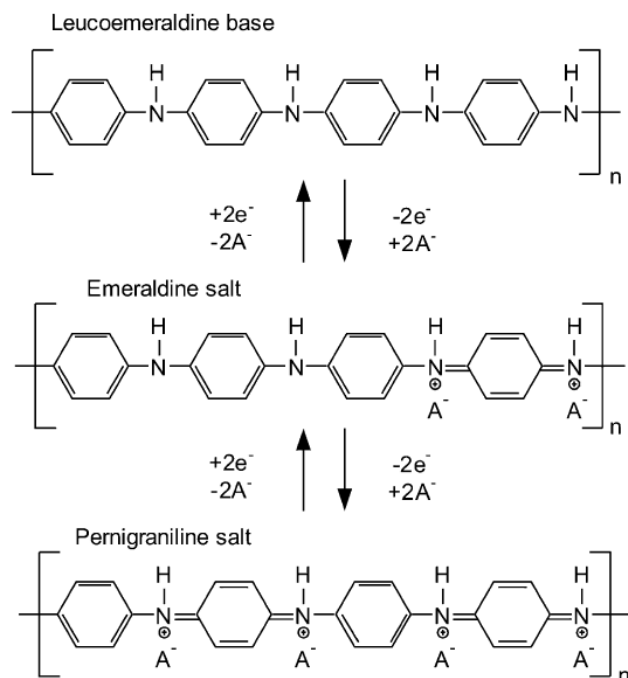
Figure 2.53. Generalized scheme of electrochemical reactions of various PANI oxidation forms [121].

3. EXPERIMENTAL

3.1. Polypyrrole - lead sulfate system

Polypyrrole was synthesized galvanostatically with current density of 2 mA cm^{-2} from electrolyte containing 0.1 M pyrrole (Aldrich p.a, previously distilled under reduced pressure), and 1 M H_2SO_4 (p.a., Merck) onto the plane 1.5 cm $\times$ 4 cm, $A = 6$ cm^2, graphite electrode with polymerization charges of 3.6 mAh, which corresponds to 4.8 mg of the doped polypyrrole.

Lead-lead sulfate electrode was prepared on pure lead (>99.9%, Alfa Aesar GmbH & Co KG, Germany) of 1.5 cm $\times$4 cm, $A = 6$ cm^2, according to modified Planté formation process as previously reported [122]. In order to remove lead oxide, naturally formed in the air, the lead sample was dipped in 8 M HNO_3 for 30 s, and rinsed with distilled water prior to immersion in 1 M H_2SO_4 and 0.05 M $KClO_4$ (p.a. Merck) for the formation process. The lead electrode was initially pre-treated cathodically at constant current of 6 mA during 5 min, and then oxidized to PbO_2 galvanostatically 750 s with current of 6 mA. Lead sulfate electrode was prepared galvanostatically by reduction of PbO_2 to Pb and then oxidized to $PbSO_4$ in the same electrolyte at a current of 6 mA. The corresponding synthesis charge was 1.25 mAh, with a calculated mass of $PbSO_4$ of 7.1 mg.

Electrodes were from one side protected by the epoxy. Before experiments, the electrodes were mechanically polished with fine emery papers (2/0, 3/0 and 4/0, respectively) and degreased in acetone in an ultrasonic bath.

All experiments were conducted in 1 M H_2SO_4 with 0.5 M $(NH_4)_2SO_4$ (p.a. Merck) using saturated calomel electrode as the reference, and in some cases Pt-mesh as a counter electrode. Electrochemical cell was made from plexiglass, with a volume of 100 cm^3, equipped with Luggin capillary for reference electrode, as shown in Fig.3.1. Experiments were performed using Gamry PC3 potentiostat/galvanostat, and cell

voltage was acquired with digital voltmeter ISO-Tech IDM 73, interfaced to a PC via RS-232.
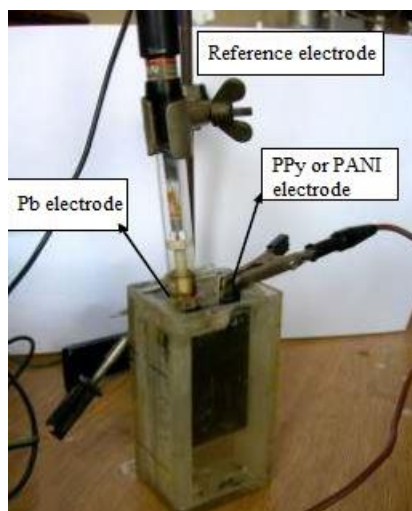
Figure 3.1. Assembly of the electrochemical cell.

3.2. Polyaniline - lead sulfate system

Polyaniline (PANI) was synthesized from aniline monomer (ANI, p.a. Merck) with concentration of 0.25 M in 1 M H_2SO_4 aqueous solution. Prior to use aniline was distilled under reduced pressure. Synthesis was carried out by the galvanostatic method with the current of 15 mA for 1900 s (7.9 mAh) onto a plane graphite electrode with dimensions 1.5 cm (4 cm, $A = 6$ cm^2, platinum gauze counter, and saturated calomel as the reference electrode. Lead sulfate was synthesized by the oxidation of one side of the thin lead foil with dimensions 1.5 cm $\times$ 4 cm, $A = 6$ cm^2, first to spongy lead dioxide, and then by reduction of lead dioxide to lead sulfate. Oxidation was conducted with a current of 9 mA over 450 s (1.125 mAh) in solution contained 1 M H_2SO_4 with the addition of 0.05 M $KClO_4$ as an oxidizing agent. Formation of the Pb|PbSO$_4$ electrode was performed in pure 1 M H_2SO_4, by the oxidation of lead sulfate to lead dioxide, and then by reduction of the dioxide to sulfate, and sulfate to pure spongy lead, with a current of 6 mA. Procedure of charge-discharge of lead sulfate to lead and vice versa, was repeated until stable charge-discharge curve was obtained, typically three times. The half-cells reactions, and the determination of the cell performances were conducted in 1 M H_2SO_4, because the addition of 0.5 M $(NH_4)_2SO_4$ leads to the poorer

characteristics of the polyaniline electrode.

The electrochemical experiments were conducted using Gamry PC3 potentiostat/galvanostat, in the Plexiglas cell with a volume of 100 cm^3, equipped with saturated calomel electrode for potential measurement, as shown in Fig. 3.1. The voltage of the cell was recorded using Peak Tech 4390 USB DMM, digital voltmeter connected to PC via USB cable.

3.3. Characterization methods

For the UV−vis study of as synthesized polypyrole and polyaniline, the product was after synthesis scratched from the graphite electrode surface using a plastic knife, and well ground in an agate mortar. The small amounts of solid product, ∼3 mg was added to 10 ml of 1 M H_2SO_4, sonicated in an ultrasound bath for 30 min, and finally, after the precipitation of the larger particles that lasted one hour, 3 ml of the solution was analyzed with an UV−vis LLG uniSPEC 2 spectrometer.

For the XRD study of as synthesized $PbSO_4$, the same procedure as for the electrode preparation was applied, only the oxidation was conducted for 2000s, to minimize the influence of pure lead from the electrode bulk. The XRD pattern of the samples was recorded with an Ital Structure APD2000 X-ray diffractometer in a Bragg−Brentano geometry using CuKα radiation and the step-scan mode (range: 15–65° 2θ, step-time: 0.50 s, step-width: 0.02°).

4. RESULTS AND DISCUSSION

4.1. Supercapacitor based on polypyrrole and lead-lead sulfate

Figure 1 shows galvanostatic synthesis of the polypyrrole. Electro-polymerization of the pyrrole occurred in the potential range of 0.55 to 0.65 V via following reaction: [123]:

$$nPy + nySO_4^{2-} = [PPy^{2y+}(SO_4^{2-})_y]_n + 2nH^+ + (2 + zy)ne \qquad (4.1)$$

where y is dopping degree and z anion charge.
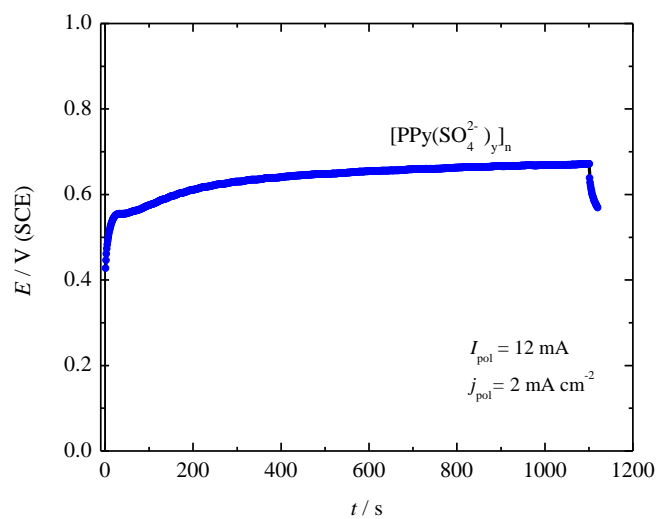
Figure 4.1. Galvanostatic synthesis of the polypyrrole in 1 M H_2SO_4 + 0.1 Py.

The most widely accepted mechanism for pyrrole polymerization was proposed by Diaz et al. [105 , 106]. The first stage of the reaction is the oxidation of monomer molecules yielding radical cations with the radical state delocalized over the pyrrole ring. The radical cations dimerise, in the rate-controlling step, during which two protons are

expelled. The dimers, owing to stronger conjugation, are more readily oxidized under the given reaction conditions than the monomer. The chain growth proceeds by addition of a newly formed radical cation to an oligomeric one. The anodic oxidation, which results in the formation of conducting polymer, has the stoichiometry of $(2+zy)F$ per mole of monomer. Of those, only $2F$ mol^{-1} are related to the polymerisation, and extra charge zyF, to the oxidation (doping) of the polymer film, usually in the PPy^{2y+}, bipolaronic states [124]. Because the oxidation potential of the monomer is always markedly higher than that for the polymer, the two processes, the formation of polymer and its oxidation proceed in parallel and are accompanied by the incorporation of counterions into the polymer matrix [125]. The yield in charge terms is close to 100%; providing a possibility of controlling the mass and thickness of the film [125].

Figure 4.2. shows UV-vis spectra of dispersed as synthetized product in distilled water. In as synthetized PPy, two bands are present at 345 and 415 nm. The absorption at 345 corresponds to bipolaron formation [126]. The absorption peaks at 415 nm, is assigned as transitions from the PPy valence band to an anti-bipolarons band. Intense, broad absorptions are also occurred above 550 nm [127]. This broad absorption is attributed to electron transitions from the polypyrrole valence band to a second bipolarons band in the band gap. So, as synthetized PPy has the well-defined features of a bipolaron formation, showing the film to be in a fully doped state [126, 127].
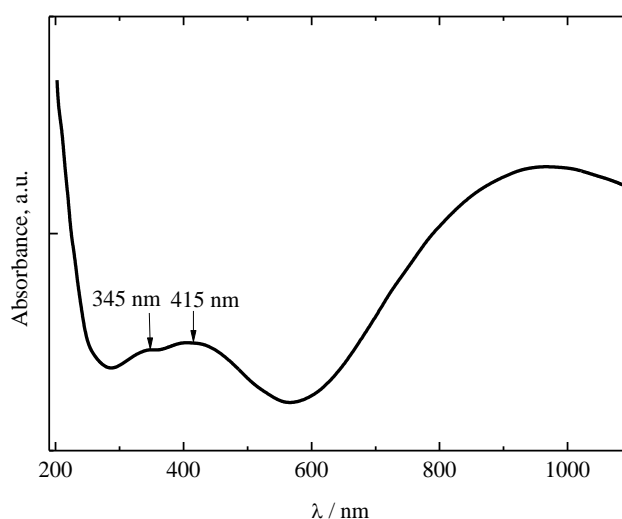
Figure 4.2. UV-vis spectra of dispersed as synthetized PPy in distilled water.

Hence, based on this findings, it could be proposed that structure of doped polypyrrole in the bipolaronic state as shown in Fig. 4.3, for the (a) single charged anions, X⁻, and divalent anions, e.g. SO_4^{2-}, (b).

a)

b)
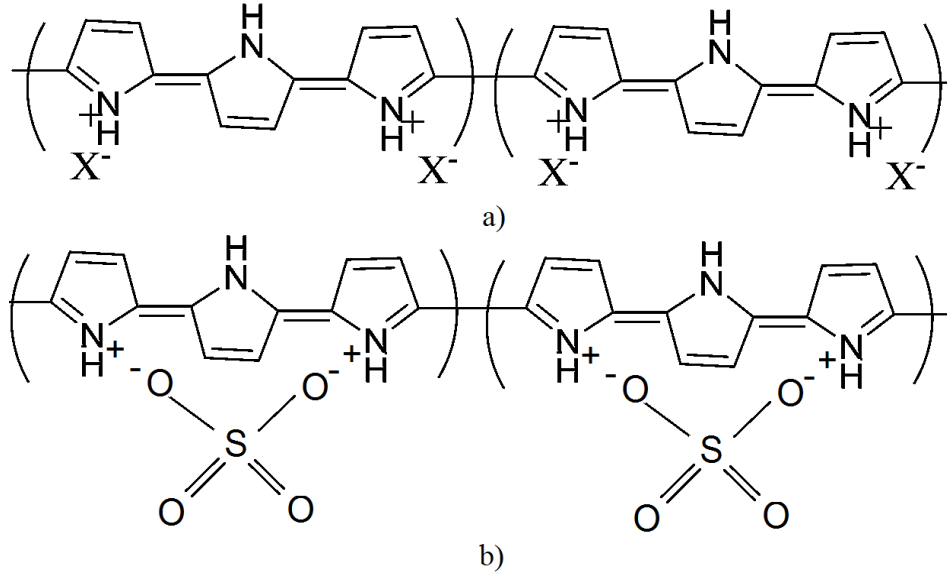
Figure 4.3. Proposed structure of doped polypyrrole in the bipolaronic state for the single charged anions (a) and divalent anions, e.g. SO_4^{2-}, (b).

Considering the polypyrrole electropolymerization reaction (Eq. 4.1), total polymerization charge, Q_p, is given as:

$$Q_p = I_p\, t_p = (2+2y)neF \qquad (4.2)$$

On the other hand, for the p-doping/dedoping reaction with sulfate anions:

$$[PPy^{2y+}(SO_4^{2-})_y]_n + 2yne = [PPy]_n + nySO_4^{2-} \qquad (4.3)$$

theoretically available capacity is given:

$$Q = It = 2nyeF \qquad (4.4)$$

Combining Eqs. (4.2) and (4.4), available capacity is connected with polymerization charge with the following equation:

$$Q = \frac{2y}{2+2y} Q_{\text{p}} = \frac{2y}{2+2y} I_{\text{p}} t_{\text{p}} \tag{4.5}$$

Therefore, for the polymerization charge of 3.6 mAh and theoretical doping degree of 0.33 (one sulfate anions per polymer units) [125], taking into account that z is 2, available dedoping charge was estimated to 0.9 mAh.

Lead sulfate was synthesized through the galvanostatic template of the PbO_2 film electrode formation and reduction, as shown in Fig. 4.4. Initially electrode was cathodically treated 300 s, to remove eventually naturally formed oxides (1). After anodic current was applied, at potential of –0.55 V the oxidation of pure lead to lead sulfate occur, via following equation:

$$Pb_{(s)} + SO_4^{2-} = PbSO_4 + 2e \quad E_{\text{r}}^{\theta}(PbSO_4 \,|\, Pb) = -0.601 \text{ V (SCE)} \tag{4.6}$$

Once, when most of the lead surface was converted into the $PbSO_4$, sharp increase of the potential up to the ~1.85 V and followed by the potential plateau at ~1.55 V (2) was connected with the transformation of $PbSO_4$ to PbO_2, given as:

$$PbSO_4 + 2H_2O = PbO_2 + SO_4^{2-} + 4H^+ + 2e$$
$$E_{\text{r}}^{\theta}(PbO_2 \,|\, PbSO_4) = 1.449 \text{ V (SCE)} \tag{4.7}$$
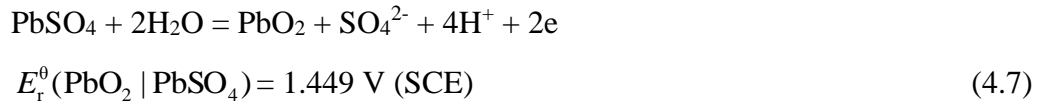
After 750 s, electrode was completely discharged to the potential of –0.6 V with the same current density (3). Lead-lead sulfate was produced by three cycles of discharge to pure lead (4) and charge (5) to lead sulfate in the same electrolyte, according to Eq. 4.6. After formation, discharged, spongy lead electrode was washed with bi-distiled water, to remove perchlorate anions and transferred into the electrochemical cell for the further investigations. For the XRD characterization the same procedure was applied.
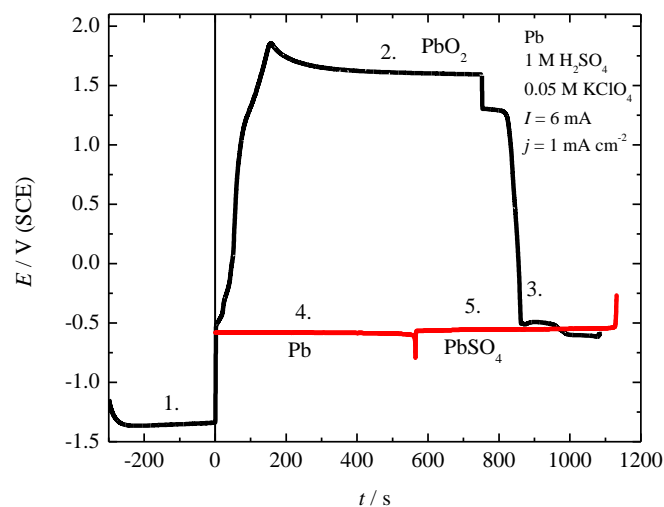
Figure 4.4. Galvanostatic synthesis of the lead - lead sulfate
in 1 M H₂SO₄ + 0.05 M KClO₄

In Fig. 4.5 the XDR spectra of as synthesized lead sulfate was shown. The peaks positioned at 2θ of: 31.21^{o}; 36.16^{o}; 52.11^{o} and 62.09^{o} corresponds to the pure lead (JCPDS No. 04-0686 Pb pdf), from the bulk of the electrode. The rest of the observed peaks were in excellent agreement with the peak positions of lead sulfate with anglesite structure (JCPDS No. 36-1461 Anglesite pdf).
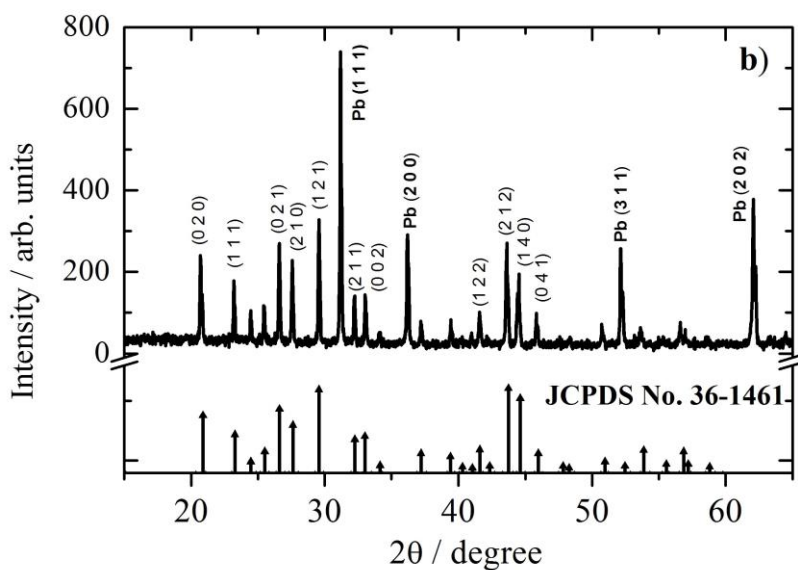
Figure 4.5. The XDR spectra of as synthesized lead sulfate.

Figure 4.6 shows cyclic voltammograms of investigated materials. Polypyrrole electrode has pceudocapacitive behavior accompanied with doping-dedoping reaction in the broad range of studied potential. In anodic direction, doping (charge) with sulfate anions started at –0.2 V, and proceeds up to the potentials of ~0.6 V, followed by an increase of the current density due to the overoxidation processes [128]. Dedoping (discharge) occurred in the potential range of 0.45 to –0.45 V, with a well-defined peak at –0.3 V. Small broad peak at the potentials more negative then –0.45 V could be associated with cation insertion [129]. Lead-lead sulfate electrode shows the reversible behavior with sharp current peaks, typical for battery electrodes. Formal potentials of the lead-lead sulfate system was estimated to –0.58 V.
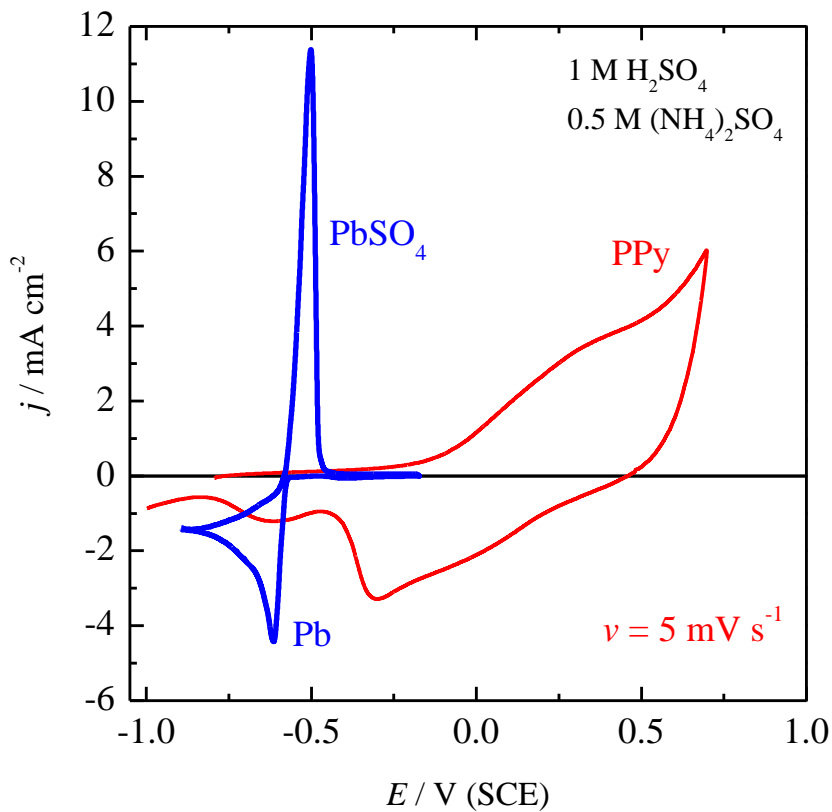
Figure 4.6. Cyclic voltammograms of lead-lead sulfate and polypyrrole electrodes.

Galvanostatic charge-discharge curves at different currents of investigated materials were shown in Fig. 4.7. From Fig. 4.7 it can be seen that lead-sulfate electrode shows typical battery charge-discharge behavior, practically, without polarization. On the other hand, polypyrrole electrode shows the typical pseudocapacitive behavior,

whereby the charge-discharge occurred in a broad potential region. Charge occur linearly from –0.1 V to 0.5 V, while discharge proceeded nonlinearly from 0.5 V to the –0.3 V, followed by a sharp decrease of the potential due counter-ions diffusion limitations.
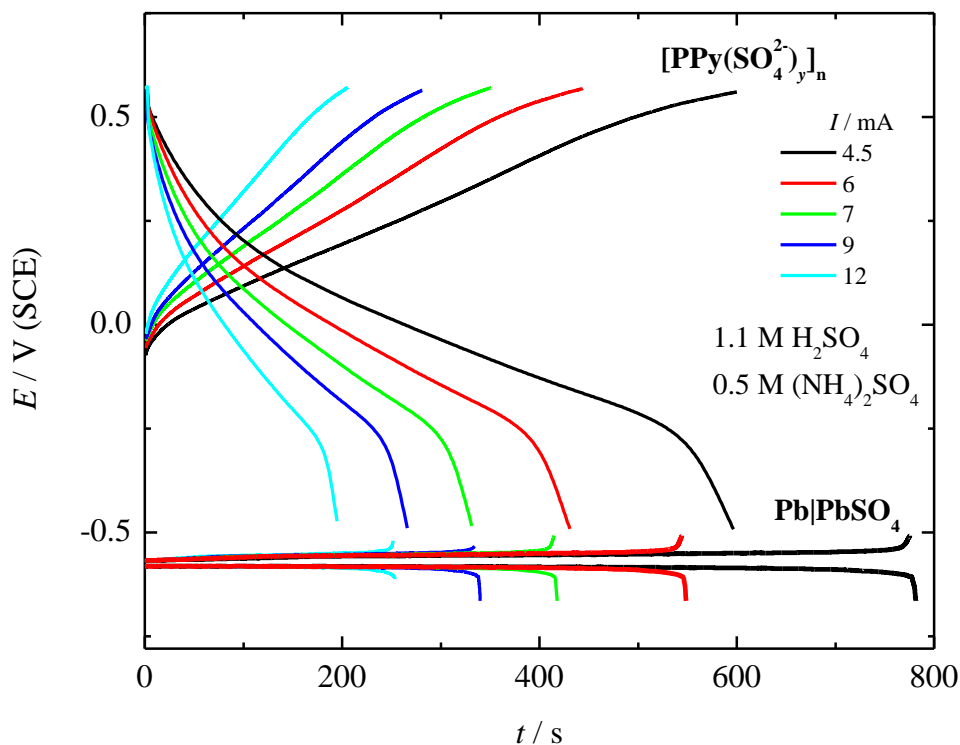
Figure 4.7. Galvonostatic charge-discharge curves of polypyrrole and lead-lead sulfate electrode at different currents.

The charge-discharge cell voltage for different applied currents, in the range of 0.6 to 18 mA, are shown in Fig. 4.8a) and b). Charge of the cell proceeds practically linearly from 0.5 V to 1.15 V, and the discharge from ~1.15 V to 0.05 V, but without linearity. Coulombic efficiency (CE) of charge-discharge, shown in the inset of Fig. 4.8a), decrease from ~107 to 93%. CE higher than 100% for low current can be explained by cation insertion in negatively charged PPy at low potentials, as is observed in cyclic voltammogram, Fig 4.6. From the inset of Fig. 4.8b), it can be seen that the capacity of the charge-discharge process, linearly increase from 0.55 to 0.75 mAh with decreasing current from 18 to ~3 mA, followed by a further increase for low currents, to practically theoretical of ~0.9 mAh. From above presented results it could be suggested that

investigated cell behaves as a supercapacitive-like systems for high current discharge rate, and more battery-like for low current discharge rate.
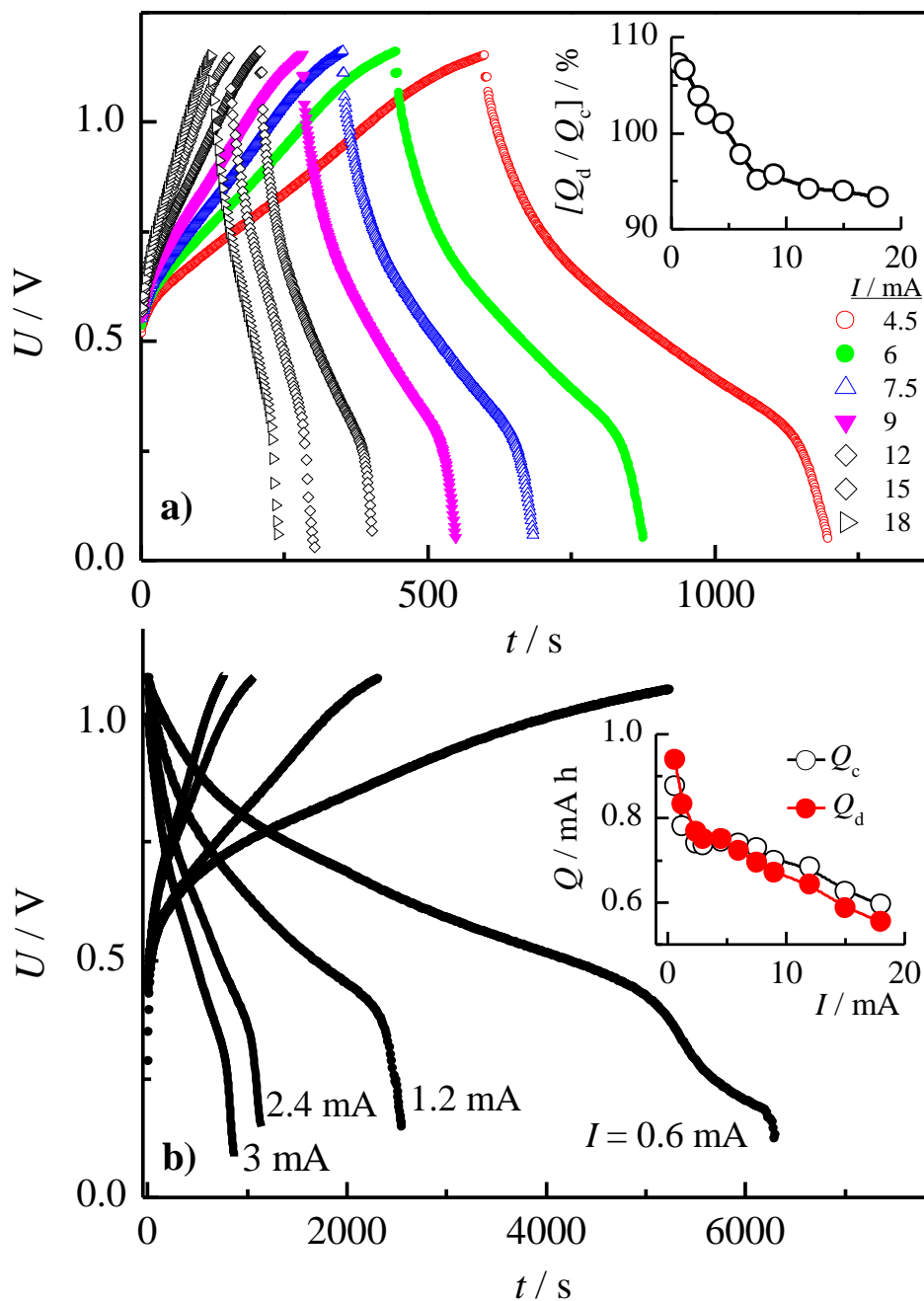
Figure 4.8. The dependence of the Pb|PPy cell voltage over time for different applied currents marked in the figure. Inset in Fig 4.8a): Coulombic efficiency of charge-discharge processes on applied current. Inset in Fig. 4.8b): Dependence of the capacity for charge-discharge process on applied current.

Reactions taking place during discharge were:

$$[PPy^{2y+}(SO_4^{2-})_y]_n + 2yne = [PPy]_n + nySO_4^{2-} \tag{4.2}$$

$$Pb + SO_4^{2-} = PbSO_4 + 2e \tag{4.6}$$

_____

$$[PPy^{2y+}(SO_4^{2-})_y]_n + nyPb = [PPy]_n + nyPbSO_4 \qquad \text{(overall reaction)} \tag{4.8}$$
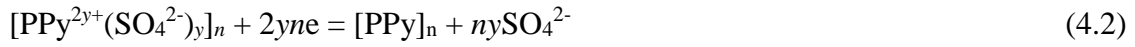
From the overall reaction (Eq. 4.8) it can be seen that there are no changes in the composition of the electrolyte, or changing its concentration (rocking-chair systems). To determine the value of the specific capacity, capacitance, energy and power, the active masses of the participants in the reaction were determined. Applying Faraday's law on Eq. 4.1, the mass of the PPy can be given as [130]:

$$m(PPy) = \frac{I_{pol}t_{pol}[M_M - 2M(H^+) + yM_A]}{(2+2y)\,F} \tag{4.9}$$

where M_M and M_A are molar mass of pyrrole monomer and sulfate anions. For the p-doping of PPy with sulfate anions, and assumed doping degree of 0.33 [124], the estimated mass was 4.8 mg. The masses of the lead sulfate were calculated based on Faraday law and passed charges during every single discharge process. Knowing the active masses:

$$m_T = m(PPy) + m(PbSO_4)$$

specific discharge current was estimated by dividing actual current with the sum of the active masses.

Owning that there was no linearity of the discharge curve, differential discharge capacitance, C_d, for constant discharge current can be calculated using the following equation:

$$dC_d = \left[\frac{\partial q_d}{\partial U} \right]_I \tag{4.10}$$

where specific discharge capacity was given in As g^{-1}. Hence, by differentiation of q_d over U curves presented in Fig. 4.9, the differential capacitance can be obtained, as shown as an example for specific current of 0.68 A g^{-1} (6 mA), in the inset of Fig. 4.9. During discharge, C_d nonlinearly increases from 100 to ~500 F g^{-1} with the maximum of 600 F g^{-1} at 0.3 V.
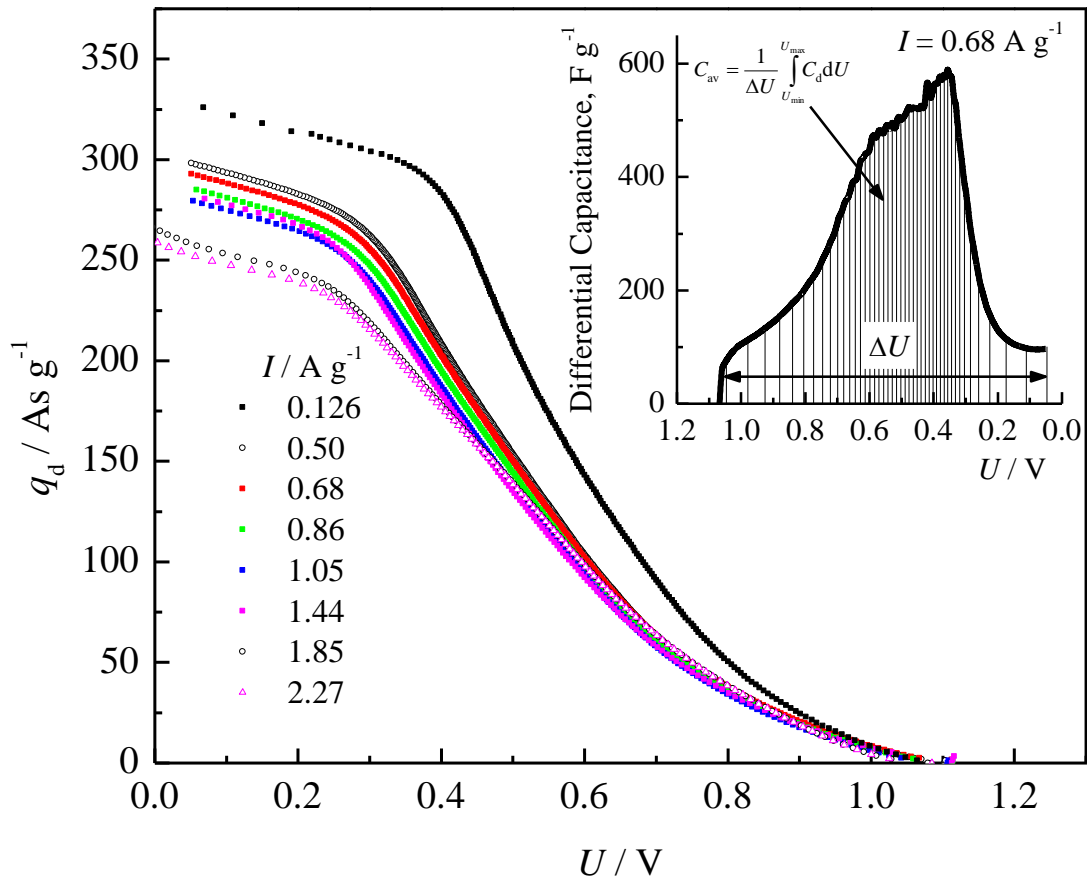
Figure 4.9. The dependence of the specific capacity on the cell voltage. Inset: The dependence of the differential specific capacitance of the cells on the cell voltage.

The average, integral specific discharge cell capacitance, can be calculated using the following equation:

$$C_{av} = \frac{1}{\Delta U} \int_{U_{min}}^{U_{max}} C_d dU \qquad (4.11)$$

and the values were shown in Fig. 4.10. Except for the low discharge current, the average capacitance was in the range of 300-250 F g^{-1}.
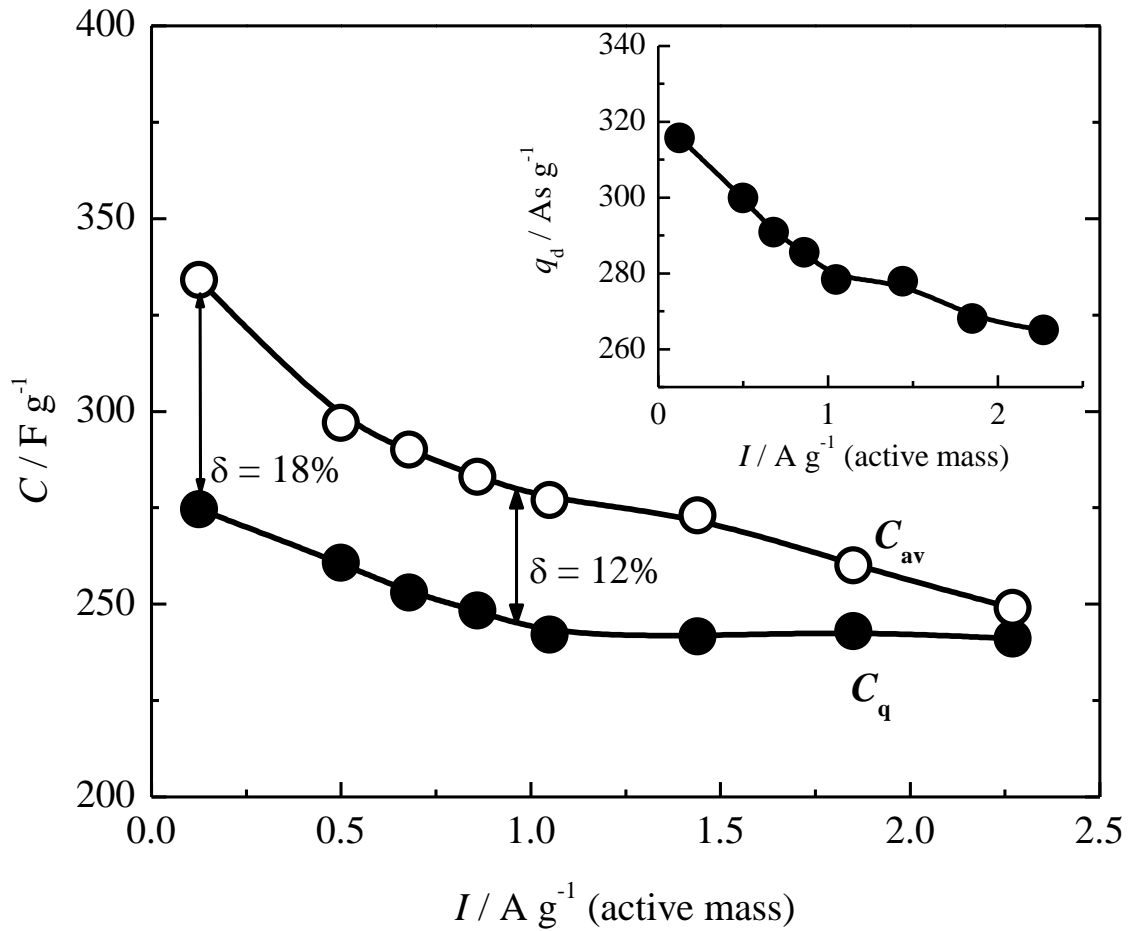
Figure 4.10. Dependence of the specific capacitance calculated using ($\circ$) Eq. 4.11 and ($\bullet$) Eq. 4.12 on the specific current. Inset: Dependence of the specific capacity of the cells on the specific current.

In the literature, the following simplified equation is usually used [67]:

$$C = \frac{\Delta q_d}{\Delta U} = \frac{I_d \, \Delta t_d}{\Delta U} \qquad (4.12)$$

Strictly, this equation can be applied only to the discharge of the EDLC's, in which voltage is practically linear function over time. To compare results obtained using Eqs. 4.11 and 4.12, specific discharge capacity, given in the inset of Fig. 4.10, was divided by $\Delta U = 1.15$ V, Fig. 4.9, and results was shown in Fig. 4.10 together with data calculated using Eq. 4.11. The specific discharge cell capacitance obtained using Eq. 12, ranging from 275 to 245 F g^{-1} was smaller for ~10% than average integral capacity for moderate discharge current, Eq. 12, but become practically equals for high discharge rate. Hence, the approximations used in Eq. 4.12 allows a relatively fast way for the rough estimation of cell capacitance.

Specific discharge energy, w_d, Wh kg^{-1}, and power, P_d, W kg^{-1}, was calculated according to the equations:

$$w_d = \frac{I}{3600} \int_0^t U dt \qquad (4.13)$$

and

$$P_d = \frac{I}{\Delta t} \int_0^t U dt \qquad (4.14)$$

where, 3600 is to convert seconds in hours, and Δt is in seconds.

Increasing specific discharge currents, a specific energy decrease from ~58 Wh kg^{-1} and stabilize to ~40 Wh kg^{-1}, while specific power increases from ~40 to 1350 W kg^{-1}, as shown in Ragone plot, Fig. 4.11. In the inset of Fig. 4.11, the dependence of the specific capacity, ranging from 92 to ~72 Ah kg^{-1}, on specific discharge current was shown.

The obtained values for specific capacity, energy and power, suggests that this system behave as a battery-like for low e.g. <0.5 A g^{-1}, and supercapacitors-like for high discharge currents, >0.5 A g^{-1}.
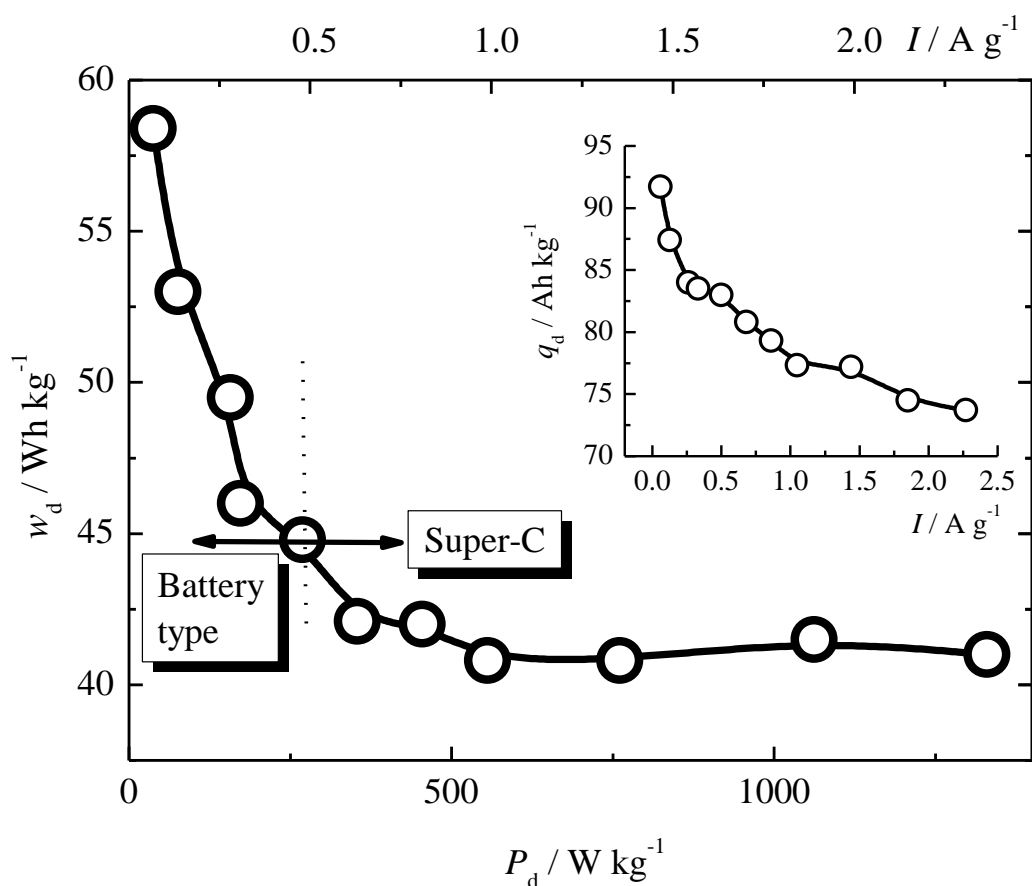
Figure 4.11. Ragone plot of the PbSO$_4$|PPy system. Inset: Dependence of the specific capacity on discharge current.

Battery-type hybrid supercapacitor should allow fast charge and a combination of fast and low discharge rate operation. In that manner, the potential applicability of such a system, was examined as follow. The cell was first cycled during twenty cycles, Fig. 12a, of the fast charge rate (1.85 A g^{-1}, 15 mA) keeping constant charge time of 140 s and capacity of 0.58 mAh, and low discharge rate (0.27 A g^{-1}, 3 mA (a) to the cutoff voltage of 0.1 V,) Fig. 12a. Discharge capacity gradually increases during first fourth cycles, and stabilizes to 0.59 mAh, reaching the Coulombic efficiency of 100%. After that, the cell was cycled fifty cycles with charge current of 15 mA (1.85 A g^{-1}) for the fixed time of 135 s, and discharged with the same current to the cutoff voltage of ~0.1 V, as shown in Fig. 12b).
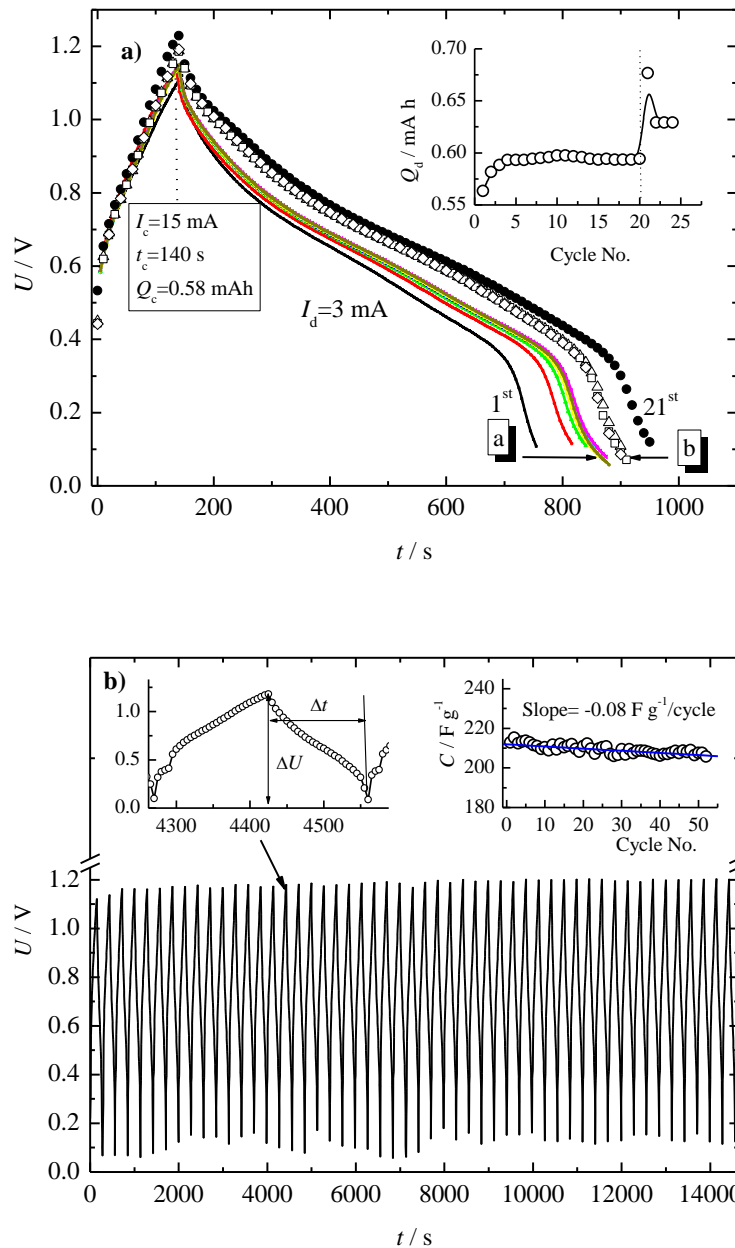
Figure 4.12. Cycle performance of Pb-PbSO$_4$|PPy cell. a) Batery-mode operation, (charge: 15 mA (1.85 A g^{-1}) during constant charge time of 140 s, discharge (3 mA, 0.27 A g^{-1}) before (a) and after (b) supercapacitors-mode cycling. Inset: calculated discharge capacity over cycle number. b) Supercapacitor-mode operation (charge: 15 mA, 1.85 A g^{-1}) for fixed time of 135 s, and discharged with same current to the cut-off voltage of ~0.1 V. Insets: magnification of charge-discharge cycle and determination of ΔU and Δt (left); Calculated specific capacitance over cycle number (right).

The discharge capacitance was calculated using Eq. 4.12, with the determined ΔU and Δt, as shown in the left inset of Fig. 12b) for each cycle. The dependence of the discharge specific capacitance over cycle numbers was shown in the right inset of Fig. 12b).. The specific capacitance gradually decreases from the initial, of ~215 F g^{-1} with the rate of ~0.08 F g^{-1} per cycle, caused by the increase of the voltage from 1.15 to ~1.2 V. Knowing this, it is possible to estimate cycle life for cell, to ~500-550 cycles for the decrease of the capacitance to 80% of its initial values. Possible deterioration of the characteristics occurred if PPy electrode was charged above potentials of ~0.55 V vs. SCE ($U_c > 1.15$ V), for a longer period of time. To avoid this, cell capacity should be limited with a smaller active mass of lead-lead sulfate electrode, which is not sensitive to over-charge. In that case, charging voltage will sharply increase after all lead sulfate was converted to lead, without hydrogen evolution reaction, due to the extremely high hydrogen overvoltages on the lead. After fifty fast charge-discharge cycles, cell was again tested in the battery mod, Fig. 12a), during fourth cycles (b). Some increase of the capacity could be explained by the expansion of the PPy layer and increased numbers of the available sites for doping/dedoping reaction, or by the reduction of overoxidized polymer backbones.

4.1.1. Comparison with the theoretical values

To compare obtained values with the theoretical one, the following analysis was performed.

Gravimetric specific capacity of a single PPy electrode is calculated from the equation:

$$q_{s,t}(\text{PPy}) = \frac{zy}{2+zy} q_{pol} = \frac{zym(\text{PPy})F}{[M_M - 2M(\text{H}^+) + yM_A]} \tag{4.15}$$

taking into account that q_{pol} is:

$$q_{pol}(\text{PPy}) = \frac{m(\text{PPy})(2+zy)F}{[M_M - 2M(\text{H}^+) + yM_A]} \tag{4.16}$$

Hence, for 1 g of PPy, doped with sulfate anions, $z = 2$, at doping degree of 0.33, theoretical specific discharge capacity is 183 mAh g^{-1}. From Fig. 4.7, it can be seen that potential window for polypyrrole is 1 V. Accordingly, theoretical specific capacitance for polypyrrole doped with sulfate anions is:

$$C_{s,t}(\text{PPy}) = \frac{q_{s,t} \times 3600}{\Delta E} = 659 \text{ F g}^{-1} \tag{4.17}$$

Theoretical specific capacitance for lead sulfate, for potential window of ~0.1 V, Fig. 4.7, is:

$$C_{s,t}(\text{PbSO}_4) = \frac{n \times F}{\Delta E \times M(\text{PbSO}_4)} = 6370 \text{ F g}^{-1} \tag{4.18}$$

For an asymmetric supercapacitor, the theoretical gravimetric cell capacitance $C_{m,t}$ can be calculated from the specific electrode capacitances according to [131]:

$$C_{m,t} = \frac{C}{m} = \left[m \left(\frac{1}{m_+ C_+} + \frac{1}{m_- C_-} \right) \right]^{-1} \tag{4.19}$$

where m is the total mass of active materials, C_+, m_+, C_-, and m_- denote the specific capacitances and the masses of the positive and negative electrodes, respectively. The corresponding mass of lead sulfate for a discharge capacity of 183 mAh, according to Faraday law is 1.03 g, so the theoretical gravimetric cell capacitance will be 296 F g^{-1}. This value is, ~15% greater than obtained for faster discharge times, Fig. 4.10, but it was approached for battery-type operation, e.g. at low discharge currents.

Corresponding theoretical specific energy, for the cell voltage of 1.15 V:

$$w_{m,t} = \frac{C \Delta U^2}{2 \times 3.6} \tag{4.20}$$

will be 54 Wh kg^{-1}. In our case, Fig 4.11, this value is obtained for low current discharge rate, but for the higher discharge rate is ~25% greater than observed.

Because specific power depends on discharge time:

$$P_{m,t} = \frac{w_{m,t} \times 3600}{\Delta t}$$

(4.21)

as an example, for specific discharge current of 2.27 A g^{-1} obtained discharge time is 110 s, and specific power is 1330 W kg^{-1}, Fig 4.11. Theoretically, according to Eq. 4.21 specific power will be 1.77 kW kg^{-1}, or ~25% greater than experimentally obtained. In an extreme case, discharge within 10 s, such device could deliver power as high as 19.5 kW kg^{-1}.

During the battery-type operation, theoretical specific capacity of the cell is defined:

$$q_{m,t}(PPy \mid PbSO_4) = \left(\frac{1}{q(PPy)} + \frac{1}{q(PbSO4)} \right)^{-1}$$

(4.22)

or:

$$q_{m,t}(PPy \mid PbSO_4) = \left[\frac{2yF}{M_M - 2M_{H^+} + yM_A} + \frac{2F}{M(PbSO_4)} \right]^{-1}$$

(4.23)

and will be 90 mAh g^{-1}, which was obtained value for low current discharge rates, Fig 4.11.

Considering the capacitive and battery type operation, according to Eq. 4.20, it can be concluded that energy limited electrode is mainly polypyrrole, due high potential drop during discharge, connected with solid state diffusion limitation of the anion doping/dedoping reaction. The influence of the electrode materials on the maximum power is more complex. It can be shown that maximum power obtained at a minimum discharge time, t_{min}, of the cell is proportional to $2CR_{sr}$, where R_{sr} is the equivalent series resistance of the cell [67]. Because $C(PbSO_4)$ is ten times higher than $C(PPy)$, t_{min} is determined by the capacitance of PbSO$_4$ electrode. On the other hand, the conductivity of the polypyrrole decrease with decrease of the doping degree, so increase in the equivalent series resistance during discharge, and decrease of power should be connected with polypyrrole electrode, as well. On more limitation on the power arise

from the slow recrystallization rate of the lead sulfate. Namely, at high currents during charge, lead sulfate crystalizes as large crystals, which are difficult to completely reduce to lead during fast discharge [132].

Based on presented values, of the specific capacity, energy and power, and bearing in mind that the cell voltage is ~1 V, such inexpensive device could be considered for the energy storage obtained from low operation voltage converters, like different photoelectrochemical cells, biofuel cells and similar.

4.2. Supercapacitor based on polyaniline and lead-lead sulfate

Figure 4.13 shows an electrochemical synthesis of polyaniline (PANI) and Pb-PbSO$_4$ active electrode materials on graphite and the thin film lead plane, respectively. Aniline electropolymerization from the aniline monomer (ANI) under galvanostatic conditions occurred at the potentials of ~0.75 V according to the following reaction:

$$n\text{ANI} + n(y/2)\text{SO}_4^{2-} \rightarrow [\text{PANI}^{y+}(\text{SO}_4^{2-})_{y/2}]_n + 2n\text{H}^+ + (2 + y)n\text{e} \qquad (4.24)$$
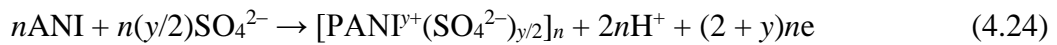
where y corresponds to the degree of doping. It was generally accepted that the first step of the polymerization of the aniline, considered as the rate-determining, involves formation of aniline radical cation, followed by coupling and elimination of two protons. After the rearomatization firstly dimer was formed, and further oligomers. The chain propagation occurred by coupling oligomer radical cation with the anilinium radical cation, with simultaneous incorporation of the anions, doping, into the polymer chain [133,134, 135].

Spongy lead sulfate was produced by the galvanostatic oxidation of pure lead to lead dioxide, PbO$_2$, in 1 M H$_2$SO$_4$ with the addition of 0.05 M KClO$_4$ as an oxidizing agent, as shown in Fig. 1 [136]. Formed lead dioxide was then reduced to the lead sulfate and lead in the same solution, according to the reactions:

$$\text{PbO}_2 + \text{SO}_4^{2-} + 4\text{H}^+ + 2\text{e} \rightleftarrows \text{PbSO}_4 + 2\text{H}_2\text{O} \qquad (4.25)$$

$$\text{PbSO}_4 + 2\text{e} \rightleftarrows \text{Pb} + \text{SO}_4^{2-} \qquad (4.26)$$

After washing, the electrode was again oxidized to spongy lead dioxide, but in pure 1 M H$_2$SO$_4$, inset in Fig. 4.13, and then few time reduced to pure lead and oxidized to lead sulfate at the potentials around ~–0.6 V.
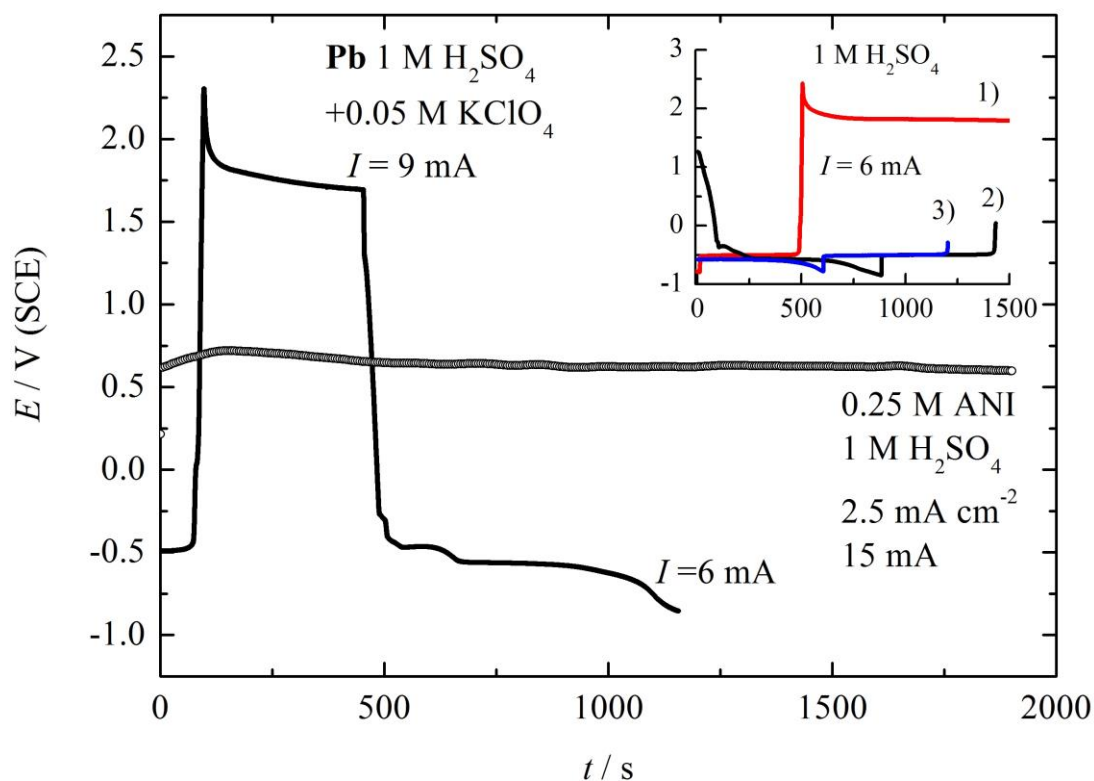
Figure 4.13. Galvanostatic formation of the active materials.

The UV-visible absorption spectra of the as synthesized PANI dispersions in 1 M H_2SO_4 aqueous solution, from 190 to 1100 nm was shown in Fig. 4.14. Spectra exhibits the local absorption maximum at 341 nm that corresponds to $\pi-\pi^*$ transition of the benzenoid ring. The band observed in the visible region at 434 nm were associated with the presence of polaron state (charged cation radical, quinoid form) and assigned to polaron$-\pi^*$, so called exciton [137]. Broad absorption above ~550 nm was associated with polaronic structures in the polyaniline, with theoretical absorption maximum at ~850 nm, corresponding to $\pi-$polaron transitions. Hence, it can be concluded that as synthesized polyaniline was in the polaronic, emeraldine salt form [138].
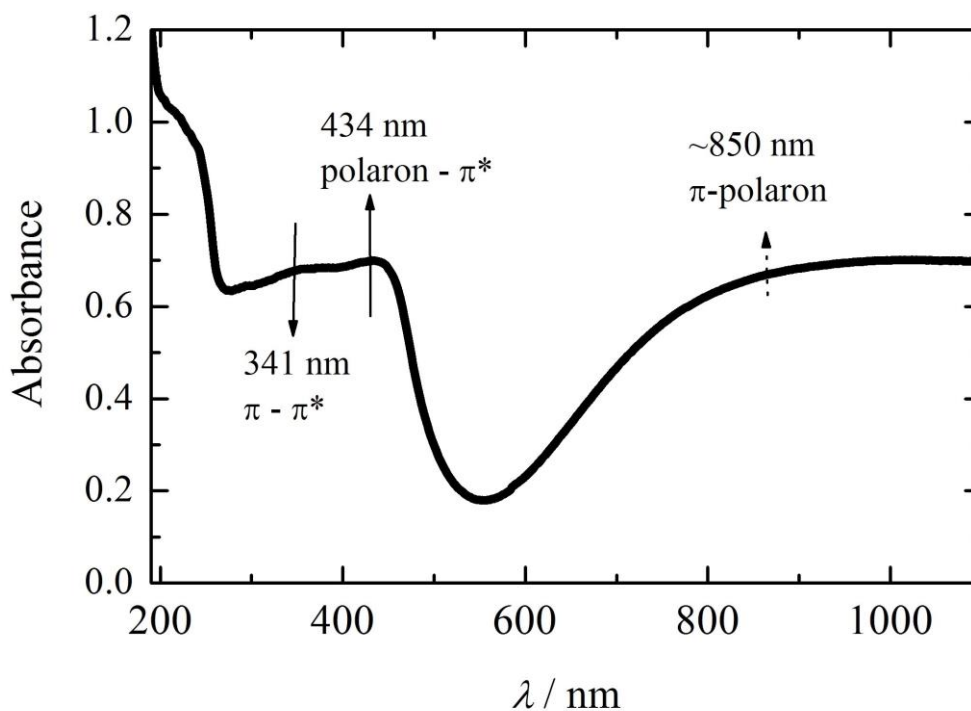
Figure 4.14. UV-vis spectra of as synthetized polyaniline.

In Fig. 4.15 the cyclic voltammograms of the examined materials were shown. Doping of the PANI in the emeraldine form starts at ~ –0.1 V, and proceed up to the potential of ~0.35 V. Above that potential, possible degradation of the PANI could occurred [139 140 141]. The dominant degradation product was proposed to be water soluble benzoquinone with the redox couple of the benzoquinone-hydroquinone [140]. Insoluble and inactive degradation products were suggested to remain on the electrode surface, like PANI strands containing quinoneimine end groups and ortho-coupled oligomers [140,141]. The dedoping reaction of the PANI occurred in the broad potential range, from 0.5 to –0.3 V.

The formal potential of the lead sulfate-lead electrode of –0.55 V was estimated from Fig. 4.15. Below that potential reduction of the lead sulfate to spongy lead occurred, and above that potentials oxidation of lead to lead sulfate, Eq. 4.26.
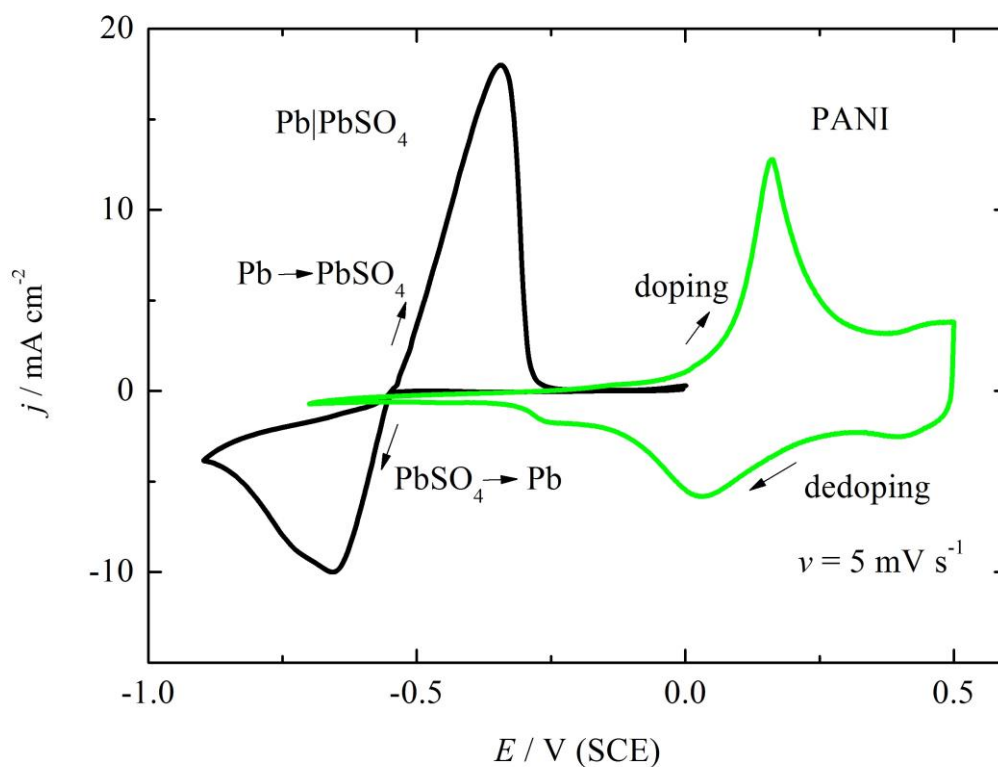
Figure 4.15. Cyclic voltammograms of the investigated materials in 1 M H_2SO_4.

In Fig. 4.16 the charge-discharge curves for investigated materials were shown. A charge of PANI electrode occurred in the potential range of 0.05 V to 0.4 V, and discharge from 0.4 to –0.15 V, followed by sharp potential decrease caused by diffusion limitations of sulfate anions in dedoping reaction to the –0.4 V. Coulombic efficiency of charge-discharge was around 100%, and obtained discharge electrode capacity depends on applied current ranging from 0.85 mAh for low currents to 0.7 mAh for higher currents, inset in Fig. 4.16. Reduction of lead sulfate occurred at potentials from ~–0.6 to –0.8 V, while most of the lead oxidation to lead sulfate occurred at potential of ~–0.5 V. The capacity of the charge-discharge was around 1 mAh, inset in Fig. 4.16.
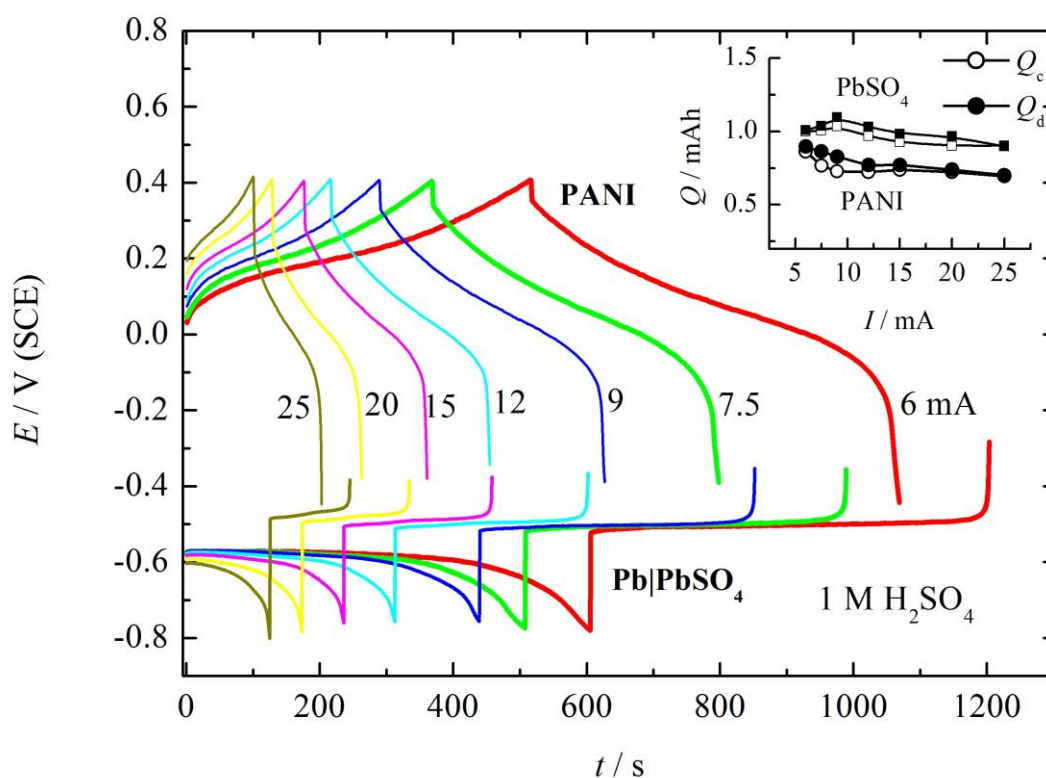
Figure 4.16. Charge-discharge curves of the investigated materials for different currents. Inset: obtained charge (open symbols) and discharge (full symbols) capacity for PANI (cycles) and PbSO₄ (squares) electrodes.

The polyaniline structure strongly depends on applied potential [142 143]. The potential regions of dominant structures in 0.1 M H_2SO_4 were reported as: –0.2 to 0.075 V (SCE) leucoemeraldine ($y = 0$); 0.075 to 0.675 V emeraldine ($y = 0.5$), with substructures: 0.075 to 0.19 V polaron, 0.19 to 0.55 V polaron lattice, 0.55 to 0.675 V bipolaron, and above 0.675 V pernigraniline ($y = 1$) [142]. It was also reported that most of the redox capacitance in 1 M H_2SO_4, ~76%, originated from the PANI polaron structure. Structural analysis of the doping of PANI with divalent anions, to the best of our knowledge, was not treated in the literature. For the single charged anions e.g. chloride, perchlorate etc. the connection of the available (Q) and polymerization charge (Q_p) can be given by the following equation:

$$Q = \frac{y}{2+y}Q_p \tag{4.27}$$

Hence, for the polymerization charge of 7.9 mAh, corresponding available charge for y = 0.5 (polaronic emeraldine state) will be 1.58 mAh, which was almost twice than obtained. Based on the average PANI doping-dedoping charge of ~0.85 to 0.7 mAh, it could be proposed that divalent sulfate anions were banded to crosslinked parallel polymer chains in the polaron state, as shown in Fig. 4.17. In that way one polymer units (consisted of four monomer units) will have a doping degree of 0.5 (emeraldine state), but whole polymer will be doped only with $n \times y/2$ anions.
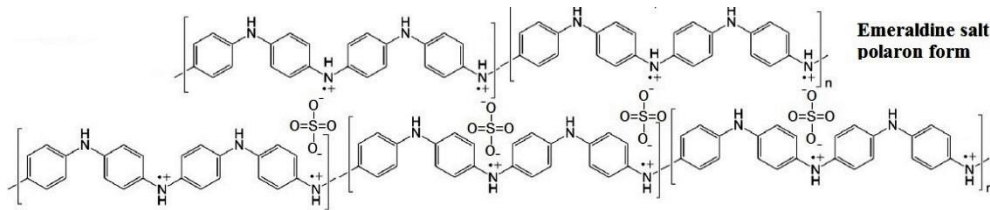
Figure 4.17. The proposed structure of polymer chain crosslinking with the sulfate anions in the emeraldine –polaron state of the polyaniline.

Based on these considerations, the total polymerization charge, Q_p, of the polyaniline electropolymerization reaction, Eq. 4.21, was given as:

$$Q_p = I_p\, t_p = (2+y)neF \tag{4.28}$$

where y is doping degree. The p-doping/dedoping reaction with sulfate anions was:

$$[\text{PANI}^{y+}(\text{SO}_4^{2-})_{y/2}]_n + (y/2)ne \rightleftarrows [\text{PANI}^0]_n + n(y/2)\text{SO}_4^{2-} \tag{4.29}$$
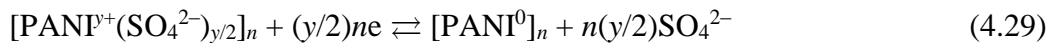
and the theoretical available doping/dedoping capacity was given as:

$$Q = It = (y/2)neF \tag{4.30}$$

Relating equations (4.28) and (4.29), available capacity can be connected with polymerization charge with the following equation:

$$Q = \frac{(y/2)}{2+y}Q_{\mathrm{p}} = \frac{(y/2)}{2+y}I_{\mathrm{p}}t_{\mathrm{p}} \qquad (4.31)$$

Consequently, for the polymerization charge of 7.9 mAh, and for the theoretical doping degree of 0.5 (two sulfate anions per polymer units) [22, 144], available dedoping charge can be estimated to 0.8 mAh, which was in excellent agreement with experimentally obtained value. For the further calculations of the specific values, it was necessary to calculate the as synthesized PANI mass. The mass of the electropolymerized PANI was related to the total polymerization charge (Q_{p}), and can be represented, according to the Faraday law, by the following equation:

$$m(\mathrm{PANI}) = \frac{I_{\mathrm{p}}t_{\mathrm{p}}[M_{\mathrm{M}} - 2M(\mathrm{H}^{+}) + (y/2)M_{\mathrm{A}}]}{(2+y)F} \qquad (4.32)$$

where, F is the Faraday constant, M_{M} and M_{A} the molar masses of the aniline monomer unit (93.13 g mol^{-1}) and the sulfate anion (96.09 g mol^{-1}), respectively. The mass of the electropolymerized PANI for $y = 0.5$ was estimated to 13 mg. From Eqs. 4.31 and 4.32, it was possible to recalculate specific capacity (q) of the doped PANI in the range of 58 mAh g^{-1}. Accordingly, the PANI specific capacitance of 262 F g^{-1}, can be obtained from the following equation:

$$C(\mathrm{PANI}) = \frac{q \times 3600}{\Delta E} \qquad (4.33)$$

where 3600 is to convert Ah g^{-1} in C g^{-1}, and ΔE was discharge potential window, ~0.8 V. On the other hand, the specific capacitance of the PbSO$_4$ electrode in the range of 1600 F g^{-1}, could be estimated for 1 g of PbSO$_4$ and using an equation:

$$C(\mathrm{PbSO}_4) = \frac{nF \times 3600}{M(\mathrm{PbSO}_4)\Delta E} \qquad (4.34)$$

where F is Faraday constant (26.8 Ah mol^{-1}), and $\triangle E$ was around 0.4 V. Consequently, for serial connection of PANI and PbSO$_4$ electrode, the overall cell capacitance, given as:

$$\frac{1}{C} = \frac{1}{C(\text{PANI})} + \frac{1}{C(\text{PbSO}_4)} \tag{4.35}$$

was in the range of 224 F g^{-1}, suggesting that $C(\text{PbSO}_4)$ slightly contributed to the capacitance of the cell. In the same manner the theoretical specific capacity of the cell:

$$\frac{1}{q_{\text{cell}}} = \frac{1}{q(\text{PANI})} + \frac{1}{q(\text{PbSO}_4)} = \frac{1}{q(\text{PANI})} + \frac{M(\text{PbSO}_4)}{2F} \tag{4.36}$$

could be estimated to 44 mAh g^{-1}.

Figure 4.18 shows charge-discharge curves of the PbSO$_4$|PANI cell for different currents, while limiting the potential of the PANI electrode to 0.4 V.
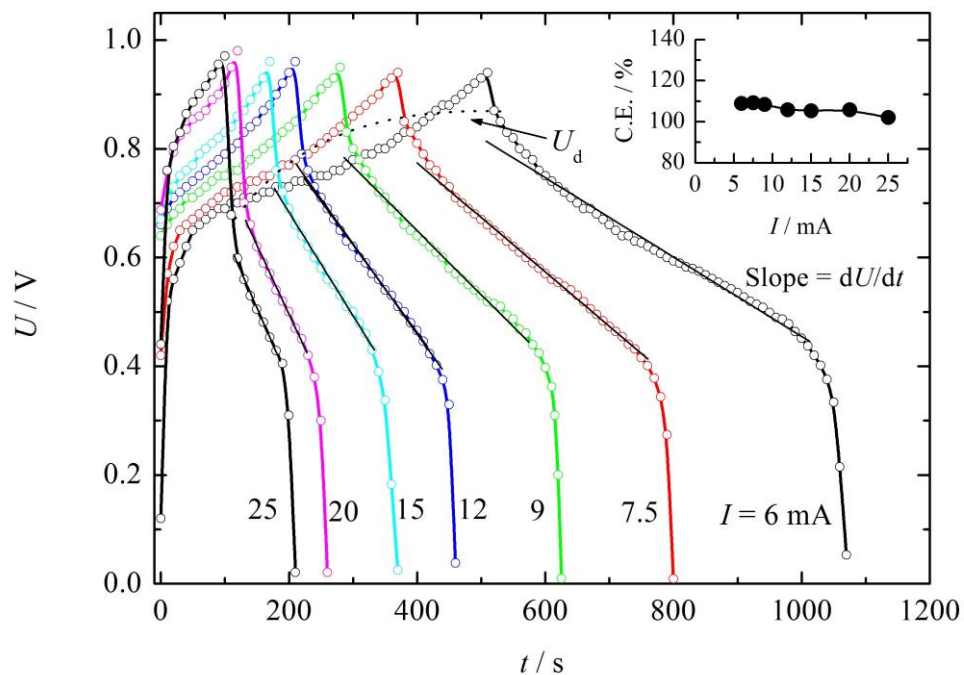
Figure 4.18. Charge-discharge curves of the PbSO$_4$|PANI cell for different currents. Inset: Coulombic efficiency of charge-discharge process.

Charge of the cell occurred above 0.5 V up to ~0.95 V, while beginning of the discharge voltage, U_d, nonlinearly decreases from 0.85 to 0.65 V with increased applied current, caused by Ohmic drop and polarization resistances of the electrodes, see Fig. 4.16. Coulombic efficiency (C.E.) slightly decreases from 108% to 101%, inset in Fig. 4.18, by increased current, probably due reduction of an overoxidized polyaniline products.

In order to determine the nature of relatively high initial voltage drops, the followed analysis was performed. In Fig. 4.19a the electrochemical impedance spectra of the charged cell, using the counter spongy lead electrode as a reference, was shown. Impedance spectra was characterized with small semicircle at higher frequencies, and straight line with the slope near 90° characteristics for pseudocapacitive materials. From the high frequency intercept with Z' axis, the cell resistance of 7.8 Ω was determined. The conductivity of 1 M H_2SO_4 was 26×10^{-2} $Ω^{-1}$ cm^{-1}, so the pure electrolyte resistance (for inter electrode distance of 2 cm and electrode area of 6 cm^2) will be in the range of ~1.3 Ω. Hence, the rest of the resistivity of ~6.5 Ω could be connected with PANI electrode, because resistance of the charged spongy lead can be neglected. Using the determined value of the cell resistance of 7.8 Ω, in Fig. 4.19 with dotted line was shown theoretical dependence of the voltage drop, $IR_Ω$, caused only with the Ohmic resistance. Experimentally determined total voltage drop, IR, during discharge, also shown in Fig. 4.19, point to Ohmic like behavior, with the slope of 13.3 Ω. The total cell resistance, R_{cell}, calculated using the Ohm law slightly depends on applied current, Fig. 4.19b. Hence, the total cell voltage drop can be given as $I(R_p+R_Ω)$, where R_p was polarization resistance. The value of R_p, to some extent depends on applied current, Fig. 4.19b, and can be mainly connected with the increased resistance of the outer surface PANI layer due fast dedoping (discharge) and slow diffusion of the dopant anion from the bulk of the polymer. Also, in some extent the voltage drop during discharge could be also connect with the initial transitions due diffusion controlled solid state reaction of the spongy lead transformation to the lead sulfate.
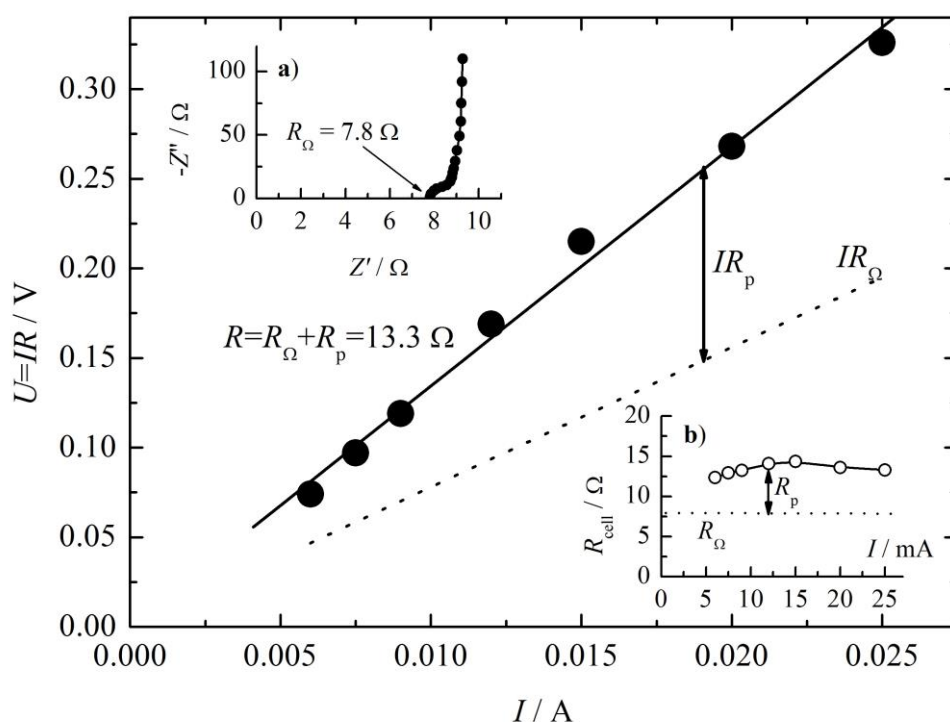
Figure 4.19. Experimentally determined voltage drop, *IR*, during initial cell discharge. Insets: a) Impedance spectra of charged cell. b) Calculated total cell resistance using the Ohms law.

Usually, in the literature the simplified method was used to obtain values of specific capacitances, energy and power. From the determined slopes, dU/dt, during discharge in Fig. 4.18 the specific capacitance of the cell was estimated by applying the following equation:

$$C_{cell} = \frac{I}{(dU/dt)\left[m(PANI)+m(PbSO_4)\right]} \qquad (4.37)$$

where I, A, was discharge current, $m(PANI)$ estimated PANI mass in a doped state of 13 mg, and $m(PbSO_4)$ was valued by the each discharge current and corresponding times using the Faraday law. The calculated values of the specific capacitances of the $PbSO_4|PANI$ cell, ranging around 450 F g^{-1}, shown in Fig. 4.20a), were practically independent on applied specific current. The obtained values using Eq 4.37, seem to be overestimated in the comparison with the theoretically calculated one of 224 F g^{-1}. It is interesting to note that the specific capacitance of the cell practically did not vary with

applied current, as usually obtained [145]. From the determined values of the specific capacitances, the maximum specific energy, w_{cell}, Wh kg^{-1}, and power, P_{cell}, W kg^{-1}, was obtained using equations:

$$w_{cell} = \frac{1}{2 \times 3.6} CU_d^2 \qquad \text{and:} \quad P_{cell} = \frac{w \times 3600}{t_d} \tag{4.38}$$

where U_d - was taken from Fig. 4.18, and t_d was in seconds. The dependence of specific energy and power was shown in Fig. 4.20, with curve 2, in the form of Ragone plot. By increasing the current, specific energy decrease from 47 to 27 Wh kg^{-1}, while specific power increased from 300 to ~1000 W kg^{-1}.

More reliable method for the determination of specific energy and power of such a cell, at constant specific discharge current, I_d, A g^{-1}, was to use the integral form of specific energy:

$$w_{cell} = \frac{I_d}{3600} \int_0^t U dt \tag{4.39}$$

and specific power:

$$P_{cell} = \frac{I_d}{\Delta t_d} \int_0^t U dt \tag{4.40}$$

The calculated values were given with line 1 in Fig. 4.20. The specific energy decrease from 30 to 20 Wh kg^{-1}, while the specific power increased from 200 to ~800 W kg^{-1}, by increasing specific current. The specific capacitance of the cell in the range of 215 to 230 F g^{-1}, were calculated using the following equation

$$C_{cell} = \frac{I_d t_d}{U_d} \tag{4.41}$$

where t_d was in seconds. These values were in good agreement with theoretically calculated of 224 F g^{-1}. Specific capacity of the cell, Fig. 4.20b), slightly decrease from 47 mAh g^{-1} to 40 mAh g^{-1} by increasing the specific current, which was in good agreement with the theoretical value of 44 mAh g^{-1}. According to the obtained specific energy and power, such device could be classified as a supercapattery cell [12].
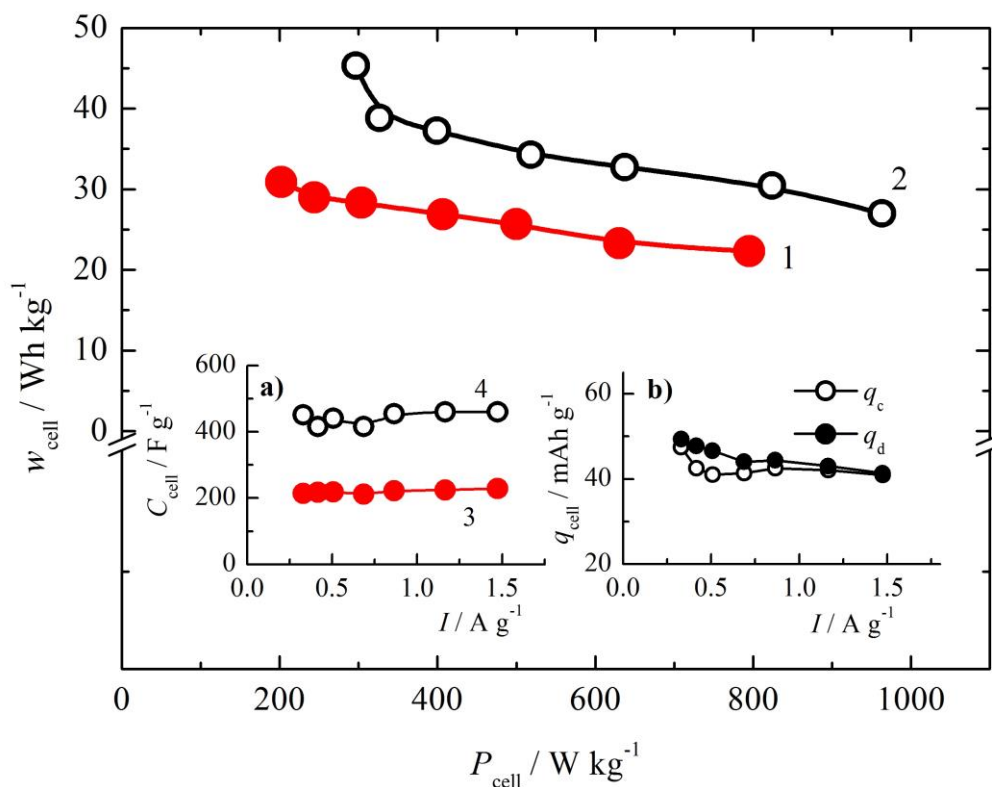
Figure 4.20. Ragone plot for PbSO$_4$|PANI cell, values calculate using 1) Eqs. 4.39 and 4.40, 2) Eq. 4.38; a) The dependence of the specific discharge capacitance calculated using 3) Eq. 4.41 and 4) Eq 4.37; b) The dependence of the cell specific capacity on applied specific currents.

The cycling performances of the cell were investigated over 44 cycles, Fig. 4.21, applying the current of 15 mA (0.864 A g^{-1}), with duration of 200 s for charge and discharge cycle, respectively. For the each discharge curve the capacitance was determined, using the simplified method given by Eq. 4.12, from the linear part of the discharge curve, Fig. 4.21a). Plotting the dependence of the obtained specific capacitance over cycle number, the decrease of -0.16 F g^{-1} per cycle was determined. Hence, it could be estimated that from an initial value of 445 F g^{-1}, 20% of capacitance loss will be achieved after ~550 to 600 cycles. Estimated cycle numbers were in good agreement reported for pure polyaniline electrode [146, 147, 148, 149] as well as for pure lead sulfate electrode [150].
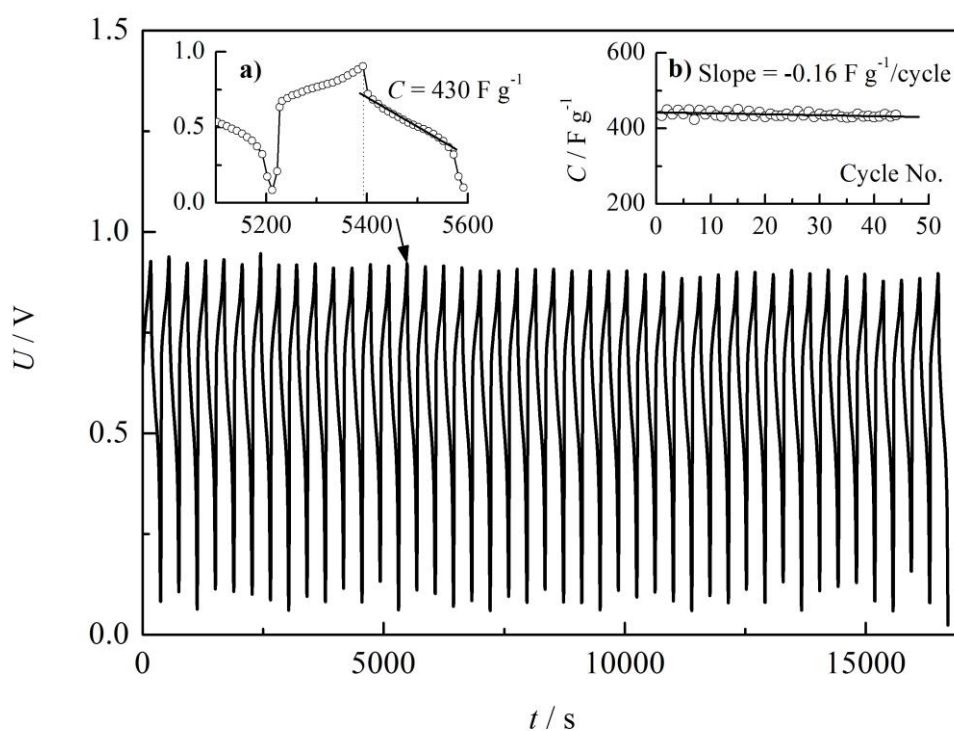
Figure 4.21. Cycling behavior of the PbSO₄|PANI call. a) The determination of the specific discharge capacitance. b) The dependence of the specific capacitance on cycle number.

Pure polyaniline electrode experience large volumetric swelling and shrinking during charge/discharge process as a result of ion doping and dedoping [151]. This volumetric interchange often leads to structural failure and thus relatively fast capacitance deterioration. Apparently, most polyaniline and polypyrrole based electrodes retain less than 50% of the initial capacitance after ~1000 cycles. Therefore, cycling instability is a major obstacle for practical applications of pure conductive polymer electrodes. Enormous stability improvement of the polyaniline and polypyrrole electrodes was recently achieved by Liu et al. [152] depositing a thin carbonaceous shell onto polymer surface, by a hydrothermal reaction using glucose as carbon precursor. Carbonaceous shell-coated polyaniline and polypyrrole electrodes reached remarkable capacitance retentions of ~95 and ~85% after 10.000 cycles. On the other hand, it was reported that 80% of the capacity loss occurred after approximately 450 to 500 cycles of pure lead sulfate under deep discharge, ~100 DOD [150]. This could be significantly improved by

adding a small amount of the different carbon materials into the active mass of lead sulfate electrode [153 154]. Addition of the carbon materials could also have beneficial effect on the cell resistivity.

4.3. Comparison with other electrochemical power source

Among batteries, electrochemical double layer supercapacitors (EDSC) and asymmetric hybrid systems, for asymmetric hybrid battery systems is expected to increase in specific power in comparison with battery and in specific energy in comparison with asymmetric hybrid supercapacitors. Typically, battery has specific energies and power up to 100 Wh kg^{-1} and 100 W kg^{-1} [87], asymmetric hybrid estimated from tables 2.5 and 2.6 [62] energy up to 30 Wh kg^{-1} and power in the range of 0.5-5 kW kg^{-1} while EDSC maximum energy up to 10 Wh kg^{-1} with power up to 20 kW kg^{-1} [6]. In Fig. 4.22 the comparisons of the typical values of existing power sources with experimentally obtained for the PbSO$_4$|PPy and PbSO$_4$|PANI systems are shown.
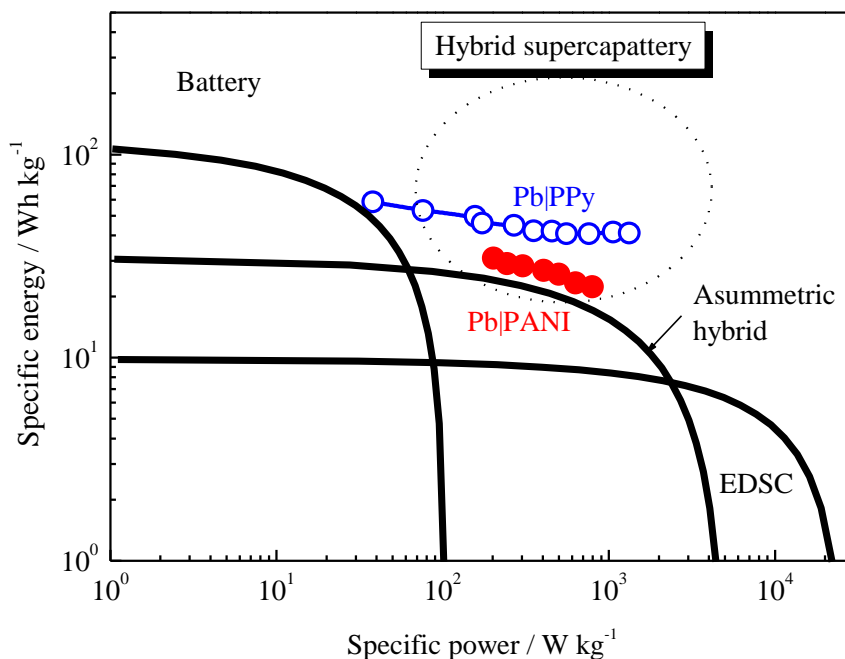
Figure 4.22. Estimated Ragone plot of typical electrochemical power sources in comparison with experimentally determined for PbSO$_4$|PPy and PbSO$_4$|PANI systems [6,62,87].

It can be seen that an increase in the specific energy is achieved in comparisons with batteries, asymmetric hybrid and especially electrochemical double layer supercapacitors. For both investigated systems, specific power is significantly increased in comparison with batteries, but are in the medium range of asymmetric supercapacitors.

The systems $PbSO_4|PPy$ shows very promising characteristics with specific energy of ~50 to 60 Wh kg^{-1}, retaining specific power of ~100 to 200 W kg^{-1}. On the other hand, for specific power of ~1 kW kg^{-1}, the specific energy of 30 Wh kg^{-1} is sufficiently higher than asymmetric hybrids.

Hence, a further modifications and improvement of both positive and negative electrode in the investigated systems should be performed, by the means of increase of the specific energy, power and especially cycle life (~600 cycles) which is in the range of a typical batteries, but lower than asymmetric hybrids. Such improvement could be achieved using the composite electrode materials. For example, modification of different carbon materials with high surface area with polypyrrole and lead sulfate, which will improve specific power and cycle life.

5. CONCLUSIONS

Polypyrrole as a positive and lead-lead sulfate electrode was investigated as a material of supercapacitors in acidic sulfate solutions. It was determined that operating cell voltage window is ~1.1 V, with the specific capacity of the cell in the range of 300-250 F g^{-1}. At low discharge rates, e.g. <0.5 A g^{-1}, the device exhibits battery-type behavior, and at a higher discharge rate supercapacitors-type behavior. Obtained values, of the specific capacity of 90-72 Ah kg^{-1}, energy of 58-40 Wh kg^{-1} and power of ~40-1350 W kg^{-1}, suggests that such inexpensive device, after further optimization, could be considered for energy storage obtained from low operation voltage converters, like different photoelectrochemical cells, biofuel cells and similar. Because, the theoretical values of experimentally determined parameters are, at least 20% higher, further optimization in the sense of the polypyrrole layer thickness, electrolyte concentration, internal resistance of the cell, possible problems with lead dendrite formations, *etc*. The main problem with such device could be degradation of polypyrrole if charged above voltage of 1.15 V (0.5 V *vs.* SCE). But this can be avoided with limitation of negative active mass weight.

The charge-discharge reactions of the electrochemically formed polyaniline ad lead-lead sulfate in 1 M H$_2$SO$_4$ were investigated. It was proposed that divalent sulfate anions were banded to crosslinked parallel polyaniline chains in the polaron state. In that way one polymer units (consisted of four monomer units) will have a doping degree of $y = 0.5$ (emeraldine state), but whole polymer will be doped only with $y/2$ anions. The two mathematical methods for the determination of the cell electric characteristic were used: treating the slopes of the charge-discharge curves, and integral form of discharge characteristics. It was shown that integral form of treating was more reliable. The cell capacitance, ranging from 216 F g^{-1} to 230 F g^{-1} was determined, which were in good agreement with theoretically calculated of 224 F g^{-1}. In the specific current range of 0.3 to 1.5 A g^{-1} based on the active masses, the specific energy decrease from 30 to

20 Wh kg^{-1}, while specific power increased from 200 to ~800 W kg^{-1}. The specific capacity of the cell, slightly decrease from 47 Ah g^{-1} to 40 Ah g^{-1} by increasing the specific current. From the cyclization experiments, it was estimated that cell will lose 20% of initial capacitance after ~550 cycles. It could be also suggested that improvement of the cycling stability as well as the relatively high resistivity of the cell, can be further achieved preparing a carbonaceous based composite electrode materials.

According to obtained specific energy and power, investigated devices could be classified as a hybrid asymmetric battery type supercapacitors or supercapattery cell.

REFERENCES

[1] A. Yu, V. Chabot, J. Zhang, Electrochemical Supercapacitors for Energy Storage and Delivery: Fundamentals and Applications, CRC press, Taylor & Francis Group, LLC, Broken Sound Parkway NW, 2013.

[2] B.E. Conway, Electrochemical Supercapacitors: Scientific Fundamentals and Technological Applications. (1999) New York, Kluwer-Plenum.

[3] R. Kötz, M. Carlen. Principles and applications of electrochemical capacitors, Electrochim. Acta 45(15-16) (2000) 2483-2498.

[4] A.S. Aricò, P. Bruce, B. Scrosati, J-M Tarascon, W. van Schalkwijk, Nanostructured materials for advanced energy conversion and storage devices. Nature Materials, 4 (2005) 366-377

[5] A. Chu, P. Braatz, Comparison of commercial supercapacitors and high power lithium-ion batteries for power-assist applications in hybrid electric vehicles I. Initial characterization, J. Powep Sources, 112(1) (2002) 236-246.

[6] Y. Zhang, H. Feng, X. Wu, L. Wang, A. Zhang, T. Xia, H. Dong, X. Li, L. Zhang, Progress of electrochemical capacitor electrode materials: A review, Int. J. Hyd. Energy. 34 (2009) 4889–4899.

[7] S. Faraji, F. Nasir Ani, The development supercapacitor from activated carbon by electroless plating: A review, Renewable and Sustainable Energy Reviews, 42 (2015) 823–834.

[8] D. P. Dubal, O. Ayyad, V. Ruiz, P. Gómez-Romero, Hybrid energy storage: the merging of battery and supercapacitor chemistries, Chem. Soc. Rev. 44 (2015) 1777-1790.

[9] A. Burke, Ultracapacitors: why, how, and where is the technology, J. Power Sources, 91 (2000) 37–50.

[10] G. Yu, X. Xie, L. Pan, Z. Bao, Y. Cui, Hybrid nanostructured materials for high-performance electrochemical capacitors, Nano Energy, 2 (2013) 213–234.

[11] P. Xiong, J. Zhu, X. Wang, Recent advances on multi-component hybrid nanostructures for electrochemical capacitors, J. Power Sources, 294 (2015) 31-50.

[12] L. Yu, G.Z. Chen, Redox electrode materials for supercapatteries, J. Power Source, 326 (2016) 604–612.

[13] L. Yua, G.Z. Chen, High energy supercapattery with an ionic liquid solution of LiClO$_4$, Faraday Discuss., 190 (2016) 231-240.

[14] J. Suarez-Guevara, V. Ruiz, P. Gomez-Romero, Hybrid energy storage: high voltage aqueous supercapacitors based on activated carbon-phosphotungstate hybrid materials, J. Mat. Chem. A: Materials for Energy and Sustainability, 2(4) (2014) 1014-1021.

[15] J. Ni, H. Wang, Y. Qu, L. Gao, PbO$_2$ electrodeposited on graphite for hybrid supercapacitor applications, Phys. Scr., 87 (2016) 045802

[16] H.R. Ghenaatian, M.F. Mousavi, M.S. Rahmanifar, High performance hybrid supercapacitor based on two nanostructured conducting polymers: Self-doped polyaniline and polypyrrole nanofibers, Electrochim. Acta ,78 (2012) 212-222.

[17] G. A. Snooka, P. Kao, A. S. Best, Conducting-polymer-based supercapacitor devices and electrodes, J. Power Sources, 196 (2011) 1–12.

[18] Y. Shi, L. Peng, Y. Ding, Y. Zhao, G. Yu, Nanostructured conductive polymers for advanced energy storage, Chem. Soc. Rev., 44 (2015) 6684-6696.

[19] R. Ramya, R. Sivasubramanian, M.V. Sangaranarayanan, Conducting polymers-based electrochemical supercapacitors-Progress and prospects, Electrochim. Acta, 101 (2013) 109– 129

[20] Y. Shi, L. Peng, Y. Ding, Y. Zhao, G. Yu, Nanostructured conductive polymers for advanced energy storage, Chem. Soc. Rev., 44 (2015) 6684-6696.

[21] E. Frackowiak, V. Khomenko, K. Jurewicz, K. Lota, F. Béguin, Supercapacitors based on conducting polymers/nanotubes composites, J. Power Sources, 153 (2006) 413–418.

[22] R. Holze, Y.P. Wu, Intrinsically conducting polymers in electrochemical energy technology: Trends and progress, Electrochim. Acta, 122 (2014) 93– 107.

[23] P. Audebert. Recent Trends in Polypyrrole Electrochemistry, Nanostructuration, and Applications, in: S. Cosnier and A. Karyakin (Eds.), Electropolymerization:

Concepts, Materials and Applications, Wiley-VCH Verlag GmbH & Co. KGaA, Weinheim, Germany. 2010, pp 77-91.

[24] T. Liu, L. Finn, M. Yu, H. Wang, T. Zhai, X. Lu, Y. Tong, Y. Li, Polyaniline and polypyrrole pseudocapacitor electrodes with excellent cycling stability, Nano Lett., 14 (2014) 2522−2527.

[25] X. Zhao, B. M. Sanchez, P. J. Dobson, P. S. Grant, The role of nanomaterials in redox-based supercapacitors for next generation energy storage devices, Nanoscale, 3 (2011) 839–855.

[26] D. P. Dubal, S. H. Lee, J. G. Kim, W. B. Kim, C. D. Lokhande, Porous polypyrrole clusters prepared by electropolymerization for a high performance supercapacitor, J. Mater. Chem., 22 (2012) 3044–3052.

[27] Q-Fu Wu, K-Xin He, H.-Yu Mi, X-Gang Zhang, Electrochemical capacitance of polypyrrole nanowire prepared by using cetyltrimethylammonium bromide (CTAB) as soft template, Mater. Chem. Phys., 101 (2007) 367–371.

[28] J. Ma, Y. Liu, Z. Hu, Z. Xu, Electrochemical synthesis and performance of PANI electrode material for electrochemical capacitor, Ionics, 19 (2013) 1405-1413.

[29] N. H. Khdary, M. E. Abdesalam, G. E. Enany, Mesoporous polyaniline films for high performance supercapacitors, J. Electrochem. Soc,. 161 (2014) G63-G68.

[30] Marin S. Halper, James C. Ellenbogen, Supercapacitors: A Brief Overview, MITRE, McLean, Virginia, USA, 2006.

[31] http://hyperphysics.phy-astr.gsu.edu/hbase/Tables/diel.html

[32] R.C. Dorf, J.A. Svoboda, Introduction to Electric Circuits (5th ed.). New York: John Wiley & Sons, 2001.

[33] M. Nakamura, N. Sato, N. Hoshi, O. Sakata, Outer Helmholtz plane of the electrical double layer formed at the solid electrode–liquid interface. Chem. Phys. Chem., 12 (2011) 1430–1434.

[34] https://en.wikipedia.org/wiki/Supercapacitor

[35] C. Peng, S. Zhang, D. Jewell, G.Z. Chen, Carbon nanotube and conducting polymer composites for supercapacitors, Prog. Nat. Sci., 18 (2008) 777–788.

[36] M.R. Lukatskaya, B. Dunn, Y. Gogotsi, Multidimensional materials and device architectures for future hybrid energy storage, Nat. Commun., 7, Article number: 12647, 2016.

[37] A. G. MacDiarmid, Nobel Lecture: ''Synthetic metals'': A novel role for organic polymers, Rev. Mod. Phys., **73**(3) (2001) 701-712.

[38] A. J. Heeger, Nobel Lecture: Semiconducting and metallic polymers: The fourth generation of polymeric materials, Rev. Mod. Phys., **73**(3) (2001) 681-700.

[39] H. Shirakawa, Nobel Lecture: The discovery of polyacetylene film—the dawning of an era of conducting polymers, Rev. Mod. Phys., 73(3) (2001) 713-718.

[40] Pandolfo, A.G.; Hollenkamp, A.F. Carbon properties and their role in supercapacitors. J. Power Sources, 157 (2006) 11–27

[41] G. Shul, D. Bélanger, Self-discharge of electrochemical capacitors based on soluble or grafted quinone, Phys. Chem. Chem. Phys., 18 (2016) 19137-19145

[42]K. Naoi, P. Simon. New Materials and New Configurations for Advanced Electrochemical Capacitors. Electrochem. Soc. Interface, 17 (2008) 34-37.

[43] Z. Li Li, Carbon-based materials as supercapacitor electrodes, Ph.D. thesis, National, University of Singapore, 2010.

[44] S. Iijima, Helical microtubules of graphitic carbon, Nature, 354 (6348) (1991) 56–58.

[45] A.J. Zarbin, Química de (nano)materiais., Quim Nova 30 (2007) 1469-1479

[46] A. Kumar, C. H. Lee, Synthesis and Biomedical Applications of Graphene: Present and Future Trends, Advances in Graphene Science, Dr. M. Aliofkhazraei (Ed.), InTech, 2013.

[47] K. S. Novoselov, A.K. Geim, S.V. Morozov, D. Jiang, Y. Zhang, S.V. Dubonos, I.V. Grigorieva, A.A. Firsov, Electric field effect in atomically thin carbon films, Science. 306 (5696) (2004) 666–669

[48] C.D. Lokhande, D.P. Dubal, Oh-Shim Joo, Metal oxide thin film based supercapacitors, Curr. Appl. Phys., 11 (2011) 255-270.

[49] P. Simon, Y. Gogotsi, Materials for electrochemical capacitors, Nat. Mater., 7 (2008) 845-854.

[50] C-C. Hu, K.-H. Chang, M.-C. Lin, Y.-T. Wu, Design and tailoring of the nanotubular arrayed architecture of hydrous RuO2 for Next Generation Supercapacitors, Nano Lett., 6 (12) (2006) 2690-2695.

[51] H. Xia, Y.S. Meng, G. Yuan, C. Cui, L.i Lu, A symmetric RuO2/RuO2 supercapacitor operating at 1.6 V by using a neutral aqueous electrolyte, Electrochem. Solid. State Lett. 15 (2012) A60-A63.

[52] I. György, Chapter 1: Introduction. In Scholz, F. Conducting Polymers: A New Era in Electrochemistry. Monographs in Electrochemistry. Springer. 2008, pp. 1–6.

[53] https://en.wikipedia.org/wiki/Conductive_polymer

[54] A. Rudge, J. Davey, I. Raistrick, S. Gottesfeld, J.P. Ferraris. Conducting polymers as active materials in electrochemical capacitors, J. Power Sources, 47 (1994) 89–107.

[55] D. Nguyen Nguyen, H. Yoon, Recent advances in nanostructured conducting polymers: from synthesis to practical applications, Polymers, 8 (2016) 118-156

[56] Jian-Gan Wang, Bingqing Weiab, Feiyu Kang, Facile synthesis of hierarchical conducting polypyrrole nanostructures via a reactive template of MnO2 and their application in supercapacitors, RSC Adv, 4 (2014) 199-202.

[57] Jingjing Mu, Guofu Maa, Hui Peng, Jiajia Li, Kanjun Sun, Ziqiang Lei, Facile fabrication of self-assembled polyaniline nanotubes doped with d-tartaric acid for high-performance supercapacitors, J. Power Sources, 242 (2013) 797-802.

[58] W. Chen, R.B. Rakhi, H. N. Alshareef, Facile synthesis of polyaniline nanotubes using reactive oxide templates for high energy density pseudocapacitors, J. Mater. Chem. A, 1 (2013) 3315-3324

[59] Q. Wang, J. Yan, Z. Fan, T. Wei, M. Zhang, X. Jing, Mesoporous polyaniline film on ultra-thin graphene sheets for high performance supercapacitors, J. Power Sources 247 (2014) 197-203.

[60] V. Khomenko, E. Raymundo-Piñero, E. Frackowiak, F. Béguin, High-voltage asymmetric supercapacitors operating in aqueous electrolyte, Appl. Phys. A, 82 (2005) 567–573.

[61] A.G. Pandolfo, N.W. Duffy, High energy asymmetric nickel-carbon supercapacitors. Proceedings of the Land Warfare Conference; Defense Science and Technology Organization: Salisbury, 2006.

[62] D. Cericola, R. Kötz, Hybridization of rechargeable batteries and electrochemical capacitors: Principles and limits, Electrochim. Acta, 72 (2012) 1– 17.

[63] A. Laforgue, P. Simon, J. F. Fauvarque, M. Mastragostino, F. Soavi, J. F. Sarrau, P. Lailler, M. Conte, E. Rossi, S. Saguatti, Activated carbon/conducting polymer hybrid supercapacitors, J. Electroch. Soc., 150(5) (2003) A645-A651.

[64] Marina Mastragostino, Catia Arbizzani, Francesca Soavi, Conducting polymers as electrode materials in supercapacitors, Solid State Ion., 148(3-4) (2002) 493-498.

[65] Jong Hyeok Park, O Ok Park, Hybrid electrochemical capacitors based on polyaniline and activated carbon electrodes, J. Power Sources, 111 (2002) 185–190,

[66] Min Zhou, Fei Lu, Xiaoshuang Shen, Weiwei Xia, Hui He and Xianghua Zeng, One-pot construction of three dimensional $CoMoO_4/Co_3O_4$ hybrid nanostructures and their application in supercapacitors, J. Mater. Chem. A, 3 (2015) 21201-21210

[67] G. Z. Chen, Understanding supercapacitors based on nano-hybrid materials with interfacial conjugation, Prog. Nat. Sci. 23(3) (2013) 245–255

[68] Z. Cai, L. Li, J. Ren, L. Qiu, H. Lin, H. Peng, Flexible, weavable and efficient microsupercapacitor wires based on polyaniline composite fibers incorporated with aligned carbon nanotubes, J. Mater. Chem. A, 1 (2013) 258–261

[69] Y. Liu, R. Wang, X. Yan, Synergistic effect between ultra-dmall nickel hydroxide nanoparticles and reduced graphene oxide sheets for the application in high-performance asymmetric supercapacitor, Sci. Rep., 5 (2015) 11095, DOI: 10.1038/srep11095

[70] Wei-dong Xue, Wen-jian Wang, Yu-feng Fu, Dong-xu He, Fan-yu Zeng, Rui Zhao, Rational synthesis of honeycomb-like $NiCo_2O_4@NiMoO_4$ core/shell nanofilm arrays on Ni foam for high-performance supercapacitors, Materials Letters, 186 (2017) 34-37.

[71] M. Xu, R. Xu, Y. Zhao, L. Chen, B. Huang, W. Wei, Hierarchically porous Ni monolith@branch-structured $NiCo_2O_4$ for high energy density supercapacitors, Prog. Nat. Sci.: Mat. Inter., 26 (3) (2016) 276-282.

[72] J. Zhao, Z. Li, M. Zhang, A. Meng, Q. Li, Vertically cross-linked and porous $CoNi_2S_4$ nanosheets-decorated SiC nanowires with exceptional capacitive performance as a free-standing electrode for asymmetric supercapacitors, J. Power Sources, 332 (2016) 355-365.

[73] X. Deng, J. Li, S. Zhu, F. He, C. He, E. Liu, C. Shi, Q. Li, N. Zhao, Metal–organic frameworks-derived honeycomb-like Co_3O_4/three-dimensional graphene networks/Ni

foam hybrid as a binder-free electrode for supercapacitors, J. Alloys Comp., 693 (2017) 16-24.

[74] X. Qiu, L. Li, Y. Sun, X. Kong, The application of nickel hexacyanoferrate/hexadecyl trimethyl ammonium bromide/graphene nanocomposites synthesized by reverse microemulsion in supercapacitors, Colloids and Surfaces A: Physicochemical and Engineering Aspects, 506 (5) (2016) 670-677.

[75] C. Yang, J. Shen, C. Wang, H. Fei, H. Bao, G. Wang, All-solid-state asymmetric supercapacitor based on reduced graphene oxide/carbon nanotube and carbon fiber paper/polypyrrole electrodes, J. Mater. Chem. A, 2 (2014) 1458-1464.

[76] Y. Song, X. Cai, X. Xu, X.-Xia Liu, Integration of nickel-cobalt double hydroxide nanosheets and polypyrrole film with functionalized partial-exfoliated graphite for asymmetric supercapacitor with improved rate capability, J. Mater. Chem. A, 3 (2015) 14712–14720.

[77] F. Grote, Y. Lein, A complete three-dimensionally nanostructured asymmetric supercapacitor with high operating voltage window based on PPy and MnO2, Nano Energy, 10 (2014) 63–70.

[78] J. Liu, L. Zhang, H. Bin Wu, J. Lin, Z. Shen, X. W. D. Lou, High-performance flexible asymmetric supercapacitors based on a new graphene foam/carbon nanotube hybrid film, Energy Environ. Sci. 7 (2014) 3709–3719.

[79] Y. Cheng, H. Zhang, C. V. Varanasi, J. Liu, Improving the performance of cobalt–nickel hydroxide-based self-supporting electrodes for supercapacitors using accumulative approaches, Energy Environ. Sci., 6 (2013)3314-3321

[80] H. Li, L. Cheng, Y. Xia, A hybrid electrochemical supercapacitor based on a 5V Li-ion battery cathode and active carbon, Electrochem. Solid State Lett., 8(9) (2005) A433-A436.

[81] X. Wang, J. P. Zheng, The optimal energy density of electrochemical capacitors using two different electrodes, J. Electroch. Soc., 151(10) (2004) A1683-A1689.

[82] A. Du Pasquier, I. Plitz, S. Menocal, G. Amatucci, A comparative study of Li-ion battery, supercapacitor and nonaqueous asymmetric hybrid devices for automotive applications, J. Power Sources, 115(1) (2003) 171-178.

[83] W. G. Pell, B. E. Conway, Peculiarities and requirements of asymmetric capacitor devices based on combination of capacitor and battery-type electrodes, J. Power Sources, 136(2) (2004) 334-345.

[84] G.G. Amatucci, F. Badway, A. Du Pasquier, T. Zheng, An asymmetric hybrid nonaqueous energy storage cell, J. Electrochem. Soc., 148(8) (2001) A930-A939.

[85] US Patent no. 6,252,762 "Rechargeable hybrid battery/supercapacitor system"

[86] B. Akinwolemiwa, C. Peng, G.Z. Chen, Redox Electrolytes in Supercapacitors, J. Electrochem. Soc., 162 (5) (2015) A5054-A5059.

[87] G.Z. Chen: Supercapacitor and supercapattery as emerging electrochemical energy stores, Int. Mat. Rev., (2016) http://dx.doi.org/10.1080/09506608.2016.1240914

[88] Hu D, Peng C, Chen GZ. Electrodeposition of nonconducting polymers: roles of carbon nanotubes in the process and products. ACS Nano. 4 (2010) 4274–4282.

[89] Y.J. Hao, Q.Y. Lai, L. Wang, X.-Y. Xu, H.Y. Chu, Electrochemical performance of a high cation-deficiency Li2Mn4O9/active carbon supercapacitor in LiNO3 electrolyte, Synth. Met., 160 (7–8) (2010) 669–674.

[90] H. Manjunatha, G.S. Suresh, T.V. Venkatesha, Electrode materials for aqueous rechargeable lithium batteries, J. Solid State Electrochem., 15 (2011) 431–445

[91] G. Wang, Q. Qu, B. Wang, Y. Shi, S. Tian, Y. Wu, An aqueous electrochemical energy storage system based on doping and intercalation: Ppy/LiMn2O4, Chem. Phys. Chem., 9 (2008) 2299–2301.

[92] G.J. Wang, L.C. Yang, Q.T. Qu, B. Wang, Y.P. Wu, R. Holze, An aqueous rechargeable lithium battery based on doping and intercalation mechanisms, J. Solid State Electrochem., 14 (2010) 865–869.

[93] W. Tang, L. Liu, Y. Zhu, H. Sun, Y. Wu, K. Zhu, An aqueous rechargeable lithium battery of excellent rate capability based on a nanocomposite of MoO3 coated with PPy and LiMn2O4, Energy Environ. Sci., 5 (2012) 6909–6913.

[94] W. Tang, X.W. Gao, Y.S. Zhu, Y.B. Yue, Y. Shi, Y.P. Wu, K. Zhu, A hybrid of V2O5 nanowires and MWCNTs coated with polypyrrole as an anode material for aqueous rechargeable lithium batteries with excellent cycling performance, J. Mater. Chem., 22 (2012) 20143–20145.

[95] L.L. Liu, X.J. Wang, Y.S. Zhu, C.L. Hu, Y.P. Wu, R. Holze, Polypyrrole-coated LiV3O8-nanocomposites with good electrochemical performance as anode material for aqueous rechargeable lithium batteries, J. Power Sources, 224 (2013) 290–294.

[96] L. Liu, F. Tian, M. Zhou, H. Guo, X. Wang, Aqueous rechargeable lithium battery based on polyaniline and LiMn2O4 with good cycling performance, Electrochim. Acta, 70 (2012) 360– 364.

[97] P. Novák, K. Müller, K.S.V. Santhanam, O. Haas, Electrochemically active polymers for rechargeable batteries, Chem. Rev., 97 (1997) 207-281.

[98] Wallace, G. G., Tsekouras, G. Wang, C. Inherently Conducting Polymers via Electropolymerization for Energy Conversion and Storage, in Electropolymerization: Concepts, Materials and Applications (eds S. Cosnier and A. Karyakin), Wiley-VCH Verlag GmbH & Co. KGaA, Weinheim, ch11, 2010.

[99] B.N. Grgur, M.M. Gvozdenovic, J. Stevanovic, B.Z. Jugovic, V.M. Marinovic, Polypyrrole as possible electrode materials for the aqueous-based rechargeable zinc batteries, Electrochim. Acta, 53 (2008) 4627-4633.

[100] H. Wang, J. Lin, Z.X. Shen, Polyaniline (PANi) based electrode materials for energy storage and conversion, Journal of Science: Advanced Materials and Devices 1 (2016) 225-255

[101] S. Muench, A. Wild, C. Friebe, B. Häupler, T. Janoschka, U.S. Schubert, Polymer-Based Organic Batteries, Chem. Rev., 116 (2016) 9438−9484.

[102] Milica M. Gvozdenović, Branimir Z. Jugović, Jasmina S. Stevanović, Branimir N. Grgur, Electrochemical synthesis of electroconducting polymers, Hem. Ind. 68 (6) (2014) 673–684.

[103] Leon A. P. Kane-Maguire, Gordon G. Wallace, Chiral conducting polymers, Chem. Soc. Rev., 39 (2010) 2545-2576

[104] F. Wolfart, D.P. Dubal, M. Vidotti, R. Holze, P. Gómez-Romero, Electrochemical supercapacitive properties of polypyrrole thin films: influence of the electropolymerization methods, J Solid State Electrochem., 20 (2016) 901-910.

[105] B. L. Funt, A. F. Diaz, Organic Electrochemistry: an Introduction and a Guide, Marcel Dekker, New York, 1991, pp. 1337.

[106] E. M. Genies, G. Bidan, A. F. Diaz, Spectroelectrochemical study of polypyrrole films, J. Electroanal. Chem., 149 (1983) 101-113.

[107] R. J. Waltman, J. Bargon, Electrically conducting polymers: a review of the electropolymerization reaction, of the effects of chemical structure on polymer film properties, and of applications towards technology, Can. J. Chem., 64 (1985) 76-95.

[108] R. J. Waltman, J. Bargon, Reactivity/structure correlations for the electropolymerization of pyrrole: An INDO/CNDO study of the reactive sites of oligomeric radical cations, Tetrahedron, 40 (1984) 3963-3970.

[109] P. Camurlu, Polypyrrole derivatives for electrochromic applications, RSC Adv., 4 (2014) 55832–55845

[110] S. Sadki, P. Schottland, N. Brodie, G. Sabouraud, The mechanisms of pyrrole electropolymerization, Chem. Soc. Rev., 29 (2000) 283-293.

[111] J. Roncali, Conjugated poly(thiophenes): synthesis, functionalization, and applications, Chem. Rev., 92 (1992) 711-738.

[112] M. Zhou, J. Heinze, Electropolymerization of Pyrrole and Electrochemical Study of Polypyrrole. 2. Influence of Acidity on the Formation of Polypyrrole and the Multipathway Mechanism, J. Phys. Chem. B, 103 (1999) 8443-8450.

[113] E. Smela, Conjugated polymer actuators for biomedical applications, Adv. Mater. 15(6) (2003) 481-494

[114] J. Stejskal, M. Trchova, P. Bober, Z. Morávková, D. Kopecký, M. Vrnata, J. Prokeš, M. Varga and E. Watzlova, Polypyrrole salts and bases: superior conductivity of nanotubes and their stability towards the loss of conductivity by deprotonation, RSC Adv., 6 (2016) 88382-88391.

[115] Li Y, Qian R. Electrochemical overoxidation of conducting polypyrrole nitrate film in aqueous solutions. Electrochim. Acta., 45(11) (2000) 1727‑1731.

[116] M. M. Gvozdenović , B. Z. Jugović, T. Lj. Trišović, J.S. Stevanović and B. N. Grgur, Materials Chemistry and Physics, Electrochemical characterization of polyaniline electrode in ammonium citrate containing electrolyte, 125, 3 (2004) 601-605.

[117] Y. Wei, X. Tang, Y. Sun, W.W. Focke, A study of the mechanism of aniline polymerization, J. Polym. Sci., 27 (1989) 2385–2396.

[118] Y. Wei, G-W Jang, Ch-Ch. Chan, K.F. Hsuen, R. Hariharan, S,A, Patel, C.K. Whitecar, Polymerization of aniline and alkyl ring-substituted anilines in the presence of aromatic additives, J. Phys. Chem., 94 (1990) 7716–7721.

[119] Chetna Dhand, Neeraj Dwivedi, Sachin Mishra, Pratima R Solanki, Venkatesh Mayandi, Roger W Beuerman, Seeram Ramakrishna, Rajamani Lakshminarayanan, Bansi D Malhotra, Polyaniline-based biosensors: A review, Nanobiosensors in Disease Diagnosis, 4 (2015) 25—46.

[120] Claudio H. B. Silva, Ana M. Da Costa Ferreira, Vera R. L. Constantino and Marcia L. A. Temperini, Hybrid materials of polyaniline and acidic hexaniobate nanoscrolls: high polaron formation and improved thermal properties, J. Mater. Chem. A, 2014, 2, 8205–8214

[121] B. Jugović, M. Gvozdenović, J. Stevanović, T. Trišović, B. Grgur, Characterization of electrochemically synthesized PANI on graphite electrode for potential use in electrochemical power sources, Mat. Chem. Phys., 114(2-3) (2009) 939-942.

[122] B.N. Grgur, A. Žeradjanin, M.M. Gvozdenović, M.D. Maksimović, T.Lj. Trišović, B.Z. Jugović, Electrochemical characteristics of rechargeable polyaniline/lead dioxide cell, J. Power Sources 217 (2012) 193-198.

[123] S. Suematsu, Y. Oura, H. Tsujimoto, H. Kanno, K. Naoi, Conducting polymer films of cross-linked structure and their QCM analysis, Electrochim. Acta, 45 (2000) 3813-3821.

[124] T.V. Vernitskaya, O.N. Efimov, Polypyrrole: a conducting polymer; its synthesis, properties, and applications, Russ. Chem. Rev., 66 (5) (1997) 443-457.

[125] P.M. Carrasco, M. Cortazar, E. Ochoteco, E. Calahorra, J.A. Pomposo, Comparison of surface and bulk doping levels in chemical polypyrroles of low, medium and high conductivity, Surf. Interface Anal. 39 (2007) 26–32.

[126] H. Masuda, D. K. Asano, Preparation and properties of polypyrrole, Synth. Met. 135-136 (2003) 43-44.

[127] J.V. Thombare, M.C. Rath, S.H. Han, V.J. Fulari, Synthesis of hydrophilic polypyrrole thin films by SILAR method, Materials Physics and Mechanics, 16 (2013) 118-125

[128] R. Mazeikiene, A. Malinauskas, Kinetics of the electrochemical degradation of polypyrrole, Polym. Degrad. Stab., 75 (2002) 255–258.

[129] C. Weidlich, K.-M. Mangold, K. Jüttner, EQCM study of the ion exchange behaviour of polypyrrole with different counterions in different electrolytes, Electrochim. Acta, 50 (2005) 1547–1552.

[130] B. N. Grgur, Metal | polypyrrole battery with the air regenerated positive electrode, J. Power Sources, 272 (2014) 1053-1060.

[131] P. Tammela, Z. Wang, S. Frykstrand, P. Zhang, I.-M. Sintorn, L. Nyholm, M. Strømme, Asymmetric supercapacitors based on carbon nanofibre and polypyrrole/nanocellulose composite electrodes, RSC Adv. 5 (2015) 16405–16413.

[132] M. Huck, J. Badeda, D.U. Sauer, Modeling the crystal distribution of lead-sulfate in lead-acid batteries with 3D spatial resolution, J. Power Sources, 279 (2015) 351-357.

[133] G. Wallace, G. Spinks, L. Kane-Maguire, P. Teasdale. Conductive Electroactive Polymers, CRC Press, Taylor & Francis Group, ISBN 978-1-4200-6709-5, Boca Raton, 2009.

[134] G. Ćirić-Marjanović, Recent advances in polyaniline research: Polymerization mechanisms, structural aspects, properties and applications, Synth. Met. 177 (2013) 1–47.

[135] M.M. Gvozdenović, B.Z. Jugović, J.S. Stevanović, T.Lj. Trišović, B.N. Grgur, Electropolymerization, Chapter 4: Electrochemical Polymerization of Aniline, Ewa Schab-Balcerzak (Ed.), InTech publ, 2011, pp 77-96.

[136] Petersson, B. Berghult, E. Ahlberg, Thin lead dioxide electrodes for high current density applications in semi-bipolar batteries, J. Power Sources, 74 (1998) 68–76.

[137] H. Xia, Q. Wang, Synthesis and characterization of conductive polyaniline nanoparticles through ultrasonic assisted inverse microemulsion polymerization, J. Nanopart. Res., 3 (2001) 401–411.

[138] H. Xia, Q. Wang, Synthesis and characterization of conductive polyaniline nanoparticles through ultrasonic assisted inverse microemulsion polymerization, J. Nanopart. Res., 3 (2001) 401–411.

[139] H.N. Dinh, J. Ding, S.J. Xia, V.I. Birss, Multi-technique study of the anodic degradation of polyaniline films, J. Electroanal. Chem. 459 (1998) 45-56.

[140] D.E. Stilwell, S.-M. Park, Electrochemistry of conductive polymers IV: Electrochemical studies on polyaniline degradation - Product identification and coulometric studies, J. Electrochem. Soc. 135 (1988) 2497-2502.

[141] A.Q. Zhang, C.Q. Cui, J.Y. Lee, Electrochemical degradation of polyaniline in HClO4 and H$_2$SO$_4$, Synth. Met. 72 (1995) 217-223.

[142] A.Q. Contractor, V.A. Juvekar, Estimation of equilibrium capacitance of polyaniline films using step voltammetry, J. Electrochem. Soc., 162 (7) (2015) A1175-A1181.

[143] L. Zhuang, Q. Zhou, J. Lu, Simultaneous electrochemical–ESR–conductivity measurements of polyaniline, J. Electroanal. Chem., 493 (2000) 135–140.

[144] M. Magnuson, J.-H. Guo, S. M. Butorin, A. Agui, C. Såthe, J. Nordgren, The electronic structure of polyaniline and doped phases studied by soft X-ray absorption and emission spectroscopies, J. Chem. Phys., 111, (1999) 4756-4764

[145] Y. Zhao, C.-A. Wang, Nano-network MnO$_2$/polyaniline composites with enhanced electrochemical properties for supercapacitors, Mater. Design., 97 (2016) 512–518.

[146] J. Mu, G. Ma, H. Peng, J. Li, K. Sun, Z. Lei, Facile fabrication of self-assembled polyaniline nanotubes doped with D-tartaric acid for high-performance supercapacitors, J. Power Sources, 242 (2013) 797-802.

[147] H. Wang, D. Liu, X. Duan, P. Du, J. Guo, P. Liu, Facile preparation of high-strength polyaniline/polyvinyl chloride composite film as flexible free-standing electrode for supercapacitors, Mater. Design., 108 (2016) 801–806.

[148] D. Gui, C. Liu, F. Chen, J. LiuSchool, Preparation of polyaniline/graphene oxide nanocomposite for theapplication of supercapacitor, Appl. Surf. Sci., 307 (2014) 172–177.

[149] S. Saranyaa, R. Kalai Selvana, N. Priyadharsinia, Synthesis and characterization of polyaniline/MnWO4 nanocomposites as electrodes for pseudocapacitors, Appl. Surf. Sci., 258 (2012) 4881– 4887.

[150] Y. Liu, P. Gao, X. Bu, G. Kuang, W. Liu, L. Lei, Nanocrosses of lead sulphate as the negative active material of lead acid batteries, J. Power Sources, 263 (2014) 1-6.

[151] G. Wang, L. Zhang, J. Zhang, A review of electrode materials for electrochemical supercapacitors, Chem. Soc. Rev., 41 (2) (2012) 797−828.

[152] T. Liu, L. Finn, M. Yu, H. Wang, T. Zhai, X. Lu, Y. Tong, Y. Li, Polyaniline and polypyrrole pseudocapacitor electrodes with excellent cycling stability, Nano Lett., 14 (2014) 2522−2527.

[153] E. Ebner, D. Burow, A. Börger, M. Wark, P. Atanassova, J. Valenciano, Carbon blacks for the extension of the cycle life in flooded lead acid batteries for micro-hybrid applications, J. Power Sources, 239 (2013) 483-489.

[154] D. Pavlov, P. Nikolov, Capacitive carbon and electrochemical lead electrode systems at the negative plates of lead–acid batteries and elementary processes on cycling, J. Power Sources, 242 (2013) 380-399.

BIOGRAFIJA

Alsadek Ali Alguail, master inženjer tehnologije, je rođen 1977 godine u mestu Melsata, Libya. Osnovne akademske studije je završio na Alfateh University, Tripoli, Libya, 1999 godine, na smeru za Hemijsko inženjerstvo. Master studije završio na Malaysian National University, Malaysia, 2006 godine na smeru za Hemijsko i procesno inženjerstvo. Bio je zaposlen na poslovima inženjera u postrojenju za desalinaciju u Alkhoms Power Station, Alkhoms, Libya (2001-2003). U periodu od 2006-2007 godine radio je kao saradnik u nastavi pri Departmanu za Hemijsku tehnologiju, na Higher Technical Institute, Msallatah, Libya, a u periodu od 2008-2011 godine je radio je kao saradnik u nastavi na Departmentu Zaštitu okoline na Faculty of Science, Nation Nasir University, Tripoli, Libya. Školske 2014/2015 upisao je doktorske studije na Tehnološko-metalurškom fakultetu, Univerziteta u Beogradu, odsek za Hemijsko inženjerstvo. Do sada je autor jednog rada u međunarodnom časopisu izuzetnih vrednosti (M21a) i autor i koautor dva rada u istaknutom međunarodnom časopis (M22) i koautor rada u međunarodnom časopisu (M23).

BIOGRAPHY

Alsadek Ali Alguail, Master Technology Engineer, was born in 1977 in Melsat, Libya. He completed his basic academic studies at Alfateh University, Tripoli, Libya, in 1999, in the Department of Chemical Engineering. He completed his MA in Malaysian National University, Malaysia, in 2006 on the direction of Chemical and Process Engineering. He was employed as an engineer at a desalinization plant in Alkhoms Power Station, Alkhoms, Libya (2001-2003). In the period 2006-2007 he worked as a teaching assistant at the Department of Chemical Technology at the Higher Technical Institute, Msallatah, Libya, and in the period 2008-2011 he worked as a teaching assistant at the Department of Environmental Protection at the Faculty of Science, Nation Nasir University, Tripoli, Libya. School year 2014/2015 he enrolled in doctoral studies at the Faculty of Technology and Metallurgy, University of Belgrade, Department of Chemical Engineering. He is the author and coauthor of four scientific papers.

Radovi proistekli iz doktorske disertacije/Papers from doctoral dissertation

<u>Međunarodni časopis izuzetnih vrednosti, M21a.</u>

1. Alguail Alsadek A., Al-Eggiely Ali H., Gvozdenović Milica M., Jugović Branimir Z., Grgur Branimir N., Battery Type Hybrid Supercapacitor Based on Polypyrrole and Lead-Lead Sulfate, - *Journal of Power Sources*, vol. 313, , pp. 240-246, 2016 **(IF= 6.395)** (ISSN: 0378-7753).

<u>Istaknuti međunarodni časopis M22.</u>

1. Alguail Alsadek A., Al-Eggiely Ali H., Grgur Branimir N., Polyaniline–Lead Sulfate Based cell with Supercapattery Behavior, - *Journal of Saudi Chemical Society*, vol. 21, no. 10, pp. 2769-2777, 2017 **(IF= 2.316)** (ISSN 1319-6103).

Изјава о истоветности штампане и електронске верзије докторског рада

Име и презиме аутора Alsadek Ali Alguail

Број индекса 4041/2014

Студијски програм Хемијско инжењерство

Наслов рада BATTERY TYPE HYBRID SUPERCAPACITOR BASED ON

CONDUCTING POLYMERS

Ментор Др Бранимир Гргур, ред. проф.

Потписани/а Alsadek Ali Alguail

Изјављујем да је штампана верзија мог докторског рада истоветна електронској верзији коју сам предао/ла за објављивање на порталу **Дигиталног репозиторијума Универзитета у Београду.**

Дозвољавам да се објаве моји лични подаци везани за добијање академског звања доктора наука, као што су име и презиме, година и место рођења и датум одбране рада.

Ови лични подаци могу се објавити на мрежним страницама дигиталне библиотеке, у електронском каталогу и у публикацијама Универзитета у Београду.

Потпис докторанда

У Београду, 07.11.2017
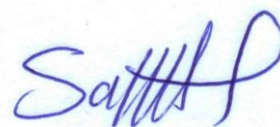
1. Ауторство - Дозвољавате умножавање, дистрибуцију и јавно саопштавање дела, и прераде, ако се наведе име аутора на начин одређен од стране аутора или даваоца лиценце, чак и у комерцијалне сврхе. Ово је најслободнија од свих лиценци.

2. Ауторство – некомерцијално. Дозвољавате умножавање, дистрибуцију и јавно саопштавање дела, и прераде, ако се наведе име аутора на начин одређен од стране аутора или даваоца лиценце. Ова лиценца не дозвољава комерцијалну употребу дела.

3. Ауторство - некомерцијално – без прераде. Дозвољавате умножавање, дистрибуцију и јавно саопштавање дела, без промена, преобликовања или употребе дела у свом делу, ако се наведе име аутора на начин одређен од стране аутора или даваоца лиценце. Ова лиценца не дозвољава комерцијалну употребу дела. У односу на све остале лиценце, овом лиценцом се ограничава највећи обим права коришћења дела.

4. Ауторство - некомерцијално – делити под истим условима. Дозвољавате умножавање, дистрибуцију и јавно саопштавање дела, и прераде, ако се наведе име аутора на начин одређен од стране аутора или даваоца лиценце и ако се прерада дистрибуира под истом или сличном лиценцом. Ова лиценца не дозвољава комерцијалну употребу дела и прерада.

5. Ауторство – без прераде. Дозвољавате умножавање, дистрибуцију и јавно саопштавање дела, без промена, преобликовања или употребе дела у свом делу, ако се наведе име аутора на начин одређен од стране аутора или даваоца лиценце. Ова лиценца дозвољава комерцијалну употребу дела.

6. Ауторство - делити под истим условима. Дозвољавате умножавање, дистрибуцију и јавно саопштавање дела, и прераде, ако се наведе име аутора на начин одређен од стране аутора или даваоца лиценце и ако се прерада дистрибуира под истом или сличном лиценцом. Ова лиценца дозвољава комерцијалну употребу дела и прерада. Слична је софтверским лиценцама, односно лиценцама отвореног кода.